博士論文

Theoretical study on the dynamics of the vortices and the Josephson junctions of superconductors

(超伝導体における渦糸およびジョセフソン接合のダイナミクスの理論的研究)

三﨑　航

Abstract

Theoretical study on the dynamics of the vortices and the Josephson junctions of superconductors

by

Kou Misaki

Doctor of Engineering in Applied Physics

University of Tokyo, Hongo

In this thesis, we will discuss the dynamics of the vortices in the superconductors and the Josephson phase. We will first discuss the suppression of superfluidity by dissipation and its relevance to "failed superconductor", and then discuss the nonreciprocity of the Josephson junctions where the two bulk superconductors exhibits different charge response property.

First, we will discuss the low temperature thermodynamic phase of superconductors in the presence of the finite magnetic field. In highly crystalline superconductors with finite magnetic field, experiments report the thermodynamic phase with very low resistance ($R \ll R_q = h/(2e)^2$, where R_q is the quantum resistance) down to the very low temperature. The theoretical understanding of this low temperature phase known as "the failed superconductor" remains unsettled.

Since the motion of vortices leads to the resistance, we believe that the dynamics of the vortices is important in understanding the failed superconductors. The difficulty of the theoretical understanding of the failed superconductor lies in the fact that, since the vortices are known to behave as bosons, they exhibit the superfluidity at low temperature. The superfluid phase of vortices physically means that the system becomes insulator, so the resistance cannot remain low at low temperature.

However, we will argue that, although the vortices are bosons, they fail to exhibit superfluidity because of the low energy continuum degrees of freedom inside the normal core, which acts as the source of dissipation. We will show this suppression of superfluidity by dissipation both in the numerical and the field-theoretical calculation, in the first-quantized and the second-quantized formulation, respectively. The physical argument for the suppression of superfluidity, the importance of the Galilean invariance breaking will be further discussed.

Our theory predict that, the failed superconductor exists for the moderately clean regime $\Delta^2/\epsilon_F \ll 1/\tau, k_B T$, where Δ is the superconducting gap, ϵ_F is the Fermi energy, τ is the relaxation time, T is the temperature of the system, while it disappears for the superclean regime $\Delta^2/\epsilon_F \gg 1/\tau, k_B T$. This prediction can be verified in experiments.

Secondly, we will discuss the theory of Josephson effect when the two bulk superconductors show different charge response property. In this case, the system lacks the inversion symmetry, and the shape of the I-V curve is not antisymmetric under the sign

change of the current bias I, i.e., $V(I) \neq -V(-I)$. This asymmetry of I-V curve is called the nonreciprocity. The important example of the nonreciprocal system is the p-n junction, where the difference of the dopant of the two bulk semiconductors lead to the drastically different behavior for positive and negative bias case.

The aim of our study is to extend this nonreciprocity caused by the difference of the bulk materials in normal junction system to the Josephson junctions. We will discuss the nonreciprocity both for the classical and quantum dynamics of the superconducting phase variable. In the classical case, the nonreciprocity is realized for the relatively small junction where the dynamics of the superconducting phase variable is underdamped. In the absence of the thermal fluctuation, we analyze the dynamics using the methods developed in the dynamical systems: We will show that the nonreciprocity is enhanced near the critical external current where the bifurcation of the dynamics occurs. For finite temperature case, the nonreciprocity in the distribution function of the energy will be discussed. In this case, not only the average value of V but also the fluctuation of V exhibits the nonreciprocity. For the quantum case, we will discuss the nonreciprocal I-V curve caused by the nonreciprocal Bloch oscillation and the nonreciprocal Zener tunneling. The experimental detection of the nonreciprocity from the 2ω measurement will be further discussed. We will show that the experimentally detectable 2ω response $V_{2\omega}$ is expected for the Josephson junctions with parameters realizable in experiments.

Contents

Contents **i**

Acknowledgements **iii**

1 Introduction **1**

2 Suppression of superfluidity by dissipation — An application to failed superconductor **9**
2.1 Background 9
2.2 Purpose and assumptions of the model 16
2.3 Model 17
2.4 Extended Feynman's argument 19
2.5 Result of the numerical calculation 22
2.6 Field theoretical Model 28
2.7 Discussion 32

3 Theory of nonreciprocal Josephson effect **35**
3.1 Background 35
3.2 Purpose and assumptions of the model 39
3.3 Models 40
3.4 Results 42
3.5 Discussion 52

4 Summary and perspectives **55**

A Appendix to chapter 2 **59**
A.1 Microscopic derivation of Green function in Keldysh formalism 59

B Appendix to chapter 3 **63**
B.1 Projection operator analysis 63
B.2 Derivation of Zener tunneling rate 70

Bibliography **77**

Acknowledgements

Foremost, I would like to express my deepest gratitude to my supervisor Prof. Naoto Nagaosa for the continuous support and many insightful comments and suggestions for my research. All the work included in this thesis started from his deep and insightful observation.
I would also like to thank all the members of Nagaosa group for fruitful discussions. My sincere thanks also goes to Tae Tokuyoshi, who has kindly helped me during the research activities.

Chapter 1

Introduction

The important effective degree of freedom inside the superconductor is the superconducting phase, which emerges because of the coherence of the wavefunction of cooper pairs established below the superconducting transition temperature. Although the superconducting phase is gauge dependent and therefore not measurable in experiments, *the difference* of the phases between two superconductors is well-defined. In Josephson junctions where the two superconductors are separated by the normal state thin film, $I-V$ curve is determined by the dynamics of the superconducting phase difference, which is described by the Josephson relation,

$$\begin{cases} \hbar\dot{\varphi} = 2eV \\ \dot{Q} + I_c \sin\varphi + \dfrac{V}{R} = I_x, \end{cases} \tag{1.1}$$

where V is the voltage drop, φ is the phase difference, i.e., Josephson phase, e is the charge of the electron, Q is the charge accumulated on the junction, I_c is the critical current of the superconductor, R is the shunt resistance, and I_x is the external current. The fact that the experimentally obtained $I-V$ curve matches with the prediction of the theory of Josephson effect is an important experimental evidence of the coherence inside the superconductors.

Another important feature of the superconductor is the rigidity against the magnetic field, known as "generalized rigidity" à la P. W. Anderson [1]. The magnetic field inside the superconductor obeys the London equation, $\nabla^2 B = [4\pi e^2 n_s/(mc^2)]B$, where B is the magnetic field, m is the electron mass, c is the speed of light, e is the electric charge of the electron, and n_s is the superfluid density. According to this equation, the magnetic field cannot penetrate into the bulk superconductor beyond the so-called London penetration depth, $\lambda = \sqrt{mc^2/(4\pi e^2 n_s)}$. The left hand side of the London equation comes from the usual Maxwell term, while the right hand side is peculiar to the superconducting system, and comes from the generalized rigidity.

The existence of the low energy superconducting phase degree of freedom and the generalized rigidity can both be understood as consequences of the spontaneous $U(1)$ gauge symmetry breaking. The superconducting phase is nothing but the Goldstone mode associated with the continuous symmetry breaking, and the generalized rigidity comes from the long ranged nature of the static current-current correlation function.

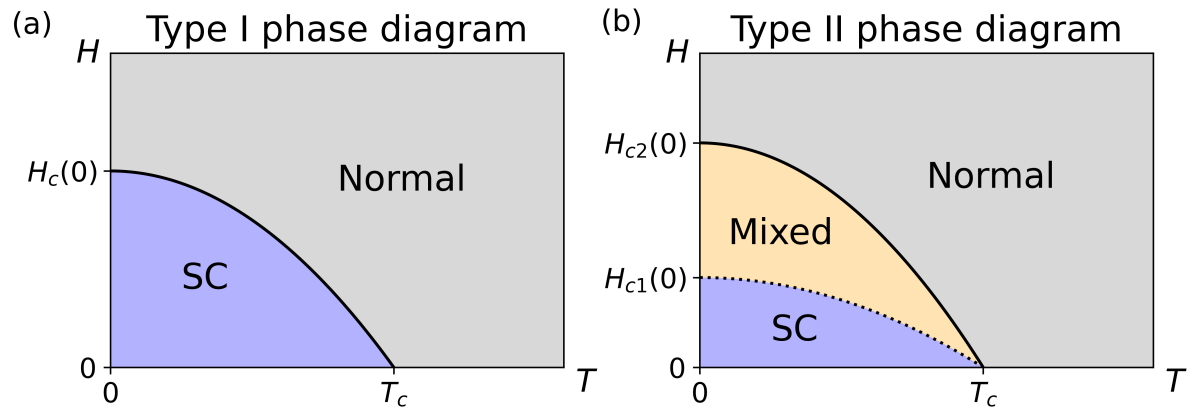

Figure 1.1: The schematic phase diagram for (a) type I superconductor and (b) type II superconductor. "SC", "Mixed" and "Normal" represent the superconducting phase, the mixed phase, and the normal phase, respectively.

In addition to the London penetration depth, there is another characteristic length scale for superconductors: The coherence length $\xi = \hbar v_F/(\pi\Delta)$, where v_F is the Fermi velocity and $\hbar$ is the Planck constant, determines the characteristic length of the variation of the superconducting gap Δ. The relative magnitude of these lengths can be quantified by the dimensionless parameter $\kappa = \lambda/\xi$, which is called the Ginzburg-Landau parameter. Since the variation of the magnetic field and the superconducting gap occurs at the boundary between the normal state system and the superconducting system, the value of κ determines the physical property of this boundary. In particular, the surface energy of the boundary is positive for $\kappa \ll 1$ and negative for $\kappa \gg 1$. To understand it, here we consider the system where the region $x \leq 0$ is in the normal state, while the region $x > 0$ is superconducting with the gap size Δ. When ξ is much larger than λ, the superconducting gap is smalller than the bulk value Δ for the region with the width $\delta x \sim \xi$, and because of the loss of the condensation energy, the surface energy is positive. When ξ is much smaller than λ, the magnetic field penetrates deep into the bulk superconductor with the width $\delta x \sim \lambda$, and because of the reduction of the diamagnetic energy of the Gibbs free energy, the surface energy is negative. The precise critical value of κ where the surface energy becomes positive from negative is at $\kappa = 1/\sqrt{2}$. The system with $\kappa < 1/\sqrt{2}$ is called the type I superconductor, while $\kappa > 1/\sqrt{2}$ is called the type II superconductor.

The consideration of the surface energy of the boundary between the normal state system and the superconducting system is crucial to understand the property of the superconductor under the application of the magnetic field. For type I superconductors, because of the Meissner effect, the magnetic field B cannot penetrate into the superconductor up to the critical field H_c. H_c satisfies the equation $H_c^2/8\pi = f_n(T) - f_s(T)$ where $f_n(T)$ and $f_s(T)$ is the normal state and the superconducting Helmholtz free energy density at temperature T, respectively. The schematic phase diagram is shown in Fig. 1.1(a). The situation is qualitatively different for type II superconductor. In this case, the magnetic field does not penetrate into the superconductor up to the lower critical field $H_{c1}(T)$, and for the magnetic field $H_{c1}(T) < H < H_{c2}(T)$, the magnetic field penetrates

into the system in the form of the thin flux lines. This phase is called the mixed phase. The thin flux line, called the vortex, has the following property: Each vortex contains the quantized flux $\Phi = h/(2e)$, and the core of the vortex is in the normal state with vanishing superconducting gap, $\Delta = 0$. The characteristic length of the variation of the magnetic flux and the normal core is again λ and ξ, i.e., the magnetic field penetrates into the superconductor up to the length λ, and the size of the normal core is determined by ξ. Since each vortex hosts the boundary between the normal and the superconducting state, for type II system where the surface energy is negative, the state where the vortices penetrate into the system is favored. The schematic phase diagram of type II superconductors is shown in Fig. 1.1(b). In particular, for the superconducting thin films, the effective London penetration depth λ is very large if the film thickness d is sufficiently small, i.e., if $d \ll \lambda$, so that thin film superconductors are type II superconductors with very small H_{c1} [2].

At low temperature, the vortices should be treated quantum mechanically, so the particle statistics of the vortices plays a crucial role. In Refs. [3–5], it was pointed out that the vortices behave as bosons. They also noted that the cooper pairs are bosons too, and there are two equivalent descriptions of the superconductor as the system of cooper pairs and the one of vortices. The transformation which relates these two theories is called "particle-vortex duality". Now, the possible low temperature phases of the vortices inside the superconductors can be stated as follows: When the vortices bose condenses, the superconductivity is destroyed and the system becomes an insulator, while when the cooper pairs bose condenses, the system remains to be a superconductor.

In Ref. [6], the interesting theoretical argument was given: When we tune a parameter, the system changes from the superconducting state to the insulating state through the superconductor-insulator transition point. In the superconducting state, the cooper pairs condense and the vortices and the antivortices are bound to pairs. In the insulating state, the vortices condense and the cooper pairs, which are charged objects, are immobile. At the transition point, neither the cooper pairs nor the vortices are condensed. The authors of Ref. [6] further assumed that, at the transition point, two descriptions are equivalent as a bosonic system, i.e., the system is *self-dual* at the transition point. The important consequence of this self-duality is the universal value of the resistance at the transition point. To understand this universal resistance, here we review the relationship between the motion of the vortex and the resistance of the system [7].

We consider the two dimensional sample with open boundary as is shown in Fig. 1.2. At $t = 0$, the vortex penetrates into the system from the left boundary $x = 0$, and it moves across the sample from left to right and reaches the right boundary $x = L$ at $t = T$. We assume that originally the superconducting phase difference along y direction, $\varphi_2 - \varphi_1$, is 0. At $t = T$, because of the branch cut emanating from the vortex, $\varphi_2 - \varphi_1 = 2\pi$. Now we use the Josephson relation (1.1):

$$\hbar\dot{\varphi} = 2eV_y \Leftrightarrow V_y = \frac{\hbar}{2e}\frac{2\pi}{T} = \frac{\hbar}{2e}2\pi\dot{n}_v, \tag{1.2}$$

where $\dot{n}_v$ is the flux of vortices and V_y is the voltage drop along y direction. Here, the supercurrent along the y direction is given as $I_y = (2e)\dot{n}_c$, where $\dot{n}_c$ is the flux of cooper

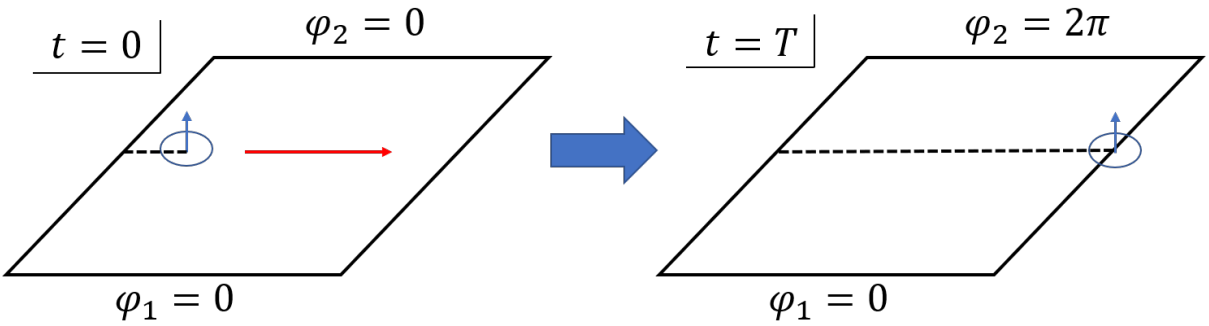

Figure 1.2: The motion of the vortex and the time evolution of the phase difference across the sample. The dashed line represents the branch cut, and the blue arrow with circle represents the vortex.

pairs. Then, the resistance is given as,

$$R = \frac{V_y}{I_y} = \frac{h}{(2e)^2}\frac{\dot{n}_v}{\dot{n}_c}. \tag{1.3}$$

Now, if the system is self-dual, we can set $\dot{n}_v = \dot{n}_c$ to get the universal resistance,

$$R = R_q = \frac{h}{(2e)^2}. \tag{1.4}$$

Early experimental study [8] supported this theoretical proposal of the self duality and the universal resistance at the transition point. As we can see from the experimental measurement of the resistance as a function of temperature shown in Fig. 1.3, as we tune the thickness of the thin film of Bismuth, the system evolves from the superconducting state to the insulator state. Here, the superconducting state is defined as the state where the resistance monotonically decreases as $T \to 0$, and the insulating state is the one where the resistance monotonically increases as $T \to 0$. We can see that these two states are separated by the single transition point where the resistance approaches constant as $T \to 0$, and, importantly, its value is very close to the universal value $R \sim R_q$.

It turned out that this was not the end of the story. As more and more experimental studies have been conducted on the highly crystalline thin film superconductors [10], it turned out that many samples do not show this behavior [11]. Rather than that, the superconducting state and the insulating state is intervened by the metallic *phase* rather than the metallic transition *point*. For example, Fig. 1.4 shows the experimentally obtained superconductor-insulator transition of the thin film of ZrNCl as we apply the magnetic field. As we can see, there is a broad range of the magnetic field where the resistance approaches constant as $T \to 0$. Therefore, the simple self-duality scenario proposed in Ref. [6] does not apply to this system. This metallic phase is known as "failed superconductor" [11].

Theoretically interesting question is the possibility of the metallic phase of bosons at $T = 0$, also known as "bose metal". In the clean system at $T = 0$, usually only two

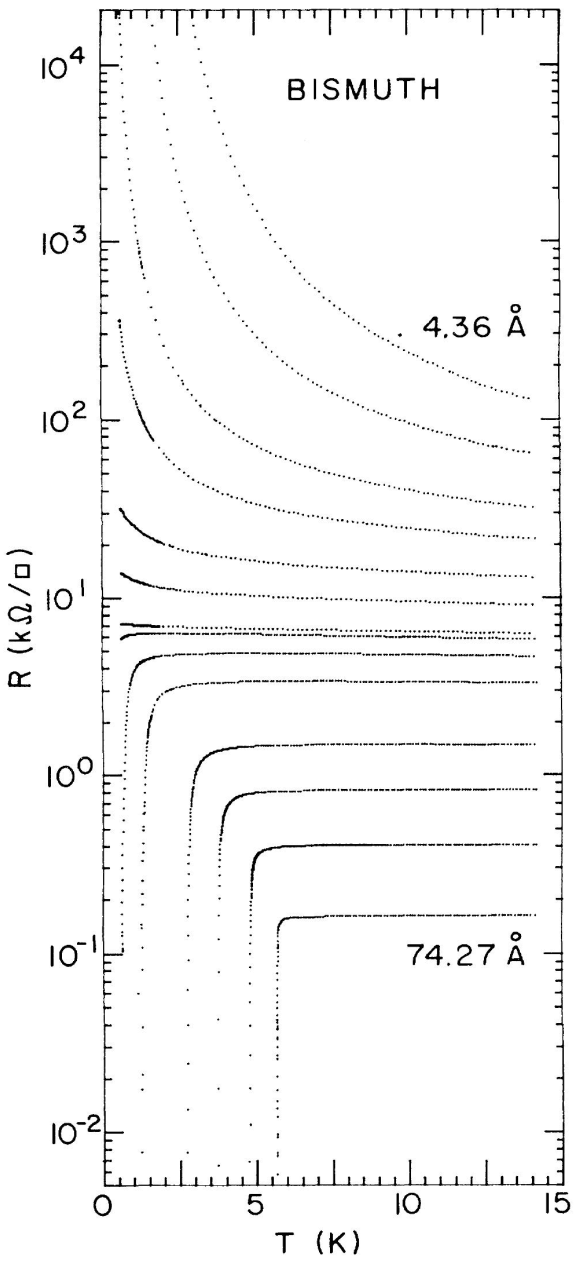

Figure 1.3: The superconductor-insulator transition with the single transition point where the resistance at the transition point is close to the universal resistance $R_q = h/(2e)^2 \sim 6.45\,k\Omega$. The transport experiment is conducted for the thin film of Bismuth, and the number in the figure indicates the thickness of the film. Reproduced with permission from [8].

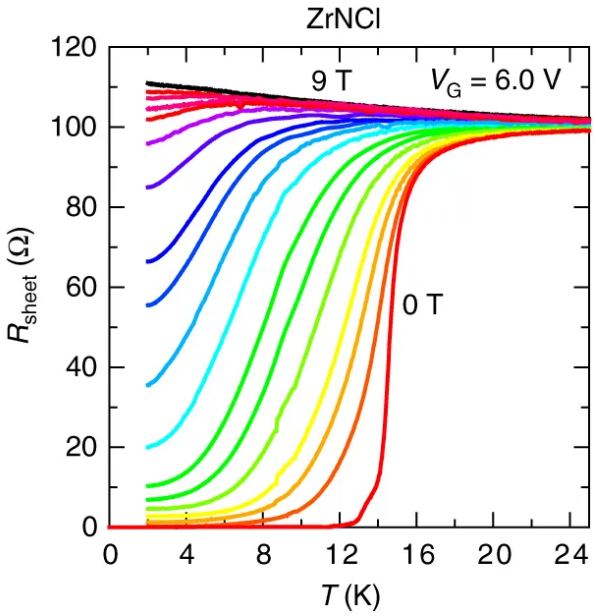

Figure 1.4: The superconductor-insulator transition in the thin film of ZrNCl. As we can see, the two phases are separated by the metallic phase, where the resistance changes in a continuous manner, rather than the transition point. The number in the figure represents the magnetic field applied perpendicularly to the system. Reproduced with permission from [9].

possibilities of the thermodynamic phase of bosons are considered: The superfluid and the insulator. In both cases, the resistance cannot be finite: it is either zero or infinity. We know the two descriptions of the superconducting system from the cooper pair picture and the vortex picture, but both of them are the bosonic systems, so that it is difficult to explain the finite resiatance observed in experiments. The theoretical understanding of this failed superconductor remains unsettled.

Another important feature of the superconducting van der Waals materials is the effect of the spatial symmetry breaking coming from the underlying crystal structure. In particular, for the inversion asymmetric materials such as MoS_2, the system exhibits the nonreciprocal response, which is defined as the following response property:

$$I(V) \neq -I(-V), \tag{1.5}$$

where V is the externally applied voltage, and I is the current response. The nonreciprocity measured in the experiment on 2H stacking of van der Waals crystal MoS_2 is shown in Fig. 1.5**F**. The nonreciprocity of this material is quantified by γ, which is defined by

$$R = V/I = R_0(1 + \gamma BI), \tag{1.6}$$

where B is the out-of-plane magnetic field, and R_0 is the resistance in the absence of B. As we can see, the nonreciprocity is enhanced for $T \lesssim 10$K where the system becomes superconductor. The large value of γ for the temperature region near the mean-field

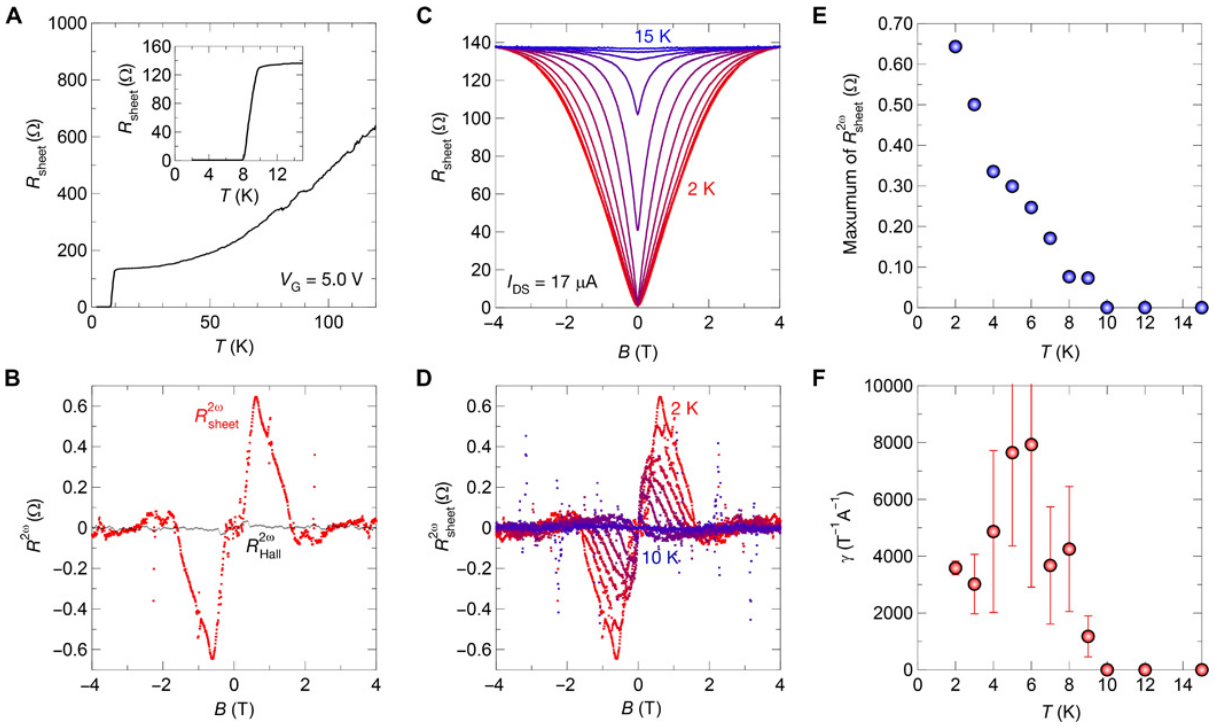

Figure 1.5: The second harmonic generation signal from 2H stacking of the two dimensional van der Waals crystal MoS_2 in the superconducting phase with the top ionic gate. Although the 2H stacking of MoS_2 is inversion symmetric, the top gate leads to the finite displacement field along the out-of-plane direction and breaks the inversion symmetry. The panel **A** shows the superconducting transition near $T \sim 8\,\mathrm{K}$. $R^{2\omega}_{\mathrm{sheet}}$, which is 2ω component of the sheet resistance against the applied bias voltage V^{ω}, as a function of the out-of-plane magnetic field B is shown in the panel **B**. The panel **C** shows the magnetoresistance for various temperature. The panel **D** shows the temperature dependence of the nonreciprocal signal $R^{2\omega}_{\mathrm{sheet}}$. The panel **E** shows the temperature dependence of the maximum value of $R^{2\omega}_{\mathrm{sheet}}$ as a function of B. If we fit the resistance by the formula $R = R_0(1 + \gamma BI)$, γ quantifies the nonreciprocity intrinsic to the material. γ obtained by the fitting to the experimentally measured $R^{2\omega}_{\mathrm{sheet}}$ as a function of the temperature T is shown in the panel **F**. We can see that γ is strongly enhanced in the superconducting phase. Reproduced with permission from [12].

transition temperature $|T - T_c|/T_c \lesssim 1$ can be understood as the consequence of the superconducting fluctuation current [12]. As we can see from Fig. 1.5**F**, in addition to the enhancement of γ in the region where the fluctuation is large, the value of γ remains to be large down to T lower than T_c. In this region, the superconductivity is fully developed and the fluctuation of the order parameter is small. Because of the finite magnetic field perpendicular to the sample, the resistance in this region is presumably caused by the motion of unpinned vortices. As is discussed in Ref. [13], the large nonreciprocity in this region can be understood as the consequence of the classical ratchet effect of the vortices from the inversion asymmetric crystal potential.

The natural question to ask is the nonreciprocal nature of the vortex dynamics for much lower temperature $T \to 0$ where the quantum effect is significant. As we can see from Fig. 1.5**F**, γ value exhibits the peak structure at the intermediate temperature scale $T \sim 5\,\mathrm{K}$, and starts to decrease towards the zero temperature where the quantum effect is not negligible. The theoretical challenge here is to show that, as is indicated by this experimental data, the quantum effect suppresses the nonreciprocity. Theoretically, the quantum effect is important already for the single particle dynamics, where the quantum dissipation leads to the nontrivial scaling theory of the quantum ratchet [14]. Even more important quantum effect is the particle statistics: As we have already discussed, since the vortices are bosons [3–5], at zero temperature without the lattice potential or disorder, the vortices exhibit superfluidity and the resistance becomes infinite. However, just as ZrNCl sample shown in Fig. 1.4, at low temperature, the resistance under the application of the magnetic field B is finite also for MoS_2, as is shown in Fig. 1.5**C**. Therefore, this MoS_2 sample at low temperature is also in the failed superconductor phase. To understand the nonreciprocal nature of the two dimensional highly crystalline superconductors at very low temperature, we first need to understand the nature of the failed superconductor phase. In particular, we need to understand why the vortices, which are bosons, do not condense at very low temperature. We will answer this question in Chapter 2, where we will show that the dissipation acting on the vortices suppresses the superfluidity.

In addition to the nonreciprocity caused by the dynamics of the vortices, we will consider the nonreciprocity caused by the dynamics of the superconducting phase variable. In contrast to the highly crystalline superconductors with failed superconductor phase, early experiments conducted on the dirty superconducting thin films reported the single transition point between the superconducting and the insulating states [8]. To understand this behavior, the model where the puddles of superconducting islands are connected by the resistive shunt, the resistively shunted Josephson junctions, was proposed [15, 16]. This model exhibits the superconductor-insulator transition as a function of the normal state resistance, and is consistent with the experiments with the single transition point, although the model is not suitable for the clean superconductors with the failed superconducting phase. If the system is inversion asymmetric, we can have a nonreciprocal response in these dirty superconducting thin films.

In Chapter 3, as a first step to understand the nonreciprocity in this resistively shunted Josephson junction model, we will consider a much simplified model, where the two superconducting islands are connected by the resistive shunt, i.e., the single Josephson junction. As we will discuss, by introducing the inversion asymmetry through the quantum capacitance, $I - V$ curve of the system exhibits the nonreciprocity. Moreover, we will show that this nonreciprocity can be detected by the 2ω component measurement for the experimentally realizable Josephson junctions. Our result is not only important to understand the nonreciprocity in the granular superconductor described by the resistively shunted Josephson junction model, but also is an important step towards the realization of the Josephson diode consisting of the single Josephson junction.

Chapter 2

Suppression of superfluidity by dissipation — An application to failed superconductor

2.1 Background

In this chapter, we will discuss the suppression of superfluidity of bosons by dissipation and its application to the understanding of failed superconductors. As we argued in Chapter 1, the theoretical difficulty of failed superconductors lies in the fact that the vortices are bosons, which usually condenses at very low temperature and leads to the diverging resistance, which contradicts the finite resistance.

We believe that, what is crucial here is the fact that the vortex is not really a pure bosonic excitation, and it is a composite object. In particular, vortex is always associated with the normal core with the low energy excitation [17, 18], which leads to the dissipation to the motion of the vortex known as "mutual friction" [18, 19]. The nature of this dissipation depends on the amount of the disorder of the system.

In the superconducting phase, according to the disorder strength, the system can be classified into three regimes: (I) dirty regime, where $\Delta \ll \hbar/\tau$, (II) moderately clean regime, where $\Delta^2/\epsilon_F \ll \hbar/\tau \ll \Delta$, and (III) superclean regime, where $\hbar/\tau \ll \Delta^2/\epsilon_F$ [20]. Here Δ and τ represent the superconducting gap and the relaxation time, respectively. When the energy scale of the disorder $\hbar/\tau$ is comparable to or larger than the superconducting gap Δ, i.e., in the dirty regime (I), the scattering length l is comparable to or smaller than the coherence length ξ which characterizes the size of the normal core of the vortex[1] [20], and the disorder potential strongly affects the motion of the vortices. As for the systems where $\hbar/\tau$ is smaller than Δ, i.e., the regime (II) and (III), in the presence of the vortex, there is another characteristic energy scale $\delta\epsilon = \Delta^2/\epsilon_F$ which is much smaller than Δ: As is shown in Fig. 2.1, the energy spectrum in the presence of the vortex has a low energy bound states in the superconducting gap, and its energy difference is given

[1]The coherence length ξ for the clean superconductor is, up to the numerical factor, $\xi \propto \hbar v_F/\Delta$, and ξ for the dirty superconductor is $\xi \propto \sqrt{\hbar v_F l/\Delta}$, so that, noting that $l = v_F\tau$, the condition $\hbar/\tau \gg \Delta$ and $\hbar/\tau \ll \Delta$ is equivalent to the condition $\xi \gg l$ and $\xi \ll l$, respectively [20].

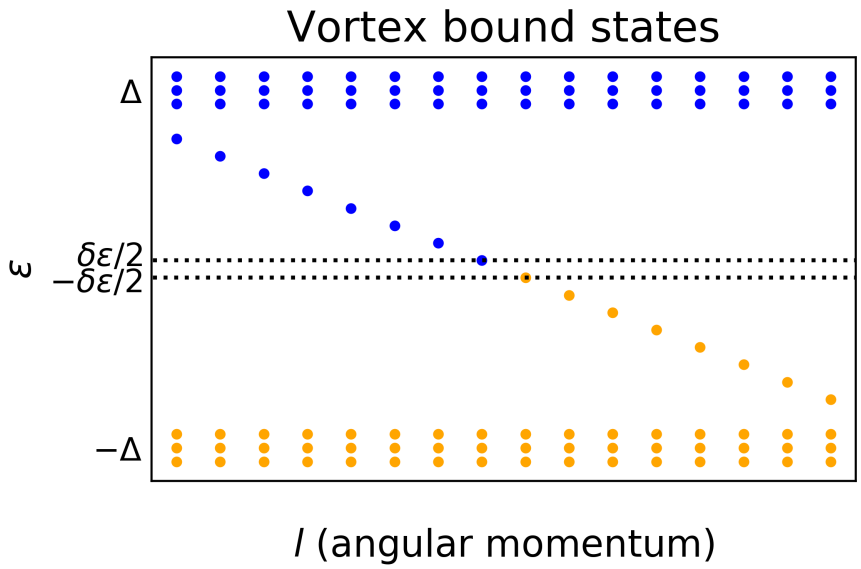

Figure 2.1: The energy spectrum of the system in the presence of the single vortex [17, 18, 20]. The linear spectrum with the energy difference $\delta\epsilon \sim \frac{\Delta^2}{\epsilon_F}$ extends over the whole range of the superconducting gap from $\epsilon = -\Delta$ to $\epsilon = \Delta$. The orange and blue dots represent the filled and empty energy levels, respectively.

by $\delta\epsilon = \Delta^2/\epsilon_F$ [17, 18, 20]. If $\hbar/\tau$ is larger than $\delta\epsilon = \Delta^2/\epsilon_F$, because of the energy broadening, the bound states energy spectrum can be regarded as continuous, and the vortex dissipates its energy into these states. This regime, where the motion of the vortex is dissipative, is called the moderately clean regime (II). If $\hbar/\tau$ is smaller than Δ^2/ϵ_F, the energy broadening is so small that the bound states spectrum should be regarded as discrete, and the vortex cannot dissipate its energy. This regime is called the superclean regime (III).

The important difference between the thin film sample of Bismuth (Fig. 1.3) and ZrNCl (Fig. 1.4) is the strength of disorder, which is characterized by the dimensionless quantity $k_F l$, where k_F is the Fermi wavenumber, or, equivalently, the quantity $\epsilon_F\tau/\hbar \sim k_F l/2$, where ϵ_F is the Fermi energy. This quantity characterizes the disorder strength in the normal state, and it can be read off from the resistivity at the normal state. In two dimensional systems, the Boltzmann theory gives the relation between the resistance and $k_F l$:

$$R_{\rm 2D} = \frac{h}{e^2}(k_F l)^{-1} \sim 26(k_F l)^{-1}\,[\mathrm{k}\Omega]. \tag{2.1}$$

From the residual resistance at the normal state around the transition point of Bismuth shown in Fig. 1.3, we can estimate $k_F l \sim 3.7$ and $\epsilon_F\tau/\hbar \sim 1.9$. As for ZrNCl sample shown in Fig. 1.3, we can estimate $k_F l \sim 260$ and $\epsilon_F\tau/\hbar \sim 130$. Since $\epsilon_F \gg \Delta$, the thin film sample of Bismuth, where $\epsilon_F\tau/\hbar \sim 1.9$, shown in Fig. 1.3, is in the dirty regime. As for ZrNCl sample shown in Fig. 1.3, since $\epsilon_F \sim 100\,\mathrm{meV}$ [21] and $\Delta(T = 0) \sim$

$1.764 k_B T_C \sim 2.2\,\mathrm{meV}$,

$$\frac{\Delta\tau}{\hbar} = \frac{\epsilon_F \tau}{\hbar}\frac{\Delta}{\epsilon_F} \sim 130 \times \frac{2.2}{100} \sim 2.9. \tag{2.2}$$

Therefore, ZrNCl sample is in the clean regime. Also,

$$\frac{\Delta^2}{\epsilon_F}\frac{\tau}{\hbar} = \frac{\epsilon_F \tau}{\hbar}\left(\frac{\Delta}{\epsilon_F}\right)^2 \sim 130 \times \left(\frac{2.2}{100}\right)^2 \sim 0.063, \tag{2.3}$$

so ZrNCl sample is in the moderately clean regime. Therefore, although the disorder strength of ZrNCl sample is weak compared to that of Bismuth sample, the disorder strength is still large, so that the motion of the vortices is dissipative.

Another important thing is that the application of the magnetic field is equivalent to the doping of the vortices into the superconductors, so we expect that the density of vortices increases continuously as we apply the magnetic field. As we noted earlier, the motion of the vortex causes the voltage drop, so, as the density of the vortex increases, we expect that the resistance also increases continuously.

Now the problem is whether or not the system of vortices can host the thermodynamic phase which is neither insulator nor superfluid, at $T = 0$, in the presence of the dissipation. Before we move on to answer this question, we will first discuss why the superfluidity is a rule rather than an exception at $T = 0$ in bosonic system without the periodic potential or the disorder. Here the Galilean invariance plays a crucial role [22–25]. The superfluidity is characterized by the order parameter ρ_s, which is defined as the free energy difference of the system when we twist the phase of the wavefunction θ at the system boundary [26, 27]:

$$\Delta f \coloneqq f(\Delta\theta) - f(0) = \frac{1}{2}\rho_s \left(\frac{\Delta\theta}{L}\right)^2, \tag{2.4}$$

where $f(\Delta\theta)$ is the free energy density when we impose the boundary condition that the phase of the wavefunction should be 0 at $x = 0$ and $\Delta\theta$ at $x = L$. In its local form, the expression becomes

$$f(\theta(\vec{r})) = \frac{1}{2}\rho_s (\nabla\theta)^2. \tag{2.5}$$

When the system is in the superfluid state, the low energy effective theory is governed by the gapless Goldstone mode, which in this case is the phase of the field operator $\psi = |\psi| e^{i\theta}$. We can explicitly derive the effective action for θ [28], but it is enough for our purpose to write down the most general expression of the effective action. First, the action should be invariant under the uniform shift of the phase $\theta \to \theta + \delta\theta$. Therefore, the Lagrangian density is given as

$$\mathcal{L}(\theta(\vec{r}, t)) = \tilde{P}(\partial_t\theta, \nabla\theta), \tag{2.6}$$

where $P(\partial_t\theta, \nabla\theta)$ is the arbitrary polynomial of $\partial_t\theta$ and $\nabla\theta$. Now, we note that, under the Galilean transform

$$t \to t' \coloneqq t, \quad \vec{r} \to \vec{r'} \coloneqq \vec{r} - \vec{v}t, \quad \psi(\vec{r}, t) \to e^{im(\vec{v}\cdot\vec{r} - v^2 t/2)}\psi(\vec{r'}, t'), \tag{2.7}$$

where $\psi(\vec{r},t)$ is the bosonic annihilation operator. Then, we get

$$\theta'(\vec{r'},t') = \theta(\vec{r},t) + mv^2t/2 - m\vec{v}\cdot\vec{r}. \tag{2.8}$$

From this equation, we get the following transformation rule for $\partial_t\theta$ and $\nabla\theta$:

$$\partial_{t'}\theta' = \vec{v}\cdot\nabla'\theta' + \partial_t\theta + mv^2/2, \quad \nabla'\theta' = \nabla\theta - m\vec{v}. \tag{2.9}$$

Therefore, $\partial_t\theta$ and $\nabla\theta$ are not singlets under Galilean transformation. Since the effective action Eq. (2.6) should be invariant under the Galilean transformation, it should be the polynomial of the Galilean singlet. Using Eq. (2.9), we can easily verify that the combination $\partial_t\theta + (\nabla\theta)^2/(2m)$ is a Galilean singlet:

$$\partial_{t'}\theta' + \frac{1}{2m}(\nabla'\theta')^2 = \vec{v}\cdot(\nabla\theta - m\vec{v}) + \partial_t\theta + mv^2/2 + \frac{1}{2m}(\nabla\theta - m\vec{v})^2 = \partial_t\theta + \frac{1}{2m}(\nabla\theta)^2. \tag{2.10}$$

Therefore, $\mathcal{L}$ should be the polynomial of this combination, and we get the following effective action:

$$\begin{aligned}\mathcal{L}(\theta(\vec{r},t)) &= P\left(\partial_t\theta + \frac{1}{2m}(\nabla\theta)^2\right) \\ &= P(0) + P'(0)\left[\partial_t\theta + \frac{1}{2m}(\nabla\theta)^2\right] + \frac{P''(0)}{2}(\partial_t\theta)^2 + \mathcal{O}((\partial_t\theta)^3, (\nabla\theta)^3).\end{aligned} \tag{2.11}$$

Now, if we set $\theta = -\mu t$ [29], we get the ground state pressure density p:

$$p = \mathcal{L}(-\mu t) = P(0) - P'(0)\mu, \tag{2.12}$$

and using the thermodynamic relation $n = \partial p/\partial\mu$ where n is the particle density, we get

$$P'(0) = -n, \tag{2.13}$$

so that, from Eq. (2.11),

$$\mathcal{L}(\theta(\vec{r},t)) = P(0) - n\left[\partial_t\theta + \frac{1}{2m}(\nabla\theta)^2\right] + \frac{P''(0)}{2}(\partial_t\theta)^2 + \mathcal{O}((\partial_t\theta)^3, (\nabla\theta)^3). \tag{2.14}$$

Then, comparing to the definition of the superfluid density, Eq. (2.5), we get

$$n = \rho_s. \tag{2.15}$$

Therefore the system is always in the superfluid phase, where $\rho_s > 0$, in the presence of Galilean invariance. We note that the superfluid density ρ_s and the condensate fraction n_0 are different quantities, and, although for the system with Galilean invariance at $T = 0$, $\rho_s = n$ holds, the condensate fraction n_0 is depleted in the presence of the interaction and $n_0 \neq n$.

At finite temperature, from the fluctuation-dissipation relationship

$$G_K(\omega,k) = \coth\left[\frac{\beta(\omega-\mu)}{2}\right](G_R(\omega,k) - G_A(\omega,k)), \tag{2.16}$$

where $G_{K,R,A}$ are the Keldysh, retarded and advanced Green functions respectively, the Galilean invariance is broken. To see this, we note that, under the Galilean transform $t \to t$, $x \to x - vt$, $\psi(x,t) \to e^{im(vx-v^2t/2)}\psi(x-vt,t)$, the Green functions transform as $G_{K,R,A}(\omega,k) \to G_{K,R,A}(\omega - vk + mv^2/2, k-mv)$[2], so the fluctuation-dissipation relationship is inconsistent with the Galilean invariance. Therefore, at finite temperature $\rho_s \neq \rho$, in accordance to the Landau's famous expression of ρ_s in terms of the thermal distribution of the quasiparticle [30].

The Galilean invariance at $T = 0$ is explicitly broken if we introduce the lattice potential or the disorder, leading to the Mott insulator [31] or the Bose glass [32–34]. Another possible source of the loss of the Galilean invariance is the nonlocal interaction along the time-direction which arises after we integrate out the gapless degrees of freedom. This depletion of superfluid component due to retarded interaction has been studied in Ref. [35], where the gapless degrees of freedom is the gauge field which mediates the interaction between vortices. In our case, it is broken by the gapless states inside the vortex, which leads to the nonlocal interaction in time when we integrate them out to get the effective action for vortices. Therefore, we expect the suppression of superfluidity by dissipation because of the explicit Galilean symmetry breaking for vortices inside the superconductor at $T = 0$.

An appropriate framework to treat the dissipation in the quantum regime is formulated by Caldeira and Leggett [36]. In this model, we couple the particle with the heat bath, and integrate them out to get the action which is nonlocal in time. We can naturally generalize their treatment for single particle system to many particle system in the first quantized formulation, as we will discuss later (see Eq. (2.31)).

Now we need the way to identify the superfluidity in the first quantized formulation. This problem was addressed by Feynman in his insightful paper [37, 38]. He not only analytically addressed the problem and revealed the essence of the superfluidity, but also laid the foundation of the later developed path integral Monte Carlo method [39, 40]. In short, the superfluidity in the first quantized picture is characterized by the exchange events with very large size [37, 38]. The partition function for the interacting bosonic system can be written as,

$$Z = \sum_{\sigma} \int \prod_i d\vec{r}_{i0} \int_{\{\vec{r}_i(\tau=0)\}=\{\vec{r}_{i0}\}}^{\{\vec{r}_i(\tau=\beta)\}=\{\vec{r}_{\sigma(i)0}\}} \prod_i D\vec{r}_i(\tau) \exp\left[-\int_0^\beta d\tau \left(\sum_i \frac{m}{2} \dot{\vec{r}}_i^2 + \sum_{i>j} V_{i,j} \right) \right], \tag{2.17}$$

where β is the inverse temperature, i is the labeling of the particles, m is the mass of the particle, $V_{i,j}$ is the interaction energy of the particles i and j. Also, σ represents the permutation of the particle number i, and the particles at $\tau = 0$ and the particles at $\tau = \beta$ can exchange their positions. This summation over the permutation is an important property of the quantum system, and for the system of fermions, for odd permutation the weight is multiplied by -1. This negative weight leads to the very slow convergence of the physical quantities well-known as the sign problem, but for bosonic particles the weight is always positive, and we do not suffer from it.

[2]This follows from $G(\omega,k) = \int dxdt e^{i(kx-\omega t)} G(x,t) \to \int dxdt e^{i((k-mv)x-(\omega-vk+mv^2/2)t)} G(x,t) = G(\omega - vk + mv^2/2, k-mv)$. We assumed the spatial and time translation invariance.

Now, the effect of the interaction is twofold. First, it renormalizes the mass of the particles. Secondly, it forces the particles to remain far apart from each other. Then we can approximate the positions of the particles at $\tau = 0$ to be some lattice, say the cubic lattice[3]. If the temperature is not too low, the particles cannot wander from $\{\vec{r}_{i0}\}$ at $\tau = 0$ to the position far apart at $\tau = \beta$. Then, the important configuration is the one where the particles exchange their positions from some vertex of the lattice at $\tau = 0$ to the next nearest vertex of the lattice at $\tau = \beta$. Here, the action of this exchange event can be approximated as,

$$y(d) = \exp\left[-\frac{m^* d^2}{2\beta\hbar^2}\right], \tag{2.18}$$

where d is the interparticle distance and m^* is the effective mass of the particle. Now, we can regard this problem as the statistical problem of the polygons on the lattice. The weight of each line of the polygons on the edge of the lattice is given by (2.18). Then, the above action can be approximated as

$$Z = \sum_L y(d)^L g(L), \tag{2.19}$$

where L represents the length of the polygon, and we represented the number of configurations of the polygon with size L on the lattice as $g(L)$. One way to roughly estimate the scaling form of $g(L)$ is as follows: We need to count the number of closed loops with the length L on the lattice. The total number of the string both open and closed with size L starting from some position is given by z^L, where z is the number of adjacent vertex on the lattice. For example, $z = 6$ for the cubic lattice, $z = 4$ for square lattice, $z = 3$ for honeycomb lattice, etc.. Now, to count the number of the *closed loops*, we regard this problem as the random walk on the lattice. The probability distribution $P(\vec{r}, t)$ of the random walk problem at position $\vec{r}$ and time t starting from $\vec{r} = 0$ at $t = 0$ is given as

$$P(\vec{r}, t) \propto t^{-d/2} \exp\left[-\frac{\vec{r}^2}{2Dt}\right], \tag{2.20}$$

where d is the dimensionality of the system. Then, the probability of the particle to come back to $\vec{r} = 0$ at time $t = L$ is $P(0, L) = L^{-d/2}$. Then, we get an estimation of the number of closed loops:

$$g(L) \propto z^L P(0, L) \propto \exp\left[L \ln z - \frac{d}{2} \ln L\right]. \tag{2.21}$$

Therefore, the partition function given by Eq. (2.19) can be written as,

$$Z \propto \sum_L \exp\left[L(\ln z - \ln y^{-1}) - \frac{d}{2} \ln L\right]. \tag{2.22}$$

Now, as we can see from Eq. (2.18), as we lower the temperature, y^{-1} monotonically increases. At $y^{-1} = z$, we can see that the configuration with diverging L has exponentially larger weight, i.e., the very large exchange events proliferate. This transition is

[3]This assumption is just for the illustrative purpose, following the analytical estimation by Feynman [38]. In the quantum Monte Carlo calculation, we will not assume any lattice order.

nothing but the superfluid transition. Therefore, to detect the superfluidity in the first quantized picture, we should look at the statistical weight of the large exchange event. More quantitatively, we can calculate the superfluid weight from the following winding number formula [39, 40]:

$$\frac{\rho_s}{\rho} = \frac{\frac{1}{N}L^2\langle \vec{W}^2 \rangle}{2d\beta\frac{\hbar^2}{2m}}, \tag{2.23}$$

where N is the number of particles, L is the linear size of the system. Here, $\vec{W}$ is the winding number vector and is defined as

$$\vec{W} = \sum_i^N \frac{\vec{r}_i(\beta) - \vec{r}_i(0)}{L}. \tag{2.24}$$

We will utilize this winding number formula to calculate the superfluid weight in the quantum Monte Carlo calculation.

We will also discuss the complementary field theoretical model formulated in the second quantized language. In this case, the superfluid density can be calculated from the transverse current-current correlation function. To see this concretely [41–43], we note that the paramagnetic current correlation function in the isotropic system can be decomposed as the sum of the longitudinal and the transverse component:

$$K_{ij}^{para}(\vec{k}) = \Pi^{\perp}(k)\left(\delta_{ij} - \frac{k_i k_j}{k^2}\right) + \Pi^{\parallel}(k)\frac{k_i k_j}{k^2} = \Pi^{\perp}(k)\delta_{ij} + \left(\Pi^{\parallel}(k) - \Pi^{\perp}(k)\right)\frac{k_i k_j}{k^2}, \tag{2.25}$$

In the normal phase, the correlation function in the real space is short-ranged. Therefore, the correlation function in momentum space, Eq. (2.25), exhibits no singularity near $k = 0$, so that the second term in Eq. (2.25) vanishes in the limit $k \to 0$, i.e.,

$$\Pi^{\perp}(k = 0) = \Pi^{\parallel}(k = 0) \quad \text{in the normal phase.} \tag{2.26}$$

When the system exhibits the superfluidity, because of the long-ranged nature of the correlation function in real space, the correlation function in momentum space exhibits the nonanalytic behavior near $k = 0$, i.e., the longitudinal and the transverse correlation function as $k \to 0$ is different:

$$\Pi^{\perp}(k = 0) \neq \Pi^{\parallel}(k = 0) \quad \text{in the superfluid phase,} \tag{2.27}$$

in sharp contrast to the normal state.

Now, the full response function can be calculated by adding the paramagnetic term, Eq. (2.25), to the diamagnetic term, which is given by

$$K_{ij}^{dia} = -\frac{\rho}{m}\delta_{ij} = -\frac{\rho}{m}\left(\delta_{ij} - \frac{k_i k_j}{k^2}\right) - \frac{\rho}{m}\frac{k_i k_j}{k^2}, \tag{2.28}$$

i.e.,

$$K_{ij}^{resp} = K_{ij}^{para} + K_{ij}^{dia} = \left(\Pi^{\perp} - \frac{\rho}{m}\right)\left(\delta_{ij} - \frac{k_i k_j}{k^2}\right) + \left(\Pi^{\parallel} - \frac{\rho}{m}\right)\frac{k_i k_j}{k^2} \tag{2.29}$$

Here, the gauge invariance imposes the condition that the full response function as $k \to 0$ be purely transverse, i.e., $\Pi^{\parallel}(k=0) = \rho/m$. Then, in the normal state, because of Eq. (2.26) $\Pi^{\perp}(k=0) = \Pi^{\parallel}(k=0) = \rho/m$ so that $K_{ij}^{resp}(k \to 0) = 0$. In contrast, in the superfluid state, because of Eq. (2.27), $\Pi^{\perp}(k=0) = \rho_n/m \neq \Pi^{\parallel}(k=0) = \rho/m$ where we defined the normal density ρ_n as the $k \to 0$ limit of $m\Pi^{\perp}(k)$, and from Eq. (2.29), we get, as $k \to 0$,

$$K_{ij}^{resp} = K_{ij}^{para} + K_{ij}^{dia} = -\frac{\rho_s}{m}\left(\delta_{ij} - \frac{k_i k_j}{k^2}\right), \quad \rho_s \coloneqq \rho - \rho_n. \tag{2.30}$$

Noting that $J_i = K_{ij}^{resp} A_j = -(\rho_s/m) A_i^T$, where A_j is the gauge potential and A_i^T is the transverse component of A_i, Eq. (2.30) represents nothing but the London equation. The London equation in the neutral bose liquid can be interpreted as the nonclassical effect of inertia [41, 44], and is one of the defining property of the superfluidity. From the argument above, we can calculate the normal density and the superfluid density from the transverse static current-current correlation function. We will calculate it using the Bogoliubov approximation.

In the following sections, we will establish the suppression of superfluidity by dissipation in two different models, and we believe that this phenomenon is rather universal, and is important when we will discuss the low temperature phase of bosons in the presence of the gapless degrees of freedom.

Here, we note the difference of our work from the previous study. There are many papers on the dissipative XY model [45–48], describing the dynamics of the resistively shunted Josephson junction array [15, 16]. However, the XY model is an effective model of bosons only at integer fillings [32, 49]. Away from integer fillings, e.g., in the dilute limit, the action contains the first order time derivative term [50], which is complex and the Monte Carlo study in the phase representation is difficult because of the sign problem. This difference is important in the context of the positive magnetoresistance of failed superconductor, since in the dilute limit the number of vortices change continuously as we increase the magnetic field. Also, the effect of dissipation on dilute boson system has been studied in Ref. [51], but their study is only for one dimensional system. The analytical argument we will discuss here is different from their argument relying on bosonization which is valid only in one dimensional system.

2.2 Purpose and assumptions of the model

Here, we explicitly state the purpose of our work and the assumption of our model.

As we discussed, our primary purpose is to understand the physics of the failed superconductor. Theoretical challenge of the failed superconductor is the presence of the zero temperature metallic phase of bosons. Once we can establish it, the experimentally observed positive magnetoresistance can be easily understood as a consequence of the increasing density of vortices, i.e., it simply comes from the flux-flow resistivity. Therefore, we focus on the discussion of the suppression of the superfluid phase of bosons at low temperature in this work.

The assumptions of our model are, (1) we can ignore the effect of the pinning of vortices coming from the point defect, and (2) the energy of the moving vortex dissipate to the lattice through the gapless excitation inside the normal core, i.e., the system is in the moderately clean regime $\Delta^2/\epsilon_F \ll 1/\tau, k_BT$ among the three regions, i.e., the dirty regime, the moderately clean regime, and the superclean regime, as we discussed.

As for the assumption (1), since the important difference of the recent experiments on the failed superconductor [9] from the early experiments [8] is that, because of the experimental progress, many recent experiments are done for the highly crystalline superconducting thin films. Therefore, we believe this assumption is legitimate. The assumption (2) is important, and this assumption leads to the experimentally possible verification or objection to our model. Namely, since the presence of the dissipation is crucial in our discussion, if the system is super clean, i.e., $\Delta^2/\epsilon_F \gg 1/\tau, k_BT$, the excitation at the normal core is discrete and there exists no source of dissipation, so the bose metal or the failed superconductor should be gone. To see this experimentally, the experimental determination of the relaxation time τ, for example by the measurement of the residual resistivity in the normal state, is important. Once τ is fixed, we can determine whether the system is in the super clean or the moderately clean regime. Our model predicts the metallic phase for the latter, while for the former case the system behaves as predicted by the original self duality scenario, since the vortices without the dissipation are simply bosons.

2.3 Model

The phenomenological action for the system of many bosons in the presence of the dissipation is,

$$S = \int_0^\beta d\tau \left(\sum_i \frac{m}{2} \dot{\vec{r}}_i^2 + \sum_{i>j} V_{i,j} \right) + \frac{\eta}{4\pi} \sum_i \int_0^\beta d\tau \int_0^\beta d\tau' \frac{\pi^2}{\beta^2} \left(\frac{\vec{r}_i(\tau) - \vec{r}_i(\tau')}{\sin \frac{\pi}{\beta}(\tau - \tau')} \right)^2, \quad (2.31)$$

where i is the labeling of the bosons, $V_{i,j}$ is the repulsive interaction between bosons, m is the mass of the bosons, β is the inverse temperature, and the last term represents the effect of the Ohmic heat bath [52, 53]. Here, η is the viscosity coefficient of the vortex, as is introduced by Bardeen and Stephen [54]. $\eta \propto \tau$ in the moderately clean regime, and $\eta \propto \tau^{-1}$ in the superclean regime [20]. We neglected the effective interaction between the bosons induced by the coupling to the heat bath [55]. For later convenience, we transform the last term in Eq. (2.31) as follows:

$$\begin{aligned} \int_0^\beta d\tau \int_0^\beta d\tau' \frac{\pi^2}{\beta^2} \left(\frac{\vec{r}_i(\tau) - \vec{r}_i(\tau')}{\sin \frac{\pi}{\beta}(\tau - \tau')} \right)^2 &= \int_0^\beta d\tau \int_0^\beta d\tau' \frac{1}{\beta^2} \sum_{n=-\infty}^{\infty} \left(\frac{\vec{r}_i(\tau) - \vec{r}_i(\tau')}{\frac{\tau - \tau' + n\beta}{\beta}} \right)^2 \\ &= \int_0^\beta d\tau \sum_{n=-\infty}^{\infty} \int_0^\beta d\tau' \left(\frac{\vec{r}_i(\tau) - \vec{r}_i(\tau')}{\tau - \tau' + n\beta} \right)^2 \\ &= \int_0^\beta d\tau \int_{-\infty}^{\infty} d\tau' \left(\frac{\vec{r}_i(\tau) - \vec{r}_i(\tau')}{\tau - \tau'} \right)^2, \end{aligned} \quad (2.32)$$

where, in the first line we used the following identity,

$$\frac{\pi^2}{\sin^2(\pi a)} = \sum_{n=-\infty}^{\infty} \frac{1}{(n+a)^2}, \tag{2.33}$$

and in the last line we extended the range of $\vec{r}_i(\tau)$ periodically from $0 \leq \tau \leq \beta$ to $-\infty < \tau < \infty$. Therefore, the last term in Eq. (2.31) is equivalent to the form given in Ref. [52].

Here, we will derive the equation of motion for Eq. (2.31) [56]. First, using the Fourier transform

$$r_{i\alpha}(\omega_n) = \int_0^\beta d\tau r_{i\alpha}(\tau) e^{i\omega_n \tau}, \tag{2.34}$$

where ω_n is the Matsubara frequency, Eq. (2.31) can be rewritten as,

$$S = \frac{1}{\beta} \sum_{\omega_n, i, \alpha} \left[\frac{m\omega_n^2}{2} + \frac{\eta}{2}|\omega_n| \right] |r_{i\alpha}(\omega_n)|^2 + \sum_{i>j} \int_0^\beta d\tau V(\vec{r}_i(\tau) - \vec{r}_j(\tau)). \tag{2.35}$$

To derive the equation of motion in real time, we need to perform the analytic continuation in time.

As for the first term, we perform the analytic continuation in frequency space, noting that the expression in the square brackets is nothing but the inverse of the Matsubara Green function. Although the analytically continued Green function is analytic on the upper and lower half plane in complex frequency space, we have a branch cut on the real axis. This branch cut is a consequence of the continuum degrees of freedom of the heat bath. In the real time, noting that the retarded and advanced Green function can be obtained from the analytic continuation from the upper and lower half plane, respectively [29], and using the fluctuation dissipation relationship,

$$G^K(\omega) = (G^R(\omega) - G^A(\omega)) \coth \frac{\beta\omega}{2}, \tag{2.36}$$

we get

$$S_1 = \sum_{i\alpha} \int \frac{d\omega}{2\pi} \begin{pmatrix} r^{cl}_{i\alpha}(-\omega) & r^{q}_{i\alpha}(-\omega) \end{pmatrix} \begin{pmatrix} 0 & -i\eta\omega + m\omega^2 \\ i\eta\omega + m\omega^2 & 2i\eta\omega \coth \frac{\beta\omega}{2} \end{pmatrix} \begin{pmatrix} r^{cl}_{i\alpha}(\omega) \\ r^{q}_{i\alpha}(\omega) \end{pmatrix}, \tag{2.37}$$

where $r^{cl/q}(\omega) = (r^+(\omega) \pm r^-(\omega))/2$, and $r^\pm$ are the position variable on the Keldysh Contour $C^\pm$, since the Green function can be obtained from the inverse of the matrix in Eq. (2.37):

$$\begin{pmatrix} G^K(\omega) & G^R(\omega) \\ G^A(\omega) & 0 \end{pmatrix} = \frac{1}{2} \begin{pmatrix} 0 & -i\eta\omega + m\omega^2 \\ i\eta\omega + m\omega^2 & 2i\eta\omega \coth \frac{\beta\omega}{2} \end{pmatrix}^{-1} = \frac{1}{2} \begin{pmatrix} \frac{-2i\eta \coth \frac{\beta\omega}{2}}{\eta^2\omega + m^2\omega^3} & \frac{1}{i\eta\omega + m\omega^2} \\ \frac{1}{-i\eta\omega + m\omega^2} & 0 \end{pmatrix}. \tag{2.38}$$

As for the second term, we can simply modify the imaginary time integration path to the Keldysh contour $C = C_+ \cup C_- = [-\infty, \infty] \cup [\infty, -\infty]$ on the real time. Then,

$$\begin{aligned} S_2 &= -\sum_{i>j} \int_0^\infty dt \left[V(\vec{r}_i^{+}(t) - \vec{r}_j^{+}(t)) - V(\vec{r}_i^{-}(t) - \vec{r}_j^{-}(t)) \right] \\ &= -\sum_{i>j} \int_0^\infty dt \left[V\left(\bar{r}_i^{cl}(t) - \bar{r}_j^{cl}(t) + \bar{r}_i^{q}(t) - \bar{r}_j^{q}(t)\right) - V\left(\bar{r}_i^{cl}(t) - \bar{r}_j^{cl}(t) - \bar{r}_i^{q}(t) - \bar{r}_j^{q}(t)\right) \right] \\ &= -2\sum_{i>j} \int_0^\infty dt \nabla V\left(\bar{r}_i^{cl}(t) - \bar{r}_j^{cl}(t)\right) \cdot (\bar{r}_i^{q}(t) - \bar{r}_j^{q}(t)) + \mathcal{O}((r_{i\alpha}^q)^3). \end{aligned} \tag{2.39}$$

Combining Eqs. (2.37) and (2.39), we get

$$\begin{aligned} S = \int_0^\infty dt \Bigg[&\sum_{i\alpha} \left(-2r_{i\alpha}^q (m\ddot{r}_{i\alpha}^{cl} + \eta \dot{r}_{i\alpha}^{cl}) \right) - 2\sum_{i>j} \nabla V\left(\bar{r}_i^{cl}(t) - \bar{r}_j^{cl}(t)\right) \cdot (\bar{r}_i^{q}(t) - \bar{r}_j^{q}(t)) \Bigg] \\ &+ \mathcal{O}((r_{i\alpha}^q)^2). \end{aligned} \tag{2.40}$$

From Eq. (2.40), if we neglect the second or higher order terms in $r_{i\alpha}^q$ (semiclassical approximation), we get the classical equation of motion with Ohmic dissipation:

$$\frac{\delta S}{\delta r_{i\alpha}^q} = 0 \Leftrightarrow m\ddot{r}_{i\alpha}^{cl} + \eta \dot{r}_{i\alpha}^{cl} = -\sum_j \nabla_\alpha V(\bar{r}_i^{cl} - \bar{r}_j^{cl}). \tag{2.41}$$

Therefore, the action (2.31) correctly describes the bosonic system with Ohmic dissipation.

2.4 Extended Feynman's argument

Here, we argue the effect of the dissipative term from the perspective of Feynman's picture of superfluidity [37, 38]. As we argued, in the absence of the dissipation, if we assume that the effect of the repulsive interaction is simply renormalizing the mass of the bosons, the action for the macroscopic exchange process can be obtained from the single particle off-diagonal density matrix of the free particle, which is given by $y(|\boldsymbol{r} - \boldsymbol{r}'|) \propto \exp[-m(\boldsymbol{r} - \boldsymbol{r}')^2/(2\beta\hbar^2)]$, so the action is proportional to β^{-1}. Therefore, as $\beta \to \infty$, the entropy of the macroscopic exchange processes, which is constant as a function of temperature, overcomes the action for the exchange process, so the bosonic system shows superfluidity at finite temperature. As we noted, the partition function is given by $Z = \sum_L y(d)^L g(L)$, where L is the number of links between vertices of the lattice, d is the lattice constant, and $g(L)$ is the total number of the polygons with L links. Here we again note that y can be approximated by the *off-diagonal* single particle density matrix, rather than the *diagonal* one as is used for the criterion of the superfluidity in a previous literature [57], although the Lindemann type criterion may be a good *necessary* condition for the superfluidity. In other word, what determines the action for the exchange is $\langle p^2 \rangle$, the second moment of the momentum, rather than $\langle r^2 \rangle$, the second moment of the position, since the off-diagonal

density matrix represents the information of the momentum distribution through the Wigner transform as $y(|\boldsymbol{r}-\boldsymbol{r}'|) \propto \exp[-(\boldsymbol{r}-\boldsymbol{r}')^2 \langle p^2\rangle/(2\hbar^2)]$. Here y is gaussian since the Caldeira-Leggett action is quadratic, and we assume that this form remains valid even in the presence of the interaction between particles. $\langle p^2\rangle^{-1}$ and $\langle r^2\rangle$ show drastically different behavior in the presence of the dissipation: The former remains constant down to $\beta \to \infty$, while the latter diverges as $\log\beta$ [58]. The reason for finiteness of $\langle p^2\rangle^{-1}$ was clearly explained by Caldeira and Leggett [52]. To see this, as we have shown in Eq. (2.32), we transform the last term in Eq. (2.31) as

$$\frac{\eta}{4\pi}\int_{-\infty}^{\infty} d\tau' \int_0^\beta d\tau \left(\frac{\vec{r}_i(\tau)-\vec{r}_i(\tau')}{\tau-\tau'}\right)^2, \tag{2.42}$$

where the finite temperature kernel is replaced by the zero temperature kernel, but now we need to consider the interaction of the boson at $0 \le \tau \le \beta$ with the infinite family of "image lines", periodically extended from $0 \le \tau' \le \beta$ to $-\infty \le \tau' \le \infty$. When we consider the process where $\vec{r}_i(0) \neq \vec{r}_i(\beta)$, i.e., the off-diagonal component of the single particle density matrix, the integral diverges because of the discontinuity at $\tau' = 0$ and $\tau' = \beta$; this divergence is regularized by the ultraviolet cutoff of the heat bath, but this contribution to the off-diagonal density matrix coming from the discontinuity remains finite even if we take the limit $\beta \to \infty$ [4].

If we assume that the effect of the interaction can be renormalized to the effective mass of the particle, from the well known result of the quantum Brownian motion [58],

$$\langle p^2\rangle = \frac{M}{\beta} + 2M\frac{\mu_1\mu_2}{\mu_1-\mu_2}\left[\psi\left(1+\mu_1\beta\right) - \psi\left(1+\mu_2\beta\right)\right], \tag{2.43}$$

where M is the effective mass of bosons, $\psi(x)$ is the digamma function, $\mu_{1/2} = \hbar(\omega_D \pm \sqrt{\omega_D^2 - 4\gamma\omega_D})/(4\pi)$, $\gamma = \eta/M$, and ω_D is the cutoff of the spectrum of the bath. Then, since $\langle p^2\rangle$ decreases as we lower the temperature and saturates at finite value, we expect that the transition temperature, which is the temperature where the entropy of macroscopic exchange $g(L)$ and the action for the exchange y^L compete, monotonically decreases and reaches zero as we increases the coupling η. To obtain the phase boundary, we transform $\frac{\langle p^2\rangle d^2}{\hbar^2}$ as,

$$\frac{\langle p^2\rangle d^2}{\hbar^2} = \frac{1}{2}\left(\frac{d^2}{\lambda\beta}\right) + \left(\frac{d^2}{\lambda\beta}\right)\frac{(\mu_1\beta)(\mu_2\beta)}{(\mu_1\beta)-(\mu_2\beta)}[\psi(1+\mu_1\beta) - \psi(1+\mu_2\beta)], \tag{2.44}$$

where $\lambda = \hbar^2/(2M)$. Eq. (2.44) has three dimensionless parameters: $d^2/(\lambda\beta)$, $\mu_1\beta$ and $\mu_2\beta$. Since $\mu_{1/2}\beta$ is given as,

$$\mu_{1/2}\beta = \frac{1}{4\pi}\left[(\hbar\omega_D\beta) \pm \sqrt{(\hbar\omega_D\beta)^2 - 8\tilde{\eta}\left(\frac{d^2}{\lambda\beta}\right)^{-1}(\hbar\omega_D\beta)}\right], \tag{2.45}$$

where $\tilde{\eta} = \eta d^2/\hbar$, the phase boundary is determined by three dimensionless parameters:

$$\frac{d^2}{\lambda\beta}, \quad \hbar\omega_D\beta, \quad \tilde{\eta}. \tag{2.46}$$

[4] We note that there is a similar problem in the treatment of the effective mass of polaron [59, 60].

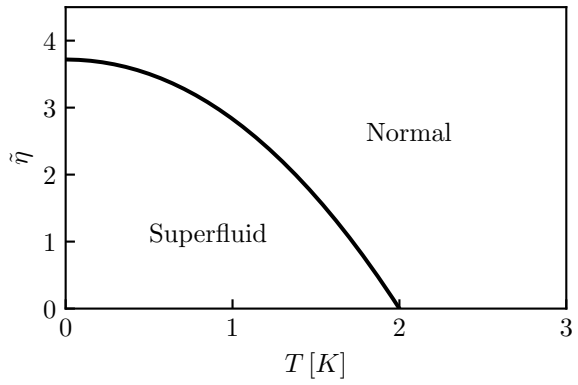

Figure 2.2: Schematic phase diagram obtained from Feynman's argument combined with the expression for the off-diagonal density matrix in the presence of the Ohmic dissipation, Eq. (2.43). $\tilde{\eta} = \eta d^2/\hbar$, where d is the interparticle distance. We set $\lambda = \hbar^2/(2M) = 6.0596\,\text{Å}^2\text{K}$, $d = 3.570\,\text{Å}$, and $\hbar\omega_D = 10\,\text{K}$. The phase boundary is calculated from the condition $\langle p^2\rangle\,(T, \tilde{\eta}) = \langle p^2\rangle\,(T = 2\,\text{K}, \tilde{\eta} = 0)$, i.e., we assumed that the transition temperature for the dissipationless system is $T = 2\,[\text{K}]$.

Now we set $\lambda = 6.0596\,\text{Å}^2\text{K}$, which is the mass parameter for ^{4}He, and $d = 3.570\,\text{Å}$ which corresponds to the particle density used in the numerical calculation for three dimensional system in section 2.5. We also set the cutoff for the bath $\hbar\omega_D = 10\,\text{K}$. The phase diagram obtained by using these parameters is shown in Fig. 2.2.

The critical η at $T = 0$ can be estimated from

$$d^2\,\langle p^2\rangle_{T=0}\,/\hbar^2 = 2Md^2\mu_1\mu_2[\ln\,(\mu_1/\mu_2)]/[\hbar^2(\mu_1 - \mu_2)] \sim 1. \tag{2.47}$$

If we further assume $\omega_D \gg \gamma$, the above condition simplifies to

$$\tilde{\eta}[\ln(\omega_D/\gamma)]/(\hbar\pi) \sim 1. \tag{2.48}$$

From Eq. (2.48), there exists the critical $\tilde{\eta} = \tilde{\eta}_c$ where the system is in the normal state for $\tilde{\eta} \geq \tilde{\eta}_c$ and in the superfluid state for $\tilde{\eta} \leq \tilde{\eta}_c$. Also, from Eq. (2.48), we can draw the schematic phase diagram of the two dimensional superconductor in $\tau^{-1}\hbar - H$ plane. As we argued, our model is applicable to the moderately clean regime where $\Delta^2/\epsilon_F \ll \hbar/\tau \ll \Delta$. Here, $n_V \propto 1/d^2 \propto H$, where n_V is the density of the vortex, d is the average distance between vortices, and H is the magnetic field perpendicular to the system. The τ dependence of η is given by [20]

$$\eta \propto \frac{\delta\epsilon\tau/\hbar}{(\delta\epsilon\tau/\hbar)^2 + 1}, \quad \left(\delta\epsilon = \frac{\Delta^2}{\epsilon_F}\right). \tag{2.49}$$

Therefore, $\eta \propto \delta\epsilon\tau/\hbar$ in the moderately clean regime where $\hbar/\tau \gg \delta\epsilon$ [54], and $\eta \propto (\delta\epsilon\tau/\hbar)^{-1}$ in the superclean regime where $\hbar/\tau \ll \delta\epsilon$. Therefore, for the moderately clean regime, ignoring the weak logarithmic dependence on η, $\tilde{\eta} = \eta d^2/\hbar \propto \tau/H$, and the vortex exhibits the superfluidity, i.e., the system is in the Bose insulator phase for

$H \geq C\tau$ and the vortex is in the normal state, i.e., the system is Bose metal for $H \leq C\tau$, where C is the constant factor independent of τ and H. The phase diagram obtained by this estimation is shown in Fig. 2.3. For the dirty regime where $\Delta \ll \hbar/\tau$, the disorder potential is strong so that the vortex introduced by H is pinned and immobile, and we can have a superconducting phase. This phase is absent for the clean regime $\hbar/\tau \leq \Delta$ where the vortex can move freely in space. In the moderately clean regime where $\hbar/\tau \gg \Delta^2/\epsilon_F$, since $\eta \propto \tau$, the metallic region enlarges as τ increases. For fixed τ in the moderately clean regime, if we increase H, there exists two critical H: The one associated with the Bose metal-Bose insulator transition, which we denote as $H_{\mathrm{BM-BI}}$, and the other one associated with the destruction of superconductivity, i.e., H_{c2}. In Fig. 2.3 (a), we assumed that $H_{c2} > H_{\mathrm{BM-BI}}$ for all $\hbar/\tau$ inside the moderately clean regime. If $H_{c2} < H_{\mathrm{BM-BI}}$ for some $\hbar/\tau$, the system should exhibit the phase transition from the Bose metal phase to the normal state without the intervening Bose insulator phase as we increase H, as is shown in Fig. 2.3 (b). To determine whether or not $H_{c2} > H_{\mathrm{BM-BI}}$ holds inside the moderately clean regime, we need to calculate $H_{\mathrm{BM-BI}}$ for τ in the moderately clean regime, and it is beyond the scope of our work. In the superclean regime where $\hbar/\tau \ll \Delta^2/\epsilon_F$, the dissipation strength becomes weak, and the Bose metal region shrinks in the phase diagram. Inside the superclean regime, we need to consider the Landau level physics of the energy spectrum, so this range is outside the scope of our work, but, because of the absence of dissipation, there cannot be Bose metal phase. For $H \geq H_{c2}$, the superconductivity is destructed so that the system is in the normal state, and we expect the finite resistance because of the applied magnetic field which counteracts the localization of electrons by disorder.

Below, we will show a strong support for this physical argument by the numerical Monte Carlo calculation of the superfluid density. This calculation confirms that the interaction between particles does not drastically affect the picture of superfluidity by Feynman even in the presence of the dissipation.

2.5 Result of the numerical calculation

We calculated the superfluid density for the boson system characterized by the action (2.31) with the worm algorithm in continuous space [61, 62] using the winding number formula [39, 40]. We implemented the canonical version [63, 64] where the Monte Carlo moves do not change the number of particles. We performed the numerical calculation for three dimensional system and two dimensional system. In both cases, we employed the Aziz potential [65] for the interaction between particles. The Aziz potential is defined

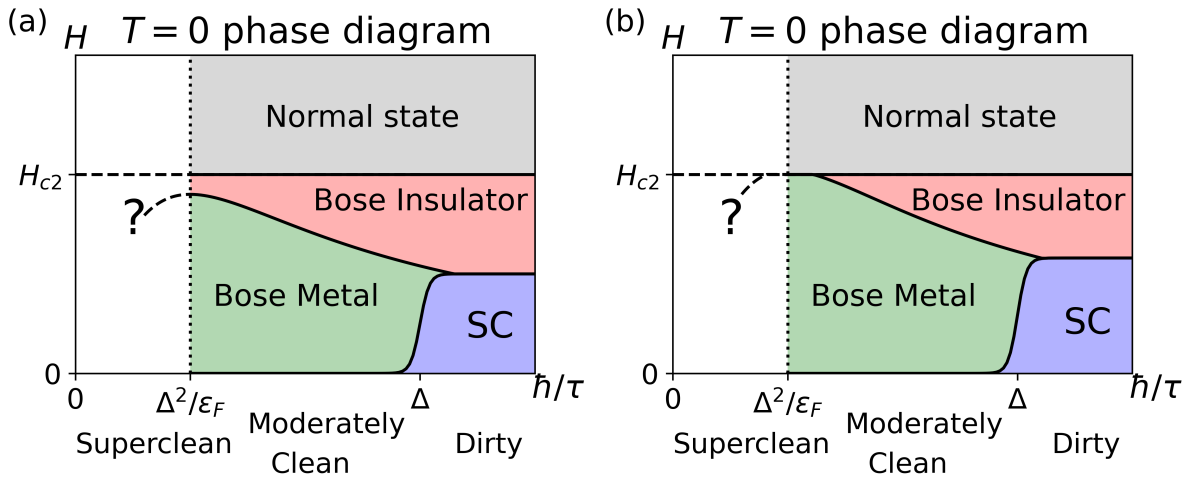

Figure 2.3: The schematic phase diagram of two dimensional superconductor in $\tau^{-1}\hbar - H$ plane for fixed superconducting coherence length ξ and H_{c2}. In (a), we assumed $H_{c2} > H_{\mathrm{BM-BI}}$ for moderately clean regime, where $H_{\mathrm{BM-BI}}$ is the critical magnetic field between the Bose metal region and the Bose insulator region. In (b), we assumed $H_{c2} < H_{\mathrm{BM-BI}}$ near $\hbar/\tau \sim \Delta^2/\epsilon_F$, and the system exhibits the direct phase transition from the Bose metal phase to the normal state near this region. It is beyond the scope of our work to determine which phase diagram is realized experimentally.

as follows:

$$V(r) = \epsilon \left[A e^{-\alpha x} - F(x) \sum_{j=0}^{2} \frac{C_{2j+6}}{x^{2j+6}} \right], \tag{2.50}$$

$$F(x) = \begin{cases} e^{-\left(\frac{D}{x}-1\right)^2} & (x < D) \\ 1 & (x > D) \end{cases}, \tag{2.51}$$

$$x = \frac{r}{r_m}, \tag{2.52}$$

where

$$\epsilon = 10.8\,\mathrm{K},\ r_m = 2.9673\,\text{Å},\ D = 1.241314,\ \alpha = 13.353384,$$
$$C_6 = 1.3732412,\ C_8 = 0.4253785,\ C_{10} = 0.1781,\ A = 0.5448504 \times 10^6.$$

This potential simulates the interaction between the ^{4}He particles. For three dimensional system, we set the particle density $\rho = 0.02198\,\text{Å}^{-3}$, where, from the numerical calculation performed on clean system [62], $T_c = 2.193 \pm 0.006\,\mathrm{K}$. For two dimensional system, we set the particle density $\rho = 0.0432\,\text{Å}^{-2}$, where the numerical estimation gave $T_c = 0.653 \pm 0.010\,\mathrm{K}$ [62]. We set the temperature $T = 2\,\mathrm{K}$ for the three dimensional system and $T = 0.5\,\mathrm{K}$ for two dimensional system, both below the numerically estimated T_c in the clean system. The convergence was checked by the binning analysis [66]. Following Ref. [62], we employed the Chin approximation [67] for the interaction term. The dissipative

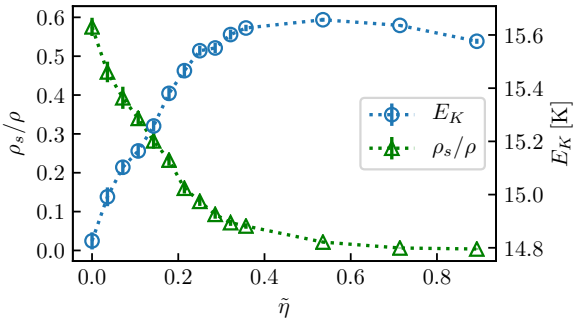

Figure 2.4: The superfluid fraction ρ_s/ρ and the kinetic energy E_K for three dimensional system as a function of $\tilde{\eta} = \eta d^2/\hbar$, where $d = 3.570\,\text{Å}$ is the interparticle distance. The number of particles is $N = 64$, the particle density ρ is $\rho = 0.02198\,\text{Å}^{-3}$, the temperature is $T = 2\,\text{K}$, the imaginary time step is $5 \times 10^{-3}\,\text{K}^{-1}$, and the cutoff of the bath is set to be $\tau_c = 0.2$. The blue circle represents the kinetic energy, while the green triangle represents the superfluid fraction.

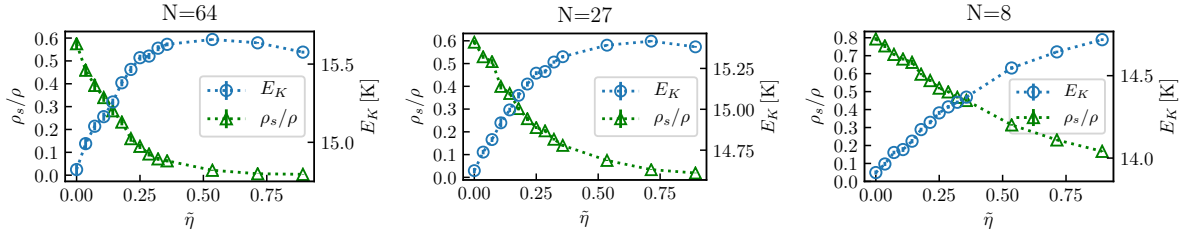

Figure 2.5: The superfluid fraction ρ_s/ρ and the kinetic energy E_K for three dimension as a function of $\tilde{\eta} = \eta d^2/\hbar$, where $d = 3.570$, as we vary the number of particles N for fixed density. The particle density ρ is $\rho = 0.02198\,\text{Å}^{-3}$, the temperature is $T = 2\,\text{K}$, the imaginary time step is $5 \times 10^{-3}\,\text{K}^{-1}$, and the cutoff of the bath is set to be $\tau_c = 0.2$.

term was discritized as [68, 69],

$$\frac{\eta}{2\pi} \sum_i \sum_{k>k'} \frac{\pi^2}{N_\tau^2} \frac{(\vec{r}_i(k) - \vec{r}_i(k'))^2}{\sin^2(\frac{\pi}{N_\tau}(k-k'))} =: \sum_i \sum_{k>k'} K(k-k')(\vec{r}_i(k) - \vec{r}_i(k'))^2, \tag{2.53}$$

where N_τ is the number of the Trotter step, k, k' is the labeling of time slice. To avoid the divergence associated with the discontinuity at $k = 0$ and N_τ, we introduce the UV cutoff for K as $K(k-k') = K((1-\tau_c)N_\tau)$ for $(1-\tau_c)N_\tau \leq k - k' \leq N_\tau - 1$; this form of cutoff is naturally realized if we introduce the ultraviolet cutoff for the spectrum of the heat bath. We set $\tau_c = 0.2$ for the cutoff in the three dimensional system and $\tau_c = 0.05$ for two dimensional systems.

Superfluid density and kinetic energy in three dimension

The result of the calculation is shown in Fig. 2.4 (green triangle). We can clearly see that ρ_s monotonically decreases as a function of η. We also calculated the kinetic energy

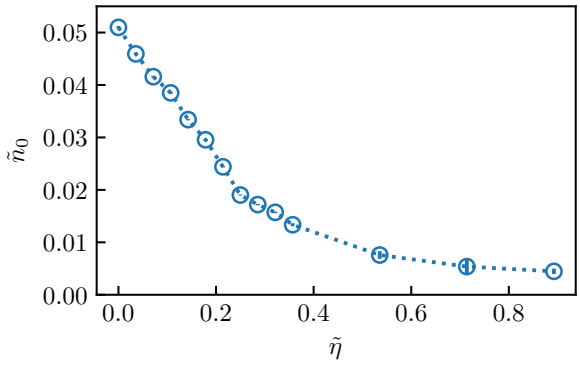

Figure 2.6: The condensate fraction at zero momentum, $\tilde{n}_0$, estimated from the off-diagonal density matrix, for three dimensional system. The number of particles is $N = 64$, the particle density ρ is $\rho = 0.02198\,\text{Å}^{-3}$, the temperature is $T = 2\,\text{K}$, the imaginary time step is $5 \times 10^{-3}\,\text{K}^{-1}$, and the cutoff of the bath is set to be $\tau_c = 0.2$. $\tilde{\eta} = \eta d^2/\hbar$, where $d = 3.570\,\text{Å}$.

(blue circle), which characterizes how strong the bosons fluctuate in the imaginary time. We can see the increase of the kinetic energy as a function of η, which comes both from the suppression of fluctuation of each boson and the suppression of the exchange event, which lowers the kinetic energy [40]. In Fig. 2.5, we show the numerical calculation of the superfluid density and the kinetic energy for the system with smaller particle number N. As we can see, the result at $N = 64$ is qualitatively similar to the result at $N = 24$. Overall the system with smaller N overestimates the superfluid density, which is reasonable since the number of the exchange event necessary for the system to have a finite winding number is smaller for smaller N.

Condensate fraction and off diagonal density matrix in three dimension

Here, we will discuss the result of the numerical calculation of the condensate fraction and the off diagonal density matrix. From the off diagonal density matrix, we can estimate the condensate fraction $\tilde{n}_0$ from the asymptotic value, and the result is shown in Fig. 2.6. We can see the monotonic decrease of $\tilde{n}_0$ as a function of η.

As for the more detailed structure of the off diagonal density matrix, we show the result for the single particle and the many particle ($N = 64$) system in Fig. 2.7. As we can see, as for the single particle case, the effect of dissipation appears in the decrease of the width of the Gaussian distribution. To see this, we showed the off-diagonal density matrix for the single particle case obtained both from the numerical calculation and the analytical expression [58],

$$n(r) = \exp\left(-\frac{\langle p^2\rangle\, r^2}{2\hbar^2}\right), \tag{2.54}$$

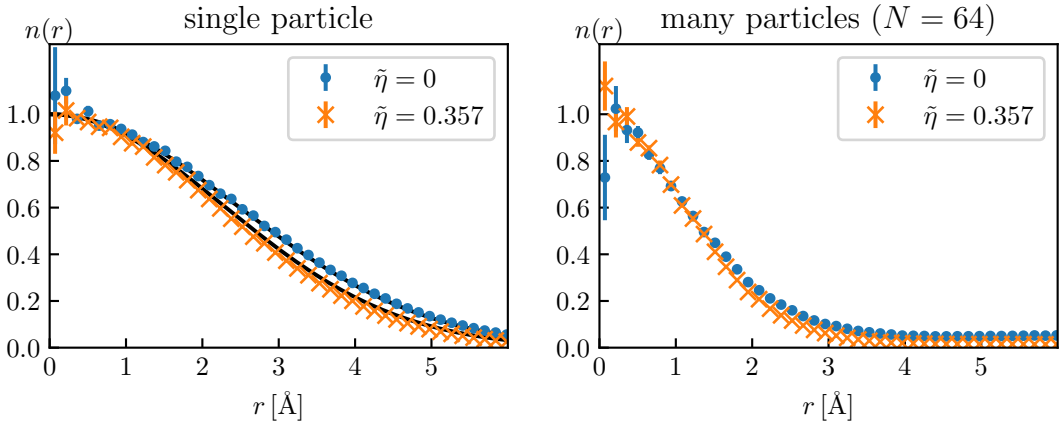

Figure 2.7: The off-diagonal density matrix in three dimension for the single particle and the particles with interaction. The number of particles is $N = 64$, the particle density ρ is $\rho = 0.02198\,\text{Å}^{-3}$, the temperature is $T = 2\,\text{K}$, the imaginary time step is $5 \times 10^{-3}\,\text{K}^{-1}$, and the cutoff of the bath is set to be $\tau_c = 0.2$. $\tilde{\eta} = \eta d^2/\hbar$, where $d = 3.570\,\text{Å}$. The solid lines for the single particle case is an analytical result based on the Eqs. (2.43) and (2.54).

where $\langle p^2 \rangle$ is given by Eq. (2.43). The cutoff for the expression Eq. (2.43) is the Drude type cutoff, i.e., $J(\omega) = \eta\omega/(1 + (\omega/\omega_D)^2)$, where $J(\omega)$ is the spectral function of the bath. Although the form of the cutoff in the numerical calculation is different from the Drude cutoff, we can see that the numerical and analytical result agrees well.

For the many particle case, the dissipation does not change the width very much, but it leads to the decrease of the condensate fraction n_0. We fitted the off diagonal density matrix with $\tilde{n}_0 + (1 - \tilde{n}_0)f(r)$, where $f(x) = \exp(-\bar{\alpha}_2 x^2/2! + \bar{\alpha}_4 x^4/4! - \bar{\alpha}_6 x^6/6!)$. The result is shown in Fig. 2.8. Although the α_2, which represents the second cumulant of the distribution, does not change drastically as a function of η, α_4 and α_6 decreases, which indicates that the distribution becomes more and more Gaussian-like distribution.

Numerical calculation in two dimension

Here, we will show the suppression of the superfluidity in two dimension to show that our scenario for the suppression of superfluidity does not depend on the dimensionality of the system. As we mentioned above, we performed the quantum Monte Carlo in two dimension with the following parameters: the temperature $T = 0.5\,\text{K}$; the particle density $\rho = 0.0432\,\text{Å}^{-2}$; the cutoff of the bath $\tau_c = 0.05$; the imaginary time step $5 \times 10^{-3}\,\text{K}^{-1}$. The result is shown in Fig. 2.9. As we can see, the superfluid fraction decreases as a function of η. Also, the tail of the off diagonal density matrix is drastically suppressed in the presence of the dissipation. The superfluid density and the kinetic energy for the systems with smaller N is shown in Fig. 2.10. We can see that the superfluid density is well converged at $N = 25$ as a function of N.

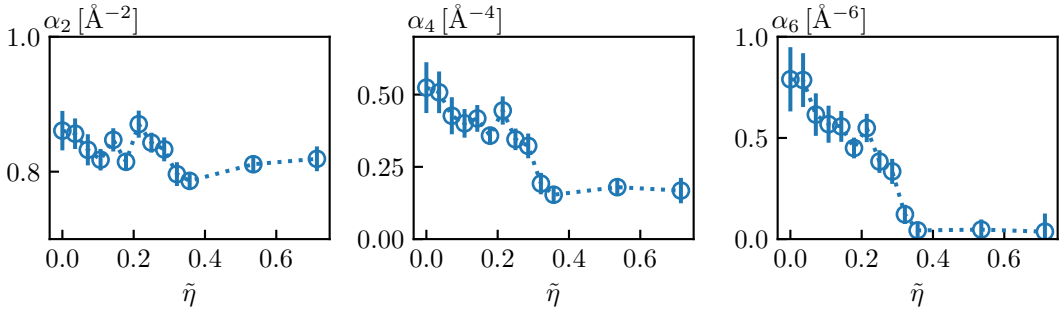

Figure 2.8: The parameters for the off diagonal density matrix in three dimension. The number of particles is $N = 64$, the particle density ρ is $\rho = 0.02198\,\text{Å}^{-3}$, the temperature is $T = 2\,\text{K}$, the imaginary time step is $5 \times 10^{-3}\,\text{K}^{-1}$, and the cutoff of the bath is set to be $\tau_c = 0.2$. $\tilde{\eta} = \eta d^2/\hbar$, where $d = 3.570\,\text{Å}$. The fitting function is $\tilde{n}_0 + (1 - \tilde{n}_0)f(r)$, where $f(x) = \exp(-\bar{\alpha}_2 x^2/2! + \bar{\alpha}_4 x^4/4! - \bar{\alpha}_6 x^6/6!)$.

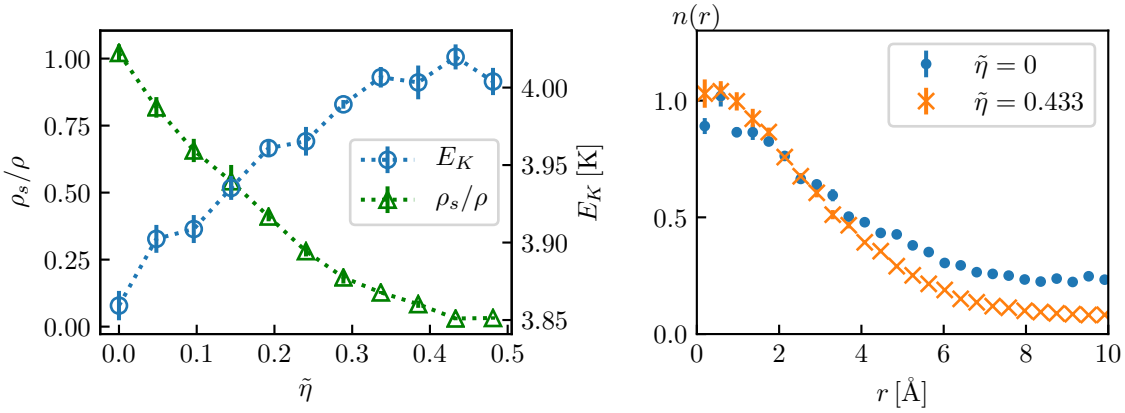

Figure 2.9: The kinetic energy E_K, the superfluid fraction ρ_s/ρ and the off diagonal density matrix for the two dimensional system. The number of particles is $N = 25$, the particle density ρ is $\rho = 0.0432\,\text{Å}^{-2}$, the temperature is $T = 0.5\,\text{K}$, the imaginary time step is $5 \times 10^{-3}\,\text{K}^{-1}$, and the cutoff of the bath is set to be $\tau_c = 0.05$. $\tilde{\eta} = \eta d^2/\hbar$, where $d = 4.811\,\text{Å}$.

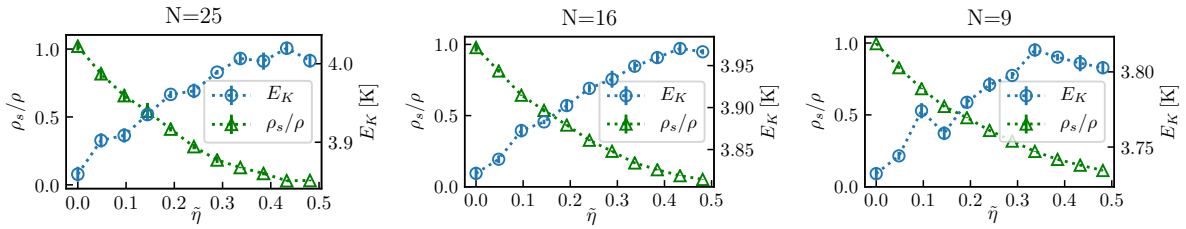

Figure 2.10: The superfluid fraction ρ_s/ρ and the kinetic energy E_K for two dimension as a function of $\tilde{\eta} = \eta d^2$, where $d = 4.811\,\text{Å}$ as we vary the number of particles N for fixed density. The particle density ρ is $\rho = 0.0432\,\text{Å}^{-2}$, the temperature is $T = 0.5\,\text{K}$, the imaginary time step is $5 \times 10^{-3}\,\text{K}^{-1}$, and the cutoff of the bath is set to be $\tau_c = 0.05$.

2.6 Field theoretical Model

Here, we discuss the effect of dissipation on the superfluidity in the following field theoretical model:

$$S = \sum_{\omega_n, \boldsymbol{k}} \left(-i\omega_n + \frac{\boldsymbol{k}^2}{2m} - \mu \right) \bar{\psi}_{n,\boldsymbol{k}} \psi_{n,\boldsymbol{k}} + \frac{g}{2} \int d\tau d\boldsymbol{r} \bar{\psi}\bar{\psi}\psi\psi + \alpha \sum_{\omega_n, \boldsymbol{k}} |\omega_n| \rho^n_{\boldsymbol{k}} \rho^{-n}_{-\boldsymbol{k}}, \quad (\rho^n_{\boldsymbol{k}} = \sum_{\omega_m, \boldsymbol{q}} \bar{\psi}_{n+m,\boldsymbol{k}+\boldsymbol{q}} \psi_{m,\boldsymbol{q}}), \tag{2.55}$$

where $\psi, \bar{\psi}$ are the bosonic annihilation and creation operator, ω_n is the Matsubara frequency for bosons, g is the interaction strength and α is the strength of the dissipation. This model obviously breaks the Galilean invariance because of the last term.

The idea behind the model Eq. (2.55) is the following. In the first quantized model above, each particle is subject to the dissipation. This can be mapped to the finite diffusion constant or the conductivity of the many-particle system, and hence the dissipation enters as the many-body interaction. More explicitly, the propagator of the density $\rho(q, \omega)$ is expressed by

$$\Pi(q, \omega) = \langle \rho(q, \omega) \rho(-q, -\omega) \rangle = \frac{N(0) D q^2}{D q^2 + |\omega|} \tag{2.56}$$

where $N(0)$ is the density of electronic states at the Fermi energy, D is the diffusion constant related to the conductivity $\sigma = e^2 N(0) D$. In the action, the inverse of $\Pi(q, \omega)$ appears in front of $\rho(q, \omega)\rho(-q, -\omega)$ which is $\frac{1}{N(0)} + \frac{|\omega|}{Dq^2}$. For simplicity, we replace Dq^2 in the denominator by a constant. Then we obtain the last term of Eq. (2.55).

We calculated the superfluid density by the Bogoliubov approximation, i.e., substitute $\psi = \sqrt{\rho_0} + \phi$ and $\bar{\psi} = \sqrt{\rho_0} + \bar{\phi}$ and retained the terms up to quadratic order in $\phi, \bar{\phi}$. From the general argument [41, 70], the normal component $\rho_n = \rho - \rho_s$ can be obtained from the transverse current-current response function $\chi^t(\omega, \boldsymbol{q})$ as $\rho_n/m = \lim_{\boldsymbol{q}\to 0} \chi^t(0, \boldsymbol{q})$. At one-loop order, it is given as [71]:

$$\frac{\rho_n}{m} = \lim_{\boldsymbol{q}\to 0} \int \frac{d\epsilon_{\boldsymbol{k}}}{2\pi} \frac{d\omega}{2\pi} \frac{\epsilon_{\boldsymbol{k}}}{4i} \mathrm{tr}[\sigma_3 G^K_{\omega,\boldsymbol{k}} \sigma_3 (G^R_{\omega,\boldsymbol{k}+\boldsymbol{q}} + G^A_{\omega,\boldsymbol{k}-\boldsymbol{q}})], \tag{2.57}$$

where we assumed the two dimensional system. The green functions are given as,

$$G^{R/A}_{\omega,\boldsymbol{k}} = \frac{1}{\omega^2 - \omega^2_{\boldsymbol{k}} \pm 2i\eta\omega\epsilon_{\boldsymbol{k}}} \begin{pmatrix} \omega + \epsilon_{\boldsymbol{k}} + g\rho_0 \mp i\eta\omega & -g\rho_0 \pm i\eta\omega \\ -g\rho_0 \pm i\eta\omega & -\omega + \epsilon_{\boldsymbol{k}} + g\rho_0 \mp i\eta\omega \end{pmatrix}, \tag{2.58}$$

and $G^K_{\omega,\boldsymbol{k}} = \coth(\beta\omega/2)[G^R_{\omega,\boldsymbol{k}} - G^A_{\omega,\boldsymbol{k}}]$, where $\eta = 2\rho_0\alpha$. The number density can be calculated as:

$$\rho = \rho_0 + \frac{1}{V}\sum_{\boldsymbol{k}} \int_{-\infty}^{\infty} \frac{d\omega}{2\pi} n_B(\omega) i((G^R_{\omega,\boldsymbol{k}})_{11} - (G^A_{\omega,\boldsymbol{k}})_{11}) \tag{2.59}$$

Here, we will discuss the derivation of the superfluid density formula (2.57) and the Green function (2.58) starting from the bosonic system coupled to the phonon bath [52]:

$$\begin{aligned} S &= \sum_{\omega_n,\boldsymbol{k}} (-i\omega_n + \xi_{\boldsymbol{k}})\bar{\psi}_{n,\boldsymbol{k}}\psi_{n,\boldsymbol{k}} + \frac{g}{2}\int d\tau \sum_i \bar{\psi}_i\bar{\psi}_i\psi_i\psi_i \\ &+ \int d\tau \sum_i \bar{\psi}_i\psi_i \sum_\alpha (V_\alpha a_{i\alpha n} + V^*_\alpha \bar{a}_{i\alpha n}) + \sum_{\omega_n,\boldsymbol{k}} (-i\omega_n + \epsilon_\alpha)\bar{a}_{i\alpha n}a_{i\alpha n} \\ &= \sum_{\omega_n,\boldsymbol{k}} (-i\omega_n + \xi_{\boldsymbol{k}})\bar{\psi}_{n,\boldsymbol{k}}\psi_{n,\boldsymbol{k}} + \frac{g}{2}\int d\tau \sum_i \bar{\psi}_i\bar{\psi}_i\psi_i\psi_i + \sum_{\omega_n,\boldsymbol{k}} A(i\omega_n)\rho^n_{\boldsymbol{k}}\rho^{-n}_{-\boldsymbol{k}} \\ &+ \sum_{\omega_n,\boldsymbol{k}} (-i\omega_n + \epsilon_\alpha)\left(\bar{a}_{n\alpha} + \frac{V_\alpha}{-i\omega_n + \epsilon_\alpha}\rho^n_i\right)\left(a_{n,\boldsymbol{k}} + \frac{V^*_\alpha}{-i\omega_n + \epsilon_\alpha}\rho^{-n}_i\right), \end{aligned}$$

where

$$\rho^n_{\boldsymbol{k}} = \sum_{\omega_m,\boldsymbol{q}} \bar{\psi}_{n+m,\boldsymbol{k}+\boldsymbol{q}}\psi_{m,\boldsymbol{q}}, \quad A(i\omega_n) = -\sum_\alpha \frac{|V_\alpha|^2\epsilon_\alpha}{\omega_n^2 + \epsilon_\alpha^2}. \tag{2.60}$$

Here, we subtract $A(0)$ to ignore the effect of potential renormalization:

$$A(i\omega_n) = \sum_\alpha |V_\alpha|^2\epsilon_\alpha \left(\frac{1}{\epsilon_\alpha^2} - \frac{1}{\omega_n^2 + \epsilon_\alpha^2}\right) \tag{2.61}$$

Then, if we assume the Ohmic bath, $A(i\omega_n) = \alpha|\omega_n|$ ($\alpha > 0$). Now we decompose $\psi, \bar{\psi}$ into $\boldsymbol{k} = 0$ condensed part ($\sqrt{N_0}$) and uncondensed $\boldsymbol{k} \neq 0$ part (ϕ) i.e., $\psi = \sqrt{N_0} + \phi$, and drop the terms higher than quadratic in the uncondensed component ϕ:

$$\begin{aligned} S = -\mu N_0 + \frac{g}{2}N_0^2 &+ \sum_{\omega_n,\boldsymbol{k}} [-i\omega_n + \xi_{\boldsymbol{k}} + 2N_0(g + A(i\omega_n))]\bar{\psi}_{n,\boldsymbol{k}}\psi_{n,\boldsymbol{k}} \\ &+ \frac{N_0}{2}\sum_{\omega_n,\boldsymbol{k}} (g + 2A(i\omega_n))\,(\bar{\psi}_{n,\boldsymbol{k}}\bar{\psi}_{-n,-\boldsymbol{k}} + \psi_{n,\boldsymbol{k}}\psi_{-n,-\boldsymbol{k}}). \end{aligned}$$

Here we introduce the Nambu spinor $\bar{\Psi}_{n,\boldsymbol{k}} = (\bar{\psi}_{n,\boldsymbol{k}}\ \psi_{-n,-\boldsymbol{k}})$. Then,

$$S = \sum_{\omega_n,\boldsymbol{k},k_x>0} \bar{\Psi}_{n,\boldsymbol{k}}(-G^{-1})\Psi_{n,\boldsymbol{k}} - \mu N_0 + \frac{g}{2}N_0^2, \tag{2.62}$$

where

$$-G^{-1} = \begin{pmatrix} -i\omega_n + \xi_{\boldsymbol{k}} + 2N_0[g + A(i\omega_n)] & N_0[g + 2A(i\omega_n)] \\ N_0[g + 2A(i\omega_n)] & i\omega_n + \xi_{\boldsymbol{k}} + 2N_0[g + A(i\omega_n)] \end{pmatrix}. \tag{2.63}$$

Then, the Green function for Bogoliubov quasiparticle $G_{\alpha\beta}(\tau) = -\langle T_\tau \Psi_\alpha(\tau)\Psi^\dagger_\beta(0)\rangle$ is:

$$G = \frac{-1}{\omega_n^2 + \omega_{\boldsymbol{k}}^2 + 4N_0\epsilon_{\boldsymbol{k}}A} \begin{pmatrix} i\omega_n + \epsilon_{\boldsymbol{k}} + N_0[g + 2A(i\omega_n)] & -N_0[g + 2A(i\omega_n)] \\ -N_0[g + 2A(i\omega_n)] & -i\omega_n + \epsilon_{\boldsymbol{k}} + N_0[g + 2A(i\omega_n)] \end{pmatrix},$$

and the total number density is given as,

$$\begin{aligned} \frac{N}{V} = \frac{N_0}{V} - G_{11}(0^-) &= \frac{N_0}{V} + \frac{1}{\beta V}\lim_{\delta\to 0}\sum_{\omega_n,\boldsymbol{k}} e^{i\omega_n\delta}\frac{i\omega_n + \epsilon_{\boldsymbol{k}} + N_0 g + 2N_0 A(i\omega_n)}{\omega_n^2 + \omega_{\boldsymbol{k}}^2 + 4N_0\epsilon_{\boldsymbol{k}}A(i\omega_n)} \\ &= \frac{N_0}{V} + \frac{1}{V}\sum_{\boldsymbol{k}}\int_{-\infty}^{\infty}\frac{d\omega}{\pi} n_B(\omega)\mathrm{Im}\left[\frac{\omega + \epsilon_{\boldsymbol{k}} + N_0 g - 2i\alpha N_0\omega}{-\omega^2 + \omega_{\boldsymbol{k}}^2 - 4i\alpha N_0\epsilon_{\boldsymbol{k}}\omega}\right] \\ &= \frac{N_0}{V} + \frac{1}{V}\sum_{\boldsymbol{k}}\int_{-\infty}^{\infty}\frac{d\omega}{\pi} n_B(\omega)\frac{\eta\omega(\epsilon_{\boldsymbol{k}} + \omega)^2}{(\omega^2 - \omega_{\boldsymbol{k}}^2)^2 + 4\eta^2\epsilon_{\boldsymbol{k}}^2\omega^2}. \end{aligned} \tag{2.64}$$

Here we assumed the relation $N_0 g = \mu$. We introduce the cutoff for the heat bath at $\omega = \omega_c$.

Assuming the two dimensional system, here we transform the above expression as,

$$\begin{aligned} 1 &= \frac{\rho_0}{\rho} + \frac{m}{\rho}\int_0^{\epsilon_c}\frac{d\epsilon}{2\pi}\int_{-\omega_c}^{\omega_c}\frac{d\omega}{\pi} n_B(\omega)\frac{\eta\omega(\epsilon + \omega)^2}{(\omega^2 - \omega_{\boldsymbol{k}}^2)^2 + 4\eta^2\epsilon^2\omega^2} \\ &= \frac{\rho_0}{\rho} + mg\int_0^{\epsilon_c/P}\frac{d\tilde{\epsilon}}{2\pi}\int_{-\omega_c/P}^{\omega_c/P}\frac{d\tilde{\omega}}{\pi} n_B(P\tilde{\omega})\frac{\eta\tilde{\omega}(\tilde{\epsilon} + \tilde{\omega})^2}{(\tilde{\omega}^2 - \tilde{\omega_{\boldsymbol{k}}}^2)^2 + 4\eta^2\tilde{\epsilon}^2\tilde{\omega}^2}, \end{aligned}$$

where

$$P = \rho g, \quad \tilde{\omega_k}^2 = \tilde{\epsilon_{\boldsymbol{k}}}^2 + \frac{2\rho_0}{\rho}\tilde{\epsilon_{\boldsymbol{k}}}. \tag{2.65}$$

The superfluid density n_s is obtained from the current-current correlation function. To derive it, we couple the system with the gauge field $\boldsymbol{A}$, and derive the effective action for $\boldsymbol{A}$. Here we define $\Delta(i\omega_n) = N_0(g + 2A(i\omega_n))$, then from Eq. (2.62) and (2.63),

$$\begin{aligned} S &= \sum_{\omega_n,\boldsymbol{k},k_x>0,\boldsymbol{k}',k_x'>0} \bar{\Psi}_{n,\boldsymbol{k}}\left(-G^{-1}\delta_{\boldsymbol{k},\boldsymbol{k}'} + \frac{i}{2m}\sigma_3([\nabla,\boldsymbol{A}])_{\boldsymbol{k},\boldsymbol{k}'} + \frac{1}{2m}(\boldsymbol{A}^2)_{\boldsymbol{k},\boldsymbol{k}'}\right)\Psi_{n,\boldsymbol{k}'} \\ &=: \sum_{\omega_n,\boldsymbol{k},k_x>0,\boldsymbol{k}',k_x'>0} \bar{\Psi}_{n,\boldsymbol{k}}\left(-G^{-1}\delta_{\boldsymbol{k},\boldsymbol{k}'} + (\chi_1)_{\boldsymbol{k},\boldsymbol{k}'} + (\chi_2)_{\boldsymbol{k},\boldsymbol{k}'}\right)\Psi_{n,\boldsymbol{k}'}. \end{aligned}$$

Then, we integrate over the Nambu spinor to obtain the effective action for $\boldsymbol{A}$:

$$\begin{aligned} S &= \mathrm{Tr}\ln(-G^{-1} + \chi_1 + \chi_2) \\ &= \mathrm{Tr}\ln(-G^{-1}) + \mathrm{Tr}\ln(1 - G\chi_1 - G\chi_2) \\ &= S_0 - \mathrm{Tr}(G\chi_2) - \frac{1}{2}\mathrm{Tr}(G\chi_1 G\chi_1) + \mathcal{O}(\boldsymbol{A}^3) \\ &\cong S_0 - \sum_q \boldsymbol{A}_q\cdot\boldsymbol{A}_{-q}\left(\sum_p \mathrm{tr}(G_{p,p}) + \frac{1}{m}\sum_p \mathrm{tr}(G_{p,p}\sigma_3 G_{p+q,p+q}\sigma_3)\frac{(\boldsymbol{p} + \boldsymbol{q}/2)^2}{2md}\right) + \mathcal{O}(\boldsymbol{A}^3), \end{aligned} \tag{2.66}$$

where $p = (i\omega_n, \boldsymbol{p}; k_x > 0)$ and we dropped higher derivative terms. The first term in the curly bracket represents the diamagnetic term, while the second term represents the paramagnetic term. Here we calculate the paramagnetic contribution:

$$\sum_p \mathrm{tr}(G_{p,p}\sigma_3 G_{p+q,p+q}\sigma_3)\frac{(\boldsymbol{p}+\boldsymbol{q}/2)^2}{2md} = \frac{1}{\beta V}\sum_{\omega_n,\boldsymbol{k}} \frac{-\omega_n^2+\omega_{\boldsymbol{k}}^2+4N_0A\epsilon_{\boldsymbol{k}}}{[\omega_n^2+\omega_{\boldsymbol{k}}^2+4N_0A\epsilon_{\boldsymbol{k}}]^2}\frac{\epsilon_{\boldsymbol{k}}}{d}. \tag{2.67}$$

Here we perform the analytic continuation, assuming the external frequency ω_l is positive. Then, there are contributions from cuts on $\mathrm{Im}(z+i\omega_l)=0$ and $\mathrm{Im}(z)=0$:

$$\begin{aligned}
&\frac{1}{\beta V}\sum_{\omega_n,\boldsymbol{k}} \mathrm{tr}(G_{i\omega_n+i\omega_l,\boldsymbol{q}+\boldsymbol{k}}\sigma_3 G_{i\omega_n,\boldsymbol{k}}\sigma_3)\frac{(\boldsymbol{k}+\boldsymbol{q}/2)^2}{2md}\\
=&\frac{1}{V}\sum_{\boldsymbol{k}}\int\frac{dz}{2\pi i}\epsilon_{\boldsymbol{k}+\boldsymbol{q}/2}\frac{\coth(\beta z/2)}{2d}\mathrm{tr}(G_{z+i\omega_l,\boldsymbol{k}+\boldsymbol{q}}\sigma_3 G_{z,\boldsymbol{k}}\sigma_3)\\
=&\frac{1}{V}\sum_{\boldsymbol{k}}\int\frac{d\omega}{2\pi i}\epsilon_{\boldsymbol{k}+\boldsymbol{q}/2}\frac{\coth(\beta\omega/2)}{2d}[\mathrm{tr}(G^R_{\omega+i\omega_l,\boldsymbol{k}+\boldsymbol{q}}\sigma_3(G^R_{\omega,\boldsymbol{k}}-G^A_{\omega,\boldsymbol{k}})\sigma_3)\\
&\qquad+\mathrm{tr}((G^R_{\omega,\boldsymbol{k}}-G^A_{\omega,\boldsymbol{k}})\sigma_3 G^A_{\omega-i\omega_l,\boldsymbol{k}-\boldsymbol{q}}\sigma_3)]\\
\to_{(i\omega_l\to\Omega)}&\frac{1}{V}\sum_{\boldsymbol{k}}\int\frac{d\omega}{2\pi i}\epsilon_{\boldsymbol{k}+\boldsymbol{q}/2}\frac{\coth(\beta\omega/2)}{2d}[\mathrm{tr}(G^R_{\omega+\Omega,\boldsymbol{k}+\boldsymbol{q}}\sigma_3(G^R_{\omega,\boldsymbol{k}}-G^A_{\omega,\boldsymbol{k}})\sigma_3)\\
&\qquad+\mathrm{tr}((G^R_{\omega,\boldsymbol{k}}-G^A_{\omega,\boldsymbol{k}})\sigma_3 G^A_{\omega-\Omega,\boldsymbol{k}-\boldsymbol{q}}\sigma_3)]\\
=&\frac{1}{V}\sum_{\boldsymbol{k}}\int\frac{d\omega}{2\pi i}\epsilon_{\boldsymbol{k}+\boldsymbol{q}/2}\frac{1}{2d}[\mathrm{tr}(G^R_{\omega+\Omega,\boldsymbol{k}+\boldsymbol{q}}\sigma_3 G^K_{\omega,\boldsymbol{k}}\sigma_3)+\mathrm{tr}(G^K_{\omega,\boldsymbol{k}}\sigma_3 G^A_{\omega-\Omega,\boldsymbol{k}-\boldsymbol{q}}\sigma_3)]\\
=&\frac{m}{V}\int\frac{d\epsilon_{\boldsymbol{k}}}{2\pi}\int\frac{d\omega}{2\pi}\epsilon_{\boldsymbol{k}+\boldsymbol{q}/2}\frac{-i}{4}\mathrm{tr}[\sigma_3 G^K_{\omega,\boldsymbol{k}}\sigma_3(G^R_{\omega+\Omega,\boldsymbol{k}+\boldsymbol{q}}+G^A_{\omega-\Omega,\boldsymbol{k}-\boldsymbol{q}})],
\end{aligned}\tag{2.68}$$

where $G^K = \coth(\beta\omega/2)(G^R - G^A)$, and in the last line we assumed two dimensional system. $\Omega\to 0$ and $\boldsymbol{q}\to 0$ limit of this term is nothing but the normal component ρ_n, and we note that this expression is the same as the one in Ref. [71], obtained from the Keldysh formalism.

Here, the retarded/advanced Green function for the Bogoliubov quasiparticle can be obtained from the analytic continuation of the imaginary time Green function from the upper/lower half plane and is given as, denoting $2\rho_0 A = \eta\omega$,

$$G^{A/R} = \frac{1}{\omega^2-\omega_{\boldsymbol{k}}^2\mp 2i\eta\omega\epsilon_{\boldsymbol{k}}}\begin{pmatrix}\omega+\epsilon_{\boldsymbol{k}}+g\rho_0\pm i\eta\omega & -g\rho_0\mp i\eta\omega\\ -g\rho_0\mp i\eta\omega & -\omega+\epsilon_{\boldsymbol{k}}+g\rho_0\pm i\eta\omega\end{pmatrix},$$

and

$$\begin{aligned}
G^K &= \coth(\beta\omega/2)[G^R-G^A]\\
&= \frac{-2i\coth(\beta\omega/2)\eta\omega}{\omega_{\boldsymbol{k}}^4-2\omega^2(\omega_{\boldsymbol{k}}^2-2\eta^2\epsilon_{\boldsymbol{k}}^2)+\omega^4}\begin{pmatrix}(\omega+\epsilon_{\boldsymbol{k}})^2 & -(\omega^2-\epsilon_{\boldsymbol{k}}^2)\\ -(\omega^2-\epsilon_{\boldsymbol{k}}^2) & (\omega-\epsilon_{\boldsymbol{k}})^2\end{pmatrix}.
\end{aligned}$$

From now on, we consider the zero temperature case, where the destruction of the superfluidity comes purely from the dissipation. The finite temperature case can be

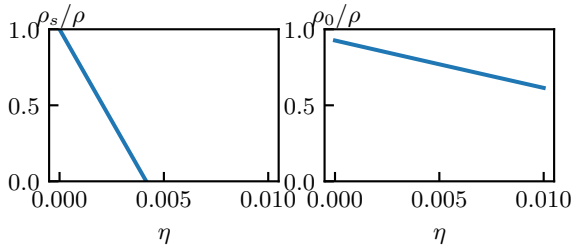

Figure 2.11: ρ_s/ρ and ρ_0/ρ obtained from Eqs. (2.57) and (2.59). The parameters are $\epsilon_c/(\rho g) = 900$, $\omega_c/(\rho g) = 1000$, $mg = 1$.

treated in a similar manner. We introduce the cutoff for η as $\eta\,\Theta(\omega_c^2 - \omega^2)$, where $\Theta(x)$ is the step function. We also introduced the cutoff for the energy $\epsilon_{\boldsymbol{k}}$ at ϵ_c, and choose $\epsilon_c < \omega_c$, so that the whole energy spectrum of the system is coupled to the heat bath. The result of the calculation is shown in Fig. 2.11. We can see that ρ_s rapidly decreases and vanishes so the superfluidity is destroyed by the dissipation. This kind of behavior is also shown in Ref. [33], where the authors discussed the destruction of the superfluid by the static impurity potential, which is in contrast to our system where the translation symmetry is preserved but the time non-local action breaks the Galilean invariance.

From Fig. 2.11, we can see that, at the critical η where $\rho_s = 0$, ρ_0 remains finite. This behavior is similar to the system with disorder [33, 34], but the depletion of ρ_0 is large in this parameter region, so our one-loop calculation cannot decide whether or not ρ_0 is finite at the critical point. In fact, assuming the smooth behavior of the single particle Green function at the critical point, the Josephson relation [72, 73] requires that both ρ_0 and ρ_s becomes zero. In spite of this uncertainty, we believe that the transition to the phase with $\rho_s = 0$ in this model remains intact, as is supported by our numerical calculation in a model with the different source of the Galilean symmetry breaking.

2.7 Discussion

At a moderately clean regime $1/\tau, k_BT \gg \Delta^2/\epsilon_F$ [20], where τ is the relaxation time, Δ is the superconducting gap and ϵ_F is the Fermi energy, the particle-hole excitation at the normal core [17, 74] can be regarded as a heat bath with a continuum spectrum, so we can regard Eq. (2.31) as a model for the vortices with normal core in that regime. Our theory does not apply to the super-clean system $1/\tau \gg \Delta^2/\epsilon_F$ at temperature below $k_BT \sim \Delta^2/\epsilon_F$. Since the motion of vortex induces the resistivity [54] and the density of vortices is proportional to the magnetic field, we expect a giant magnetoresistance, as is observed experimentally [9, 11]. In particular, since the vortices do not exhibit superfluidity even at lowest temperature, the vortex can be treated as a classical object and we expect the flux-flow resistivity $\rho \propto \rho_n(B/H_{c2})$ [2], which is linear in the magnetic field B, where ρ_n is the residual resistivity of the normal state and H_{c2} is the critical magnetic field of the type II superconductor. This behavior is observed over finite range of magnetic field [9]. For a weak magnetic field, the resistance can be much smaller than

the quantum resistance $h/(4e^2)$. We note that the long range interaction between the vortices does not spoil our scenario if we include the effect of the screening [35, 75–77]. Also, the Berry phase of vortices [78], which is absent in the present study since we assume the integer-filling of the electrons, leads to the interference of the exchange events so that the superfludity is further suppressed if we include the Berry phase term.

We also speculate that the effect of the normal core or dissipation discussed above affects the phase transition associated with the proliferation of the vortices, i.e., the transition not associated with the magnetic field. The point is that, if we extend the above dissipative action to the closed loop in the space-time, in the parameter region where the typical size of the vortex ring in the space-time is macroscopic, the exchange process between the rings is still suppressed from the same reason as above. Therefore, we expect a different phase compared to the usual proliferation of vortices in the bosonic superfluid.

In summary, we have shown both analytically and numerically that the presence of the heat bath, which is the continuous degrees of freedom, drastically affects the thermodynamic phase realized by the bosons. Our first model is in a first-quantized form, and we discussed the reduction of the superfluid density because of the modification of the *off-diagonal* density matrix of each particle in the presence of dissipation. We also numerically showed the reduction of the superfluid density at finite temperature to show the strong support for our scenario. Our second model is a second-quantized field theoretical model, and we calculated the superfluid density from the transverse current-current correlation function at zero temperature.

Chapter 3

Theory of nonreciprocal Josephson effect

3.1 Background

The nonreciprocal effect of the material is characterized by the difference of the current response property when we apply higher voltage bias on the left/right side of the material[1]. Concretely, as for the electric current, the nonreciprocity is defined by the following current response property:

$$\vec{I}(\vec{E}) \neq -\vec{I}(-\vec{E}), \tag{3.1}$$

where $\vec{E}$ and $\vec{I}$ are the external electric field and the electric current, respectively. Equivalently, if we represent the voltage bias as $V = V_L - V_R$, where $V_{L/R}$ are the voltage at the left and right side of the sample, respectively,

$$\vec{I}(V) \neq -\vec{I}(-V). \tag{3.2}$$

Physically, it is obvious that the system does not exhibit the nonreciprocity (3.2), if the material is symmetric between left and right. In fact, if the material has certain symmetry which acts on $\vec{I}$ and $\vec{E}$ as

$$\vec{I} \to -\vec{I}, \quad \vec{E} \to -\vec{E}, \tag{3.3}$$

then we get the reciprocal response $\vec{I}(\vec{E}) = -\vec{I}(-\vec{E})$ as is expected. The examples of such symmetries are the inversion symmetry $\mathcal{P}$ and the mirror symmetry $\mathcal{M}$.

The nonreciprocal responses in noncentrosymmetric materials in general have been intensively studied both from the theoretical and the experimental viewpoint [79]. It often happens that broken $\mathcal{T}$ is needed in addition to broken $\mathcal{P}$ to obtain the nonreciprocal responses, but there are cases where only $\mathcal{P}$ breaking is enough. The p-n junction is a representative example, where the hetero junction of n-type and p-type semiconductors acts as a rectifier without magnetic field or magnetization. On the other hand, the direction of the arrow of time is determined by the dissipation associated with the resistivity,

[1] In this work, we focus on the nonreciprocal electric transport at $\vec{q} = 0$, i.e., at zero wavenumber, although the nonreciprocal response at finite $\vec{q}$ like the natural circular dichroism is also an important research topic [79].

i.e., irreversibility. In the case of p-n-junction, the existence of the depletion layer due to the Coulomb interaction is essential for its rectification function. Another example of the nonreciprocal response without $\mathcal{T}$-breaking is the Zener tunneling [80]. In this case, the inter-band tunneling probability across the band gap differs between right and left directions due to the shift vector originating from the Berry connection [81] even without the broken $\mathcal{T}$. This shift vector is also relevant to the shift current for the interband photoexcitation [82]. Therefore, the quantum geometry, which encodes the information of the microscopic inversion asymmetry inside a unit cell, plays an important role. The nonreciprocity in optical systems has been widely studied [83], and in particular, the quantum diode of light has been theoretically studied [84] and experimentally realized [85]. Here the two isolated two level system act as nonlinear mirrors and lead to left-right asymmetric Fabry-Perot interferometer.

The nonreciprocal signal in solids can be utilized to experimentally detect the inversion symmetry breaking coming from the magnetic order, the structural phase transition, the inversion asymmetric crystal structure, etc.. For the range of the strength of the external voltage imposed in experiments, the nonreciprocal signal is relatively small compared to the linear response signal, so that it is hard to detect the nonreciprocity in the DC transport experiment. Instead, we can impose AC voltage V_ω, and measure DC current component I_0 [82, 86] (see Fig. 3.1) or the 2ω current component $I_{2\omega}$ [12, 87] using the band pass filter. In the inversion symmetric system, both components are forbidden from the general group theoretical argument [88], so they directly quantify the nonreciprocity of the material. Also, the conversion from the AC signal to the DC signal, i.e., the rectification effect, is important from the engineering perspective, since the earth is filled with the AC electromagnetic wave coming from the sun, and to utilize this energy, we first need to convert them to DC signal, which is done by the solar cells where the inversion symmetry is structurally broken by the junction structure.

Theoretical challenge of the nonreciprocal transport lies in the fact that the nonreciprocal nature can only be captured by the nonlinear response, since at linear order in $\vec{E}$, from $I_\alpha = \sigma_{\alpha\beta}E_\beta$, we always get the reciprocal response, $\vec{I}(\vec{E}) = -\vec{I}(-\vec{E})$. In the perturbative treatment in $\vec{E}$, the nonreciprocity arises only at even orders of $\vec{E}$, so we need to calculate at least the second order nonlinear response. This can be done by calculating the third order current correlation function by the nonlinear extension of the Kubo formula [89], directly calculating the current expectation value by the Keldysh formalism [82], or resorting to the higher order expansion in the electric field $\vec{E}$ in the Boltzmann equation [90].

Aside from the perturbative calculation of $I-V$ curve mentioned above, we can show the nonreciprocity by the nonperturbative exact calculation of $I-V$ curve, which is usually very difficult in solid state systems because of the large number of degrees of freedom. In this respect, the Josephson junction system is convenient since its $I-V$ curve is fully governed by the dynamics of the single Josephson phase φ which is the difference of the superconducting phases of left and right bulk superconductors. There are studies on the Josephson diode [91–98], but the nonreciprocity of the single Josephson junction system has not been much explored.

The Josephson effect is important both theoretically and experimentally. From the

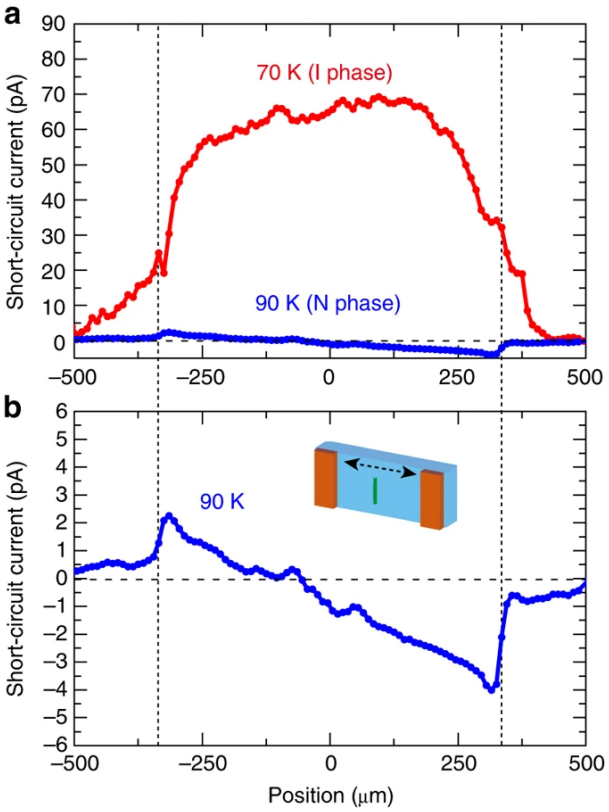

Figure 3.1: The experimental measurement of DC shift current associated with the local photo irradiation on the tetrathiafulvalene-p-chloranil (TTF-CA) sample. In this material, the inversion symmetry is intact in N phase, while it is broken in I phase with the appearance of the macroscopic electric polarization. In N phase, we can only see the small signal coming from the difference of the distance between the photo irradiation point and the left/right electrode. In I phase, we can see the giant uniform DC signal associated with the microscopic inversion symmetry breaking of TTF-CA. Reproduced with permission from [86].

theoretical side, it is a clear evidence of the coherence of the wave function inside the superconductors. From the experimental side, since the phase degree of freedom φ is almost isolated from the other degrees of freedom due to the superconducting gap and exhibits the quantum nature, it is an important building block of the quantum computers. The dynamics of φ in the dissipationless case is described by the following Hamiltonian:

$$H = \frac{Q^2}{2C} + E_J\left(1 - \cos\frac{2e\phi}{\hbar}\right) - I_x\phi, \tag{3.4}$$

where $\phi = \hbar\varphi/(2e)$, C is the capacitance of the Josephson circuit, Q is the charge accumulated at the capacitance, E_J is the Josephson coupling energy, $-e < 0$ is the charge of an electron, $[\phi, Q] = i\hbar$, and I_x is the external current bias, which is assumed to be constant. Here we assumed the symmetric charging energy $Q^2/(2C)$, i.e., Q and $-Q$ are equivalent. We will discuss the consequences of the asymmetric charging energy later.

Eq. (3.4) can be regarded as the Hamiltonian of a particle under the tilted cosine type potential with the period $\delta\phi = \pi\hbar/e$, where Q and ϕ represent the momentum and the position, respectively. When I_x is small, near the local minimum, the potential energy can be approximated by the one of the harmonic oscillator where the mass $m = C$ and the characteristic frequency $\omega = (2e/\hbar)\sqrt{E_J/C}$. Then, the width of the wavefunction is given by $\Delta\phi = \sqrt{\hbar/(m\omega)}$, and the overlap of the wavefunction between the adjacent minima is negligible when $\Delta\phi \ll \delta\phi \Leftrightarrow E_J/E_Q \gg 1$ (case (I)), and large when $\Delta\phi \gg \delta\phi \Leftrightarrow E_J/E_Q \ll 1$ (case (II)), where $E_Q = e^2/(2C)$. We also include the resistive shunt, and the Josephson circuit we will discuss is schematically shown in Fig. 3.2.

In the case (I), ϕ is well-localized inside the minima, and including the resistive shunt, the dynamics is described by the semiclassical Josephson equation given by [2]

$$\hbar\dot{\varphi} = 2eV, \tag{3.5}$$

$$\dot{Q}|_{\text{cap.}} + I_c \sin\varphi + \frac{V}{R} = I_x, \tag{3.6}$$

where $I_c = 2eE_J/\hbar$, $Q|_{\text{cap.}}$ is the charge accumulated at the capacitance, V is the chemical potential (voltage) drop, and R is the shunt resistance. Here we neglected the quantum decay probability, which is known [52] to be expressed as $P \propto \exp[-AE_J/(\hbar\omega)] = \exp[-A\sqrt{E_J/(8E_Q)}]$ at zero temperature in the dissipationless case, where A is the constant factor. We note that the dissipation further suppresses the quantum decay probability [52].

In the absence of the capacitance, i.e., $\dot{Q}|_{\text{cap.}} = 0$, the $I_x - V$ characteristic is solved easily to be $V = 0$ for $|I_x| < I_c = 2eE_J/\hbar$ and the time-averaged voltage $\bar{V} = \text{sign}(I_x)R\sqrt{I_x^2 - I_c^2}$ for $|I_x| > I_c = 2eE_J/\hbar$. Therefore, there occurs no nonreciprocal response in this case. In the presence of the capacitance C, i.e., $Q|_{\text{cap.}} = CV$, the differential equation becomes second order, i.e., the inertia term appears, which results in the coexistence of the two solutions for a range of I_x and hysteresis behavior of $I_x - V$ characteristic, see Fig. 3.3B, blue curve. We will numerically show that, in this case, the nonreciprocal $I_x - V$ curve is realized if we include the effect of the asymmetry coming from $\dot{Q}|_{\text{cap.}}$. To understand why $\dot{Q}|_{\text{cap.}}$ term is necessary for the nonreciprocal effect, here we discuss the inversion symmetry, $\mathcal{P}$, and the time reversal symmetry, $\mathcal{T}$, of Eqs. (3.5) and (3.6), in the absence of $\dot{Q}|_{\text{cap.}}$ term. $\mathcal{T}$ transforms $I_x \to -I_x$, $\varphi \to -\varphi$,

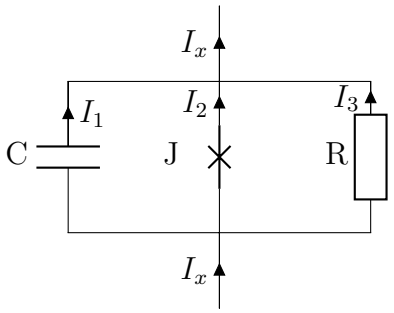

Figure 3.2: **The Josephson circuit.** The Josephson circuit, where C, J and R represent the capacitor, the Josephson junction, and the resistive shunt, respectively.

while $V \to V$ as we can see from Eq. (3.5). Note here that the last term on the l.h.s. of Eq. (3.6) changes sign when $\mathcal{T}$ is applied, although V is even with respect to $\mathcal{T}$. This is usual since $1/R$ represents the dissipation and irreversiblity, and introduces the asymmetry between the two directions of time. As for the inversion symmetry $\mathcal{P}$, on the other hand, the transformation gives $I_x \to -I_x$, $\varphi \to -\varphi$, and $V \to -V$ since the two superconductors are exchanged. Therefore, the nonreciprocal response, it it exists, comes from the term $\dot{Q}|_{\text{cap.}}$ in Eq. (3.6) when the spatial inversion symmetry $\mathcal{P}$ is broken.

In the case (II), since the cosine potential is small, Q is almost the good quantum number. In the same spirit as the nearly free electron approximation, $E_J(1-\cos[2e\phi/\hbar])$ term in the Hamiltonian can be treated perturbatively, and it leads to the Bragg reflection and opens up a gap at the momentum $Q = \pm\hbar\pi/\delta\phi = \pm e$. The size of the gap is proportional to E_J, and the energy at Brillouin zone edge is E_Q, so the dimensionless quantity E_J/E_Q is roughly the ratio of the bandgap to the bandwidth. The last term in Eq. (3.4) can be regarded as the potential coming from the external electric field $E = I_x$, and, including the dissipation term, the dynamics is described by

$$\frac{dQ}{dt} = I_x - \frac{1}{R}\frac{\partial \tilde{E}_{ch}(Q)}{\partial Q}, \tag{3.7}$$

where $\tilde{E}_{ch}(Q)$ is the band energy with the gap at $Q = \pm e$.

In the present work, we study theoretically the nonreciprocal nature of I_x-V characteristics of the asymmetric Josephson junction, which is modeled by the asymmetric charging energy $E_{ch}(Q)(\neq E_{ch}(-Q))$. We will show that, both for case (I) and case (II), the asymmetry of $E_{ch}(Q)$ leads to the nonreciprocity.

Before getting into the detailed analysis, here we discuss the origin of the asymmetric charging energy. The capacitance of small junction system originates from two contributions: One is the classical capacitance, determined by the electrostatic energy inside the thin film, and the other one is the quantum capacitance, which depends on the property of the charge response of two sandwiching bulk systems [99–103]. Among these two contributions, the latter one is in general nonlinear. In the discussion section, we will estimate the order of the quantum capacitance in real systems and discuss how to experimentally measure the nonreciprocity.

3.2 Purpose and assumptions of the model

The purpose of our work is to clarity that the nonreciprocity is present in the usual Josephson junction system if the charge response property of the left/right superconductor is different. Quantitatively, the nonreciprocity is caused by the nonlinearity of the charging energy. We will estimate the charging energy for the realistic system and discuss that it is possible to detect the nonreciprocity by 2ω measurement.

There are three experimental parameters which affects the behavior of the dynamics of ϕ and $I-V$ curve: The shunt resistance R, the capacitance C, and the Josephson energy E_J. We ignore the quasiparticle tunneling, which is suppressed exponentially at low temperature because of the superconducting gap.

The quasiparticle tunneling and the shunt can be regarded as the parallel circuit, so if the tunneling conductance is comparable or large relative to the shunt conductance, we cannot ignore the effect of quasiparticle tunneling. Experimentally, this happens if the temperature is comparable to or larger than the superconducting gap, and also the shunt conductance is small, i.e., if the junction structure is S-I-S type rather than S-N-S. We do not consider this case in our work. However, we note that our theory is still applicable to S-I-S junction if the temperature is small enough.

The capacitance C and the Josephson energy $E_J \propto I_c$ are both proportional to the junction area S. Those parameters determine the two dimensionless quantities, $E_J/E_Q = 2CE_J/e^2$ and $r = R\sqrt{(2eCI_c)/\hbar}$. E_J/E_Q is proportional to S^2, and is large for large junctions. Therefore, our model (I) is applicable to the large junctions, while our model (II) is applicable to the small junctions. r is proportional to RS, so its smallness depends on the shunt resistance. Our theory for model (I) predicts the nonreciprocity for the system with $r \gg 1$, so the larger junction and/or the large shunt resistance is better suited for the measurement of the nonreciprocity.

We will estimate the nonlinear capacitance using the Thomas-Fermi approximation [102, 103], and show that the 2ω signal $V_{2\omega} \sim 10$nV is expected for the usual Josephson junction system. This can be measured in the current experimental technology.

3.3 Models

Model for case (I)

The dc Josephson effect is described by the constant φ, Q and $V = 0$, where φ is determined by $I_x = \frac{2eE_J}{\hbar}\sin\varphi = I_c \sin\varphi$. For $|I_x| > I_c$, there is no solution for constant φ and the voltage V appears. In this picture, I_c is identical for both directions, while one needs to solve the dynamics, i.e., the time dependence, of Q and φ when finite voltage appears. In this case, the functional form of $E_{ch}(Q)$, which is related to the voltage V by $V = \frac{\partial E_{ch}}{\partial Q}$, is important. Often the form $E_{ch}(Q) = Q^2/(2C) - V_g Q$ is taken with C being the capacitance and V_g the gate voltage. This seems to break the symmetry between right and left, i.e., Q and $-Q$, but the shift in the origin of Q recovers that symmetry. Therefore, the essential asymmetry between right and left comes from the higher order terms in Q such as

$$E_{ch} = \frac{Q^2}{2C} + \alpha Q^3 + \alpha' Q^4. \tag{3.8}$$

Then we consider the following generalized Josephson equation as

$$\frac{\hbar}{2e}\dot{\varphi} = \frac{\partial E_{ch}}{\partial Q}, \quad \dot{Q} = I_x + \tilde{I}(t) - I_c \sin\varphi - \frac{1}{R}\frac{\partial E_{ch}}{\partial Q}, \tag{3.9}$$

where we added the fluctuating current $\tilde{I}$ satisfying $\langle \tilde{I}(t)\tilde{I}(t')\rangle = 2(\beta R)^{-1}\delta(t-t')$, to discuss the finite temperature system.

It is useful to rewrite Eqs. (3.8) and (3.9) with the dimensionless parameters $\tilde{i} = \tilde{I}/I_c$, $i_x = I_x/I_c$, $r^{-1} = R^{-1}\sqrt{\hbar/(2eCI_c)}$, $A = \alpha C^{3/2}\sqrt{E_J}$, $A' = \alpha' C^2 E_J$ and $\tilde{T}^{-1} = E_J\beta$. Also,

we rescale t and Q as $\tau = t\sqrt{2eI_c/(\hbar C)}$ and $q = \sqrt{2e/(\hbar C I_c)}Q$. Then, Eq. (3.9) becomes

$$\frac{d\varphi}{d\tau} = \frac{\partial \epsilon_{ch}}{\partial q}, \quad \frac{dq}{d\tau} = i_x + \tilde{i}(t) - \sin\varphi - r^{-1}\frac{\partial \epsilon_{ch}}{\partial q}, \tag{3.10}$$

where

$$\epsilon_{ch} = \frac{q^2}{2} + Aq^3 + A'q^4. \tag{3.11}$$

Let us discuss here the analogy of Eq. (3.10) with the particle motion under the periodic potential. The Josephson phase φ corresponds to the position x, while the charge transfer q to the momentum p. In this particle picture, the potential energy is $-\cos x$ and the kinetic energy is $\epsilon_{ch}(q \to p)$. In this sense, one can define the "time-reversal symmetry" $\mathcal{T}'$ and "inversion symmetry" $\mathcal{P}'$ as

$$\begin{aligned} &\mathcal{T}' : x \to x, p \to -p, \\ &\mathcal{P}' : x \to -x, p \to -p. \end{aligned} \tag{3.12}$$

Then, our system breaks both $\mathcal{P}'$ and $\mathcal{T}'$, while it preserves $\mathcal{P}'\mathcal{T}'$ except the dissipative term in Eqs. (3.9) and (3.10). Namely, the periodic potential is inversion symmetric, while the kinetic energy is asymmetric with respect to p and $-p$. In the quantum mechanical case, this leads to the asymmetric dispersion $\varepsilon(k) \neq \varepsilon(-k)$.

We will discuss the nonreciprocity of Eq. (3.10) with Eq. (3.11) for two cases: First, we discuss the system with no thermal fluctuation, at $T = 0$. For $|i_x| > 1$, where the bias is so strong that the potential barrier disappears, the dynamics is characterized by the limit cycle in (φ, q) space. For $|i_x| < 1$ and sufficiently small r^{-1}, there coexists the stable fixed point and the limit cycle [104, 105], which represents the metastable steady state. Secondly, we discuss the system with thermal fluctuation at finite temperature $T > 0$, where the phase slip is caused by the thermal fluctuation [106, 107]. In both cases, we will show that the asymmetry of the charging energy leads to the nonreciprocity.

Here we note that, since the voltage drop V in the presence of A satisfies $V(A, -i_x) = -V(-A, i_x)$, the nonreciprocity characterized by $V_{\rm asym} = [V(A, i_x)+V(A, -i_x)]/[V(A, i_x)-V(A, -i_x)]$ can be rewritten as $[V(A, i_x) - V(-A, i_x)]/[V(A, i_x) + V(-A, i_x)]$, so we calculate the voltage drop $V(A, i_x)$ for positive i_x and change the sign of A. We set the parameters $A = \pm 0.6$ and $A' = 0.3$ in the following.

Model for case (II)

As we mentioned in section 3.1, the dynamics in this case is governed by Eq. (3.7), and E_J/E_Q characterizes the ratio of the band gap to the bandwidth, see Fig. 3.12C.

In this case, because of the periodicity of the Brillouin zone, the system starts to exhibit Bloch oscillation, which affects the $I_x - V$ curve in a substantial way [108, 109]. Physically, the Bloch oscillation in Q space corresponds to the cooper pair tunneling through the Josephson junction [108], and it reduces the current flowing through the resistive shunt, so the voltage drop V is suppressed. The Bloch oscillation is hindered by the Zener tunneling process where the state is excited to higher energy bands, and

$I_x - V$ curve is determined by the competition between the Bloch oscillation and the Zener tunneling process [109–111].

For the discussion of Bloch oscillation, for simplicity, we work in the lowest order approximation in E_J, i.e., we neglect the gap at Brillouin zone boundary but assume the periodic structure of the energy dispersion, $\tilde{E}_{ch}$, i.e.,

$$\tilde{E}_{\rm ch}(Q) = \min_{n\in\mathbb{Z}} E_{\rm ch}(Q - 2ne). \tag{3.13}$$

Setting $Q = e\tilde{q}$, $t = RC\tilde{\tau}$, $I_x = \tilde{i}_x e/(RC)$, Eq. (3.7) becomes

$$\frac{d\tilde{q}}{d\tilde{\tau}} = \tilde{i}_x - \frac{\partial\tilde{\epsilon}}{\partial\tilde{q}}, \tag{3.14}$$

where

$$\tilde{\epsilon}(\tilde{q}) = \min_{n\in\mathbb{Z}} E'_{ch}(\tilde{q} - 2n), \quad E'_{\rm ch}(\tilde{q}) = \frac{\tilde{q}^2}{2} + \tilde{A}\tilde{q}^3 + \tilde{A}'\tilde{q}^4, \tag{3.15}$$

where $\tilde{A} = \alpha Ce$, $\tilde{A}' = \alpha' Ce^2$. We set $\tilde{A} = 0.6$ and $\tilde{A}' = 0.3$ in the following.

3.4 Results

Nonreciprocal $I_x - V$ curve at $T = 0$ for case (I)

In Fig. 3.3 (blue curves), we show the $I_x - V$ curve for the system without the $\dot{Q}|_{\rm cap.}$ term (panel A) and the system with $\mathcal{P}$ breaking $\dot{Q}|_{\rm cap.}$ term (panel B) at $T = 0$. As we mentioned in the background section, the nonreciprocity is realized only for the latter system, see panel C.

An important feature of $I_x - V$ curve at $T = 0$ with finite $\dot{Q}|_{\rm cap.}$ (Fig. 3.3B, blue curve) is the hysteresis at $i^R_{c1} < i_x < i_{c3}$ and $-i^L_{c3} < i_x < -i^L_{c1}$. This comes from the coexistence of the limit cycle and the stable fixed point [104, 105]. As can be seen from Figs. 3.4B and C, because of the presence of the limit cycle, for the initial condition inside the dark blue region, the stationary state at long time is governed by the limit cycle so that the finite voltage drop results. On the contrary, for the initial condition inside the green region, the particle is attracted to the fixed point and the voltage drop is zero. Sweeping i_x from the large value to the small value corresponds to the former case, while sweeping i_x from the small value to the large value corresponds to the latter case. Namely, the hysteresis behavior occurs. On the contrary, there exists no hysteresis for $I_x - V$ curve at $T = 0$ without $\dot{Q}|_{\rm cap.}$ term (Fig. 3.3A, blue curve).

Here we review the qualitative aspect of the bifurcation of limit cycle in the system with $T = 0$ [104, 105] for $i_x > 0$. The system shows qualitatively different behavior depending on the value of the dissipation strength r, defined above Eq. (3.10).

For $r^{-1} \gg 1$ (Fig. 3.3A), we can neglect the inertia term (the capacitance)[2] and the equation becomes

$$r^{-1} d\varphi/d\tau = i_x - \sin\varphi. \tag{3.16}$$

[2]This approximation is called "overdamped approximation" in the literature. This is the first order term of the systematic γ^{-1} expansion as we will discuss in Appendix B.1. We will also show that, up to the third order terms, the system does not exhibit nonreciprocity.

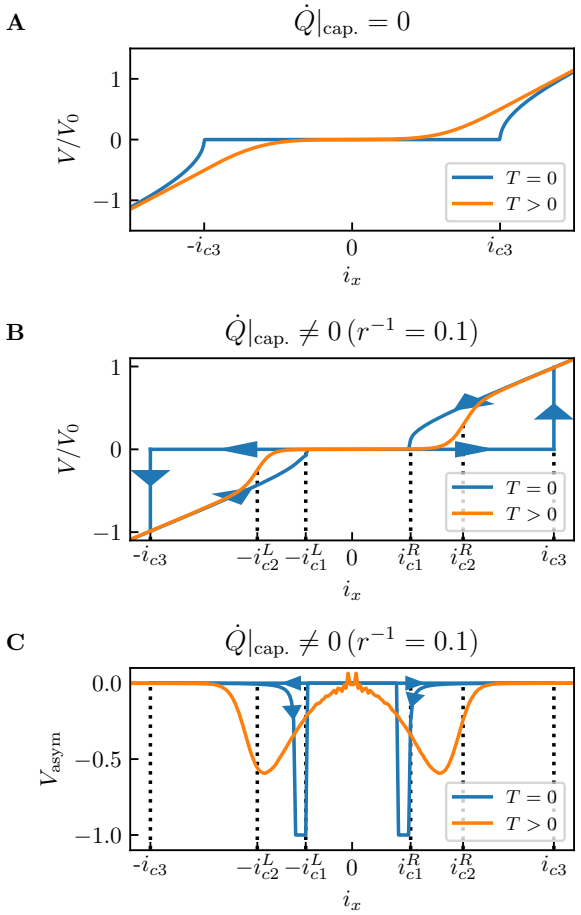

Figure 3.3: $I_x - V$ curve for case (I) at $T = 0$ and $T > 0$. $I_x - V$ curve calculated by the classical Langevin equation (3.10) and (3.11) (case (I)), for the system (**A**) without $\dot{Q}|_{\text{cap.}}$ term and (**B** and **C**) with $\dot{Q}|_{\text{cap.}}$ term (for the definition of r^{-1}, see Eq. (3.10)), where $i_x = I_x/I_c$ and $V_0 = RI_c$ with $I_c = 2eE_J/\hbar$. In (**C**), we show $V_{\text{asym}}(i_x) = [V(i_x) + V(-i_x)]/[V(i_x) - V(-i_x)]$ which quantifies the degree of nonreciprocity calculated from the $I_x - V$ curve (**B**). We note that $V_{\text{asym}} = 0$ identically for the $I_x - V$ curve (**A**), i.e., when $\dot{Q}|_{\text{cap.}} = 0$. The arrows on blue curves represents the direction of the sweep of i_x. We set $\tilde{T} = 0.25$ for $T > 0$ data, i.e., for orange curves, and $A = 0.6$, $A' = 0.3$ in Eqs. (3.10) and (3.11).

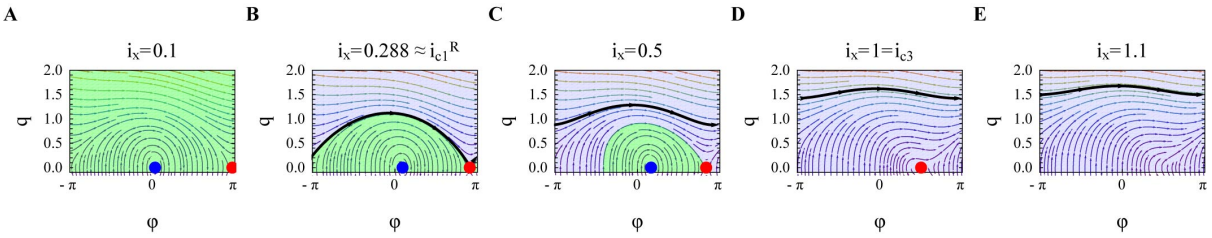

Figure 3.4: The bifurcation of the system with $\dot{Q}|_{\text{cap.}} \neq 0$. The bifurcation of the system with finite capacitance, Eqs. (3.10) and (3.11). We set $A = 0.6$, $A' = 0.3$, $r^{-1} = 0.1$ and (**A**) $i_x = 0.1$, (**B**) $i_x = 0.288 \cong i_{c1}^R$, (**C**) $i_x = 0.5$, (**D**) $i_x = 1 = i_{c3}$ and (**E**) $i_x = 1.1$. The blue and red dots represent the stable fixed point and the saddle point, respectively. Black curves are (meta)stable limit cycle, and the green and dark blue regions are the basins of attraction of the stable fixed point (blue dot) and the limit cycle (black curve), respectively. We present the case of positive i_x, while the behavior is similar also for $i_x < 0$. However, the critical i_{c1}^L is different from i_{c1}^R.

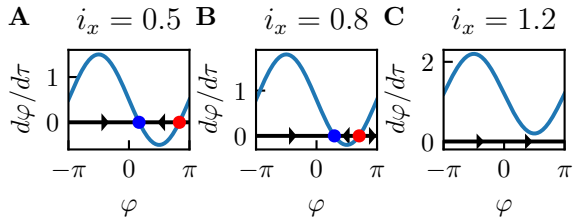

Figure 3.5: The bifurcation of the system with $\dot{Q}|_{\text{cap.}} = 0$. The bifurcation of the system with $\dot{Q}|_{cap} = 0$, Eq. (3.16) for (**A**) $i_x = 0.5$, (**B**) $i_x = 0.8$ and (**C**) $i_x = 1.2$. The blue curve represents $d\varphi/d\tau$ and the arrow on the black curve represents the direction of the velocity. The blue and red dots represent the stable fixed point and the saddle point, respectively. We can see that the limit cycle disappears for $i_x < 1$.

For $i_x > 1$, $d\varphi/d\tau > 0$ and there is only a limit cycle (Fig. 3.5C). At $i_x = i_{c3} = 1$, the saddle-node (blue-sky) bifurcation leads to the vanishing of the limit cycle and the birth of the stable and unstable fixed points at $\varphi = \sin^{-1} i_x$ and $\pi - \sin^{-1} i_x$ for $i_x < 1$, respectively, see Figs. 3.5 B and C. For $i_x < 1$, the long time dynamics is governed by the stable fixed point, see Figs. 3.5A and B. Therefore, in this case the disappearance of the limit cycle and the birth of the stable fixed point occur simultaneously, i.e., $i_{c1}^R = i_{c3} = 1$. Above i_{c3}, the flow of φ occurs, and the time-average of $d\varphi/d\tau$ gives that of the voltage drop $\bar{V} = \text{sign}(I_x) R\sqrt{I_x^2 - I_c^2}$ as we mentioned in the introduction.

For $r^{-1} \ll 1$ (Fig. 3.3B), we cannot neglect the inertia term (the capacitance) and the bifurcation mentioned above splits into two bifurcations. One is at $i_x = i_{c3} = 1$, where the saddle-node bifurcation leads to the birth of the stable fixed point and the saddle point at $(\varphi, q) = (\sin^{-1} i_x, 0)$ and $(\pi - \sin^{-1} i_x, 0)$, as is shown in Figs. 3.4 C, D and E; The other one is the homoclinic bifurcation at $i_x = i_{c1}^R$, where the limit cycle collides with the saddle point at $(\varphi, q) = (\pi - \sin^{-1} i_x, 0)$ to become the homoclinic orbit and then disappears, as is shown in Figs. 3.4A and B. We will review what a homoclinic orbit is

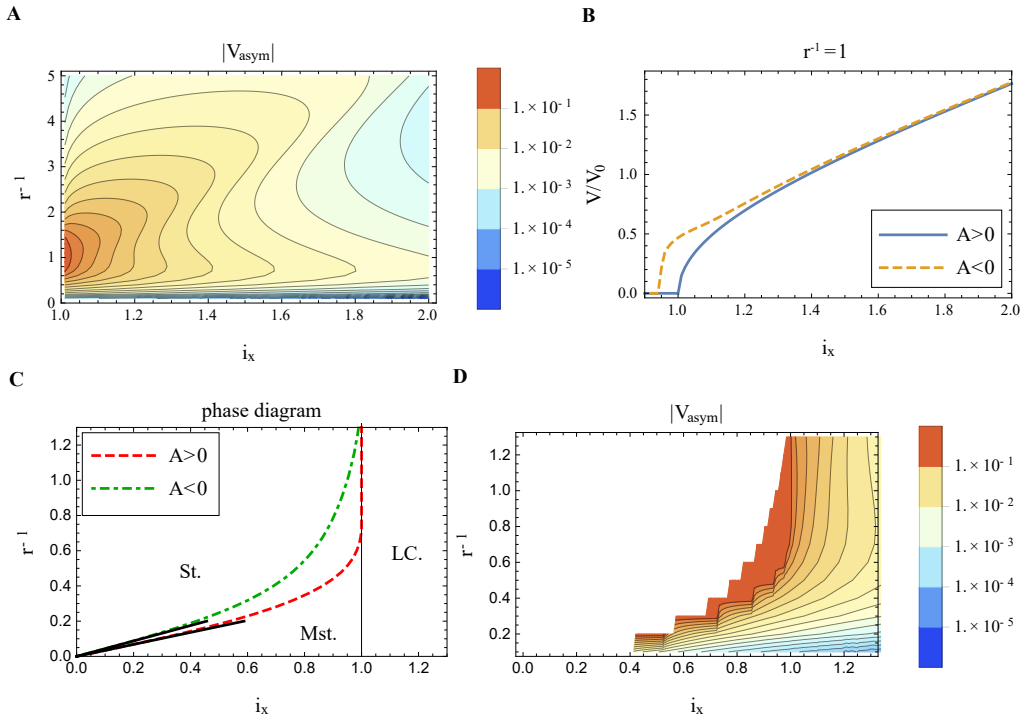

Figure 3.6: Nonreciprocity for various i_x and r^{-1} for case (I) at $T = 0$. (**A**) $V_{\rm asym}(i_x) = [V(i_x) + V(-i_x)]/[V(i_x) - V(-i_x)]$ as a function of i_x and r^{-1} calculated by Eqs. (3.10) and (3.11) with $\tilde{T} = 0$. (**B**) The voltage drop V/V_0 where $V_0 = RI_c$ for $A > 0$ and $A < 0$ with $r^{-1} = 1$ and $\tilde{T} = 0$ in Eqs. (3.10) and (3.11). Here $V_{\rm asym} < 0$ for the parameter region shown in (**A**). (**C**) The phase diagram in (i_x, r^{-1}) space for Eqs. (3.10) and (3.11) with $\tilde{T} = 0$. St., Mst. and LC. represent the phase with stable fixed point only, stable fixed point coexisting with limit cycle, and limit cycle only, respectively. The black curves are the phase boundary calculated from Eq. (3.17). (**D**) $V_{\rm asym}(i_x) = [V(i_x) + V(-i_x)]/[V(i_x) - V(-i_x)]$ near the phase boundary, where $V(i_x)$ is calculated for the metastable limit cycle of Eqs. (3.10) and (3.11) with $\tilde{T} = 0$, i.e., the plot corresponds to the sweeping of i_x from the large value in Fig. 3.3D. $V_{\rm asym} < 0$ for the parameter region shown in (**B**).

and discuss its role in the phase diagram later. As for the bifurcations for $i_x < 0$, the qualitative nature of the bifurcations are the same, but importantly, $i_{c1}^L \neq i_{c1}^R$ because of the asymmetry of the charging energy. It leads to the enhancement of $V_{\rm asym}$ near i_{c1}^L and i_{c1}^R as can be seen in Fig. 3.3C.

Nonreciprocity for various i_x and r^{-1} at $T = 0$ for case (I)

For $|i_x| > 1$, $V_{\rm asym}$ as a function of i_x and r^{-1} is shown in Fig. 3.6A. We can see that the nonreciprocity is enhanced for small i_x and r^{-1}. Since $|i_x| > 1$, the dynamics is governed by the limit cycle traversing from $\varphi = -\pi$ to π at finite q as is shown in Figs. 3.7A and B. As we can see, finite A modifies the limit cycle and leads to the asymmetry.

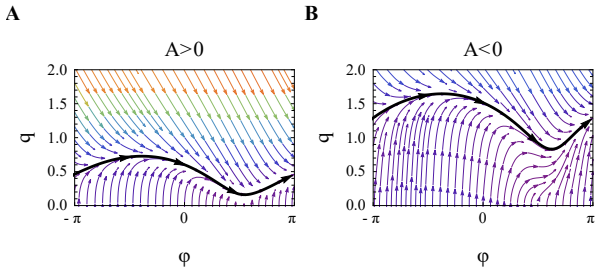

Figure 3.7: The limit cycle for $i_x > 1$. The limit cycle, shown by black curves with Eqs. (3.10) and (3.11) for $i_x = 1.2$, $r^{-1} = 1$, and (**A**) $A > 0$ and (**B**) $A < 0$.

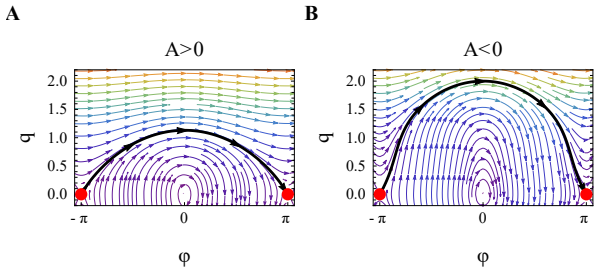

Figure 3.8: The homoclinic orbit for $i_x = r^{-1} = 0$. The homoclinic orbit (black curves) at $r^{-1} = i_x = 0$ for (**A**) $A > 0$ and (**B**) $A < 0$ in Eqs. (3.10) and (3.11). The red dots represent the fixed point. Note that $(\varphi, q) = (\pi, 0)$ and $(-\pi, 0)$ are equivalent.

For $|i_x| < 1$, the homoclinic bifurcation occurs at i_{c1}^R and $-i_{c1}^L$. As we explained in the last section, at this bifurcation point the limit cycle becomes the homoclinic orbit. In short, a homoclinic orbit is a variant of a limit cycle. However, in contrast to a limit cycle, there exists a fixed point on it, so its time period is infinite, since it takes infinite time to reach and depart from the fixed point. For example, the black curves in Figs. 3.4B and 3.8A and B are homoclinic orbits where the fixed point is shown by red dots. In our case, the presence of the homoclinic orbit indicates the homoclinic bifurcation, so by identifying the parameter where there exists a homoclinic orbit on the (i_x, r^{-1}) plane, we can identify the phase boundary.

For small i_x and r^{-1}, we can perturbatively calculate the phase boundary from the parameter point $i_x = r^{-1} = 0$, where we can analytically obtain the homoclinic orbit, see Figs. 3.8A and B. For that, we calculate the simple zero of the following Melnikov function [112]:

$$\begin{aligned}&\int_{-\infty}^{\infty} dt \dot{\varphi}_0(t)(i_x - r^{-1}\dot{\varphi}_0(t)) \\ =&2\pi i_x - 2r^{-1}\int_0^{q_{\max}} dq \left(\frac{d\epsilon_{ch}(q)}{dq}\right)^2 \frac{1}{\sqrt{\epsilon_{ch}(q)[2-\epsilon_{ch}(q)]}},\end{aligned} \tag{3.17}$$

where $\varphi_0(t)$ is the homoclinic orbit for $i_x = r^{-1} = 0$ shown in Fig. 3.8, and $q_{\max}$ is the maximum of q along the orbit. As we can see, the homoclinic orbit for $A > 0$ (Fig. 3.8A, black curve) and $A < 0$ (Fig. 3.8B, black curve) is quite different and that leads to the

difference of the Melnikov function and the phase boundary in two cases. In Fig. 3.6C, we show the phase boundary obtained from direct numerical calculation (red dotted and green dot-dashed curves) and the one obtained from the condition that Eq. (3.17) should be zero (black solid curve). We can see that the prediction of Eq. (3.17) agrees well with the numerically obtained boundary for small i_x and r^{-1}. For (i_x, r^{-1}) such that metastable limit cycle does exist for $A < 0$ but not for $A > 0$, we observe very large $|V_{\rm asym}|$, as is shown in Fig. 3.6D, since the time-averaged velocity $\overline{d\varphi/d\tau} = 0$ for $A > 0$ but $\overline{d\varphi/d\tau}$ is finite for $A < 0$. We also note that the large $|V_{\rm asym}|$ for $i_x \gtrsim 1$ (Fig. 3.6A) can be understood as a consequence of the difference of i_{c1} for $A > 0$ and $A < 0$: As we can see from Fig. 3.6B, the voltage drop V is larger at $i_x \gtrsim 1$ for $A < 0$, because i_{c1} is smaller for $A < 0$.

Nonreciprocal $I_x - V$ curve at finite temperature $T > 0$ for case (I)

For the finite temperature $T > 0$ case, we numerically simulated the Langiven equation Eq. (3.9) with stochastic Heun's scheme [113] to calculate the physical quantities and then took an ensemble average. Numerically calculated $I_x - V$ curve is shown in Fig. 3.3 (orange curves). As is shown in Fig. 3.3B, we can see that the voltage drop V suddenly increases around i_{c2}^R and $-i_{c2}^L$ and merges to the curve $V/V_0 = i_x$. This behavior can be understood as the dynamical transition, from the state where the dominant probabilistic weight is on the stable fixed point so that the voltage drop is around zero, to the one where the limit cycle is primarily realized and the finite voltage drop results [114, 115]. Since the system is at the finite temperature, the transition is not sharp, but as $T \to +0$ this transition becomes sharper and sharper and the jump of V from 0 to finite value occurs at $i_x = i_{c2}^R$ and $-i_{c2}^L$ when $T = +0$. At the same time, the relaxation time between the two configurations diverges as $T \to +0$, and when the experimental measurement time is shorter than the relaxation time, we observe the hysteresis behavior as we discussed above for $T = 0$ case. In the similar manner to $T = 0$ case, the large $V_{\rm asym}$ near i_{c2}^R and $-i_{c2}^L$ is realized because $i_{c2}^R \neq i_{c2}^L$.

Nonreciprocity for various i_x and r^{-1} at $T > 0$ for case (I)

We numerically calculated the nonreciprocity for various i_x and r^{-1}, and the result of the numerical calculation is shown in Fig. 3.9.

As we can see, the nonreciprocity is enhanced for small r^{-1}, i.e., small dissipation, region. This is consistent with the fact that, for $r^{-1} \gg 1$, we can neglect the inertia term in Eq. (3.10) to obtain the usual inversion-symmetric overdamped Langevin equation[3]. In addition, we can see the peak structure at finite value of i_x for fixed r^{-1}. To understand this behavior, it is useful to plot the normalized mobility $r^{-1}\mu = V/(V_0 i_x)$, where $V_0 = RI_c$, as a function of i_x [114], see Fig. 3.10A. We can see that for small i_x, the mobility is almost zero, but at some finite i_x the mobility jumps to $\mu = r$ and saturates. This

[3]For the derivation, see Appendix B.1. We will also show that up to third order terms in γ^{-1}, the system does not exhibit nonreciprocity.

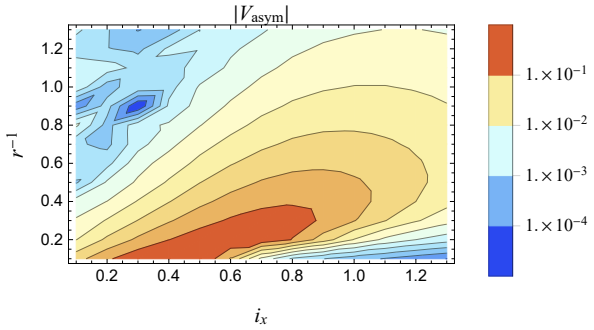

Figure 3.9: Nonreciprocity for various i_x and r^{-1} for case (I) at $T > 0$. $V_{\rm asym}(i_x) = [V(i_x)+V(-i_x)]/[V(i_x)-V(-i_x)]$ at finite temperature. For the parameter region shown in the plot, $V_{\rm asym} < 0$. We used Eqs. (3.10) and (3.11) with $\tilde{T} = 0.25$.

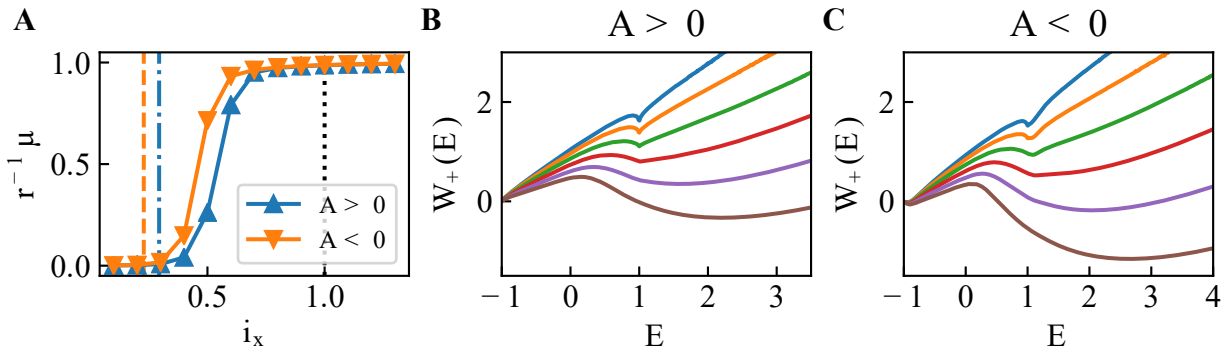

Figure 3.10: Normalized mobility and distribution function for case (I) at $T > 0$. (**A**) Normalized mobility $r^{-1}\mu$, where $r^{-1}\mu = V/(V_0 i_x)$ and $V_0 = RI_c$, as a function of i_x for fixed r^{-1}. The value where the limit cycle appears is shown by the dot-dashed blue and the dashed orange curves, and the value where the stable fixed point vanishes is shown by black dotted curve. (**B** and **C**) $W_+(E)$ from $i_x = 0.1$ (blue curve) to $i_x = 0.6$ (brown curve), for $A > 0$ and $A < 0$. The parameters are set to be $r^{-1} = 0.1$, $\tilde{T} = 0.25$ in Eqs. (3.10) and (3.11).

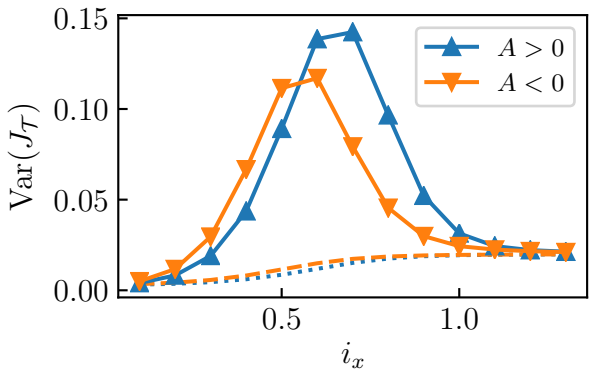

Figure 3.11: Variance of $J_\mathcal{T} = \int_0^\mathcal{T} d\tau \frac{d\varphi}{d\tau}$ for case (I) at $T > 0$. Variance of $J_\mathcal{T}$ as a function of i_x. The blue dotted and orange dashed curves are the lower bound predicted by the thermodynamic uncertainty relation, $\mathrm{Var}(J_\mathcal{T}) \geq 2\langle J_\mathcal{T}\rangle^2/(\mathcal{T}\sigma)$, where σ is the entropy production rate and is calculated as $\sigma = i_x\langle J_\mathcal{T}\rangle/\tilde{T}$ [116]. We numerically simulated the Langevin equation (3.10) and (3.11) for 100 ensembles with time $\tau = 10^7$ and $\Delta\tau = 10^{-2}$ by the stochastic Heun scheme, and set $\mathcal{T} = 1000$. The parameters are set to be $r^{-1} = 0.1$, $\tilde{T} = 1$.

kind of behavior can be understood from the distribution function of the energy $W_\pm(E)$, defined as

$$P(E) = \begin{cases} \mathcal{N}_+ e^{-W_+(E)/\tilde{T}} & (q \geq 0) \\ \mathcal{N}_- e^{-W_-(E)/\tilde{T}} & (q < 0) \end{cases}, \; E = \epsilon_{ch}(q) - \cos\varphi. \tag{3.18}$$

where $\mathcal{N}_{+/-}$ is the normalization factor, $P(E)$ is the distribution function of E, and we introduced two functions W_+ and W_-, corresponding to the two branches of momentum q as a function of the energy E [114]. Numerically calculated $W_+(E)$ for $A > 0$ and $A < 0$ is shown in Figs. 3.10B and C. We can see that, as we increase the bias i_x, $W_+(E)$ at large E becomes small and eventually the local minimum at $E > 1$ drops below the value at $E = -1$. This corresponds to the dynamical transition of the typical trajectory from the static one at $E = -1$ to the running one at $E > 1$. We can see that the critical value of i_x which we denote i_{c2}, where this transition occurs is different for $A > 0$ case ($i_{c2} \sim 0.6$) and $A < 0$ case ($i_{c2} \sim 0.5$). The fact that i_{c2} is larger for $A > 0$ is consistent with the larger i_{c1} where the limit cycle emerges, as is shown by blue dot-dashed and orange dashed curves in Fig. 3.10A.

Because of the presence of the thermal fluctuation, we can discuss not only the average value of the velocity, but also the whole distribution of the time-averaged current $J_\mathcal{T} = \int_0^\mathcal{T} d\tau \frac{d\varphi}{d\tau}$ [116]. The numerically calculated variance is shown in Fig. 3.11. Since the system does not have $\mathcal{T}'$ symmetry (For the definition of $\mathcal{T}'$ and $\mathcal{P}'$ symmetry, see section 3.3), we might have a violation of the lower bound of the variance known as thermodynamic uncertainty relation [116–118], as is observed in the underdamped Langevin system with magnetic field [119], but we did not observe any violation as far as for the parameter regions we have checked. As we can see, the fluctuation of the current becomes large for

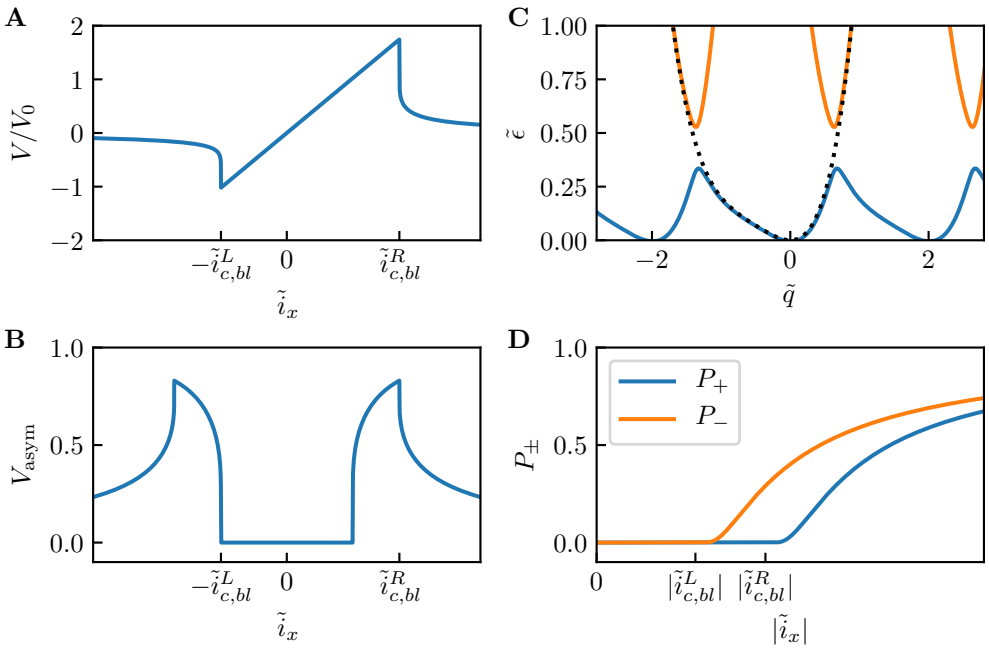

Figure 3.12: $I_x - V$ curve, energy dispersion and nonreciprocal Zener tunneling for case (II). (**A**) $I_x - V$ curve and (**B**) $V_{\rm asym}(\tilde{i}_x) = [V(\tilde{i}_x) + V(-\tilde{i}_x)]/[V(\tilde{i}_x) - V(-\tilde{i}_x)]$ in the presence of the Bloch oscillation, calculated from Eqs. (3.20) and (3.21), where $V_0 = e/C$. (**C**) Energy dispersion of the two lowest energy bands with the asymmetric changing energy $E'_{ch}(\tilde{q}) = \tilde{q}^2/2 + \tilde{A}\tilde{q}^3 + \tilde{A}'\tilde{q}^4$ with $\tilde{A} = 0.6$ and $\tilde{A}' = 0.3$, and we set $E_J/E_Q = 0.2$, where $E_Q = e^2/(2C)$, to open up a gap in the spectrum. Dotted curve represents the energy dispersion without the Josephson coupling term $E_J \cos\varphi$ in the Hamiltonian. (**D**) The LZ rate calculated from Eq. (3.22) with $E_J/E_Q = 0.1$ ($E_Q = e^2/(2C)$) and $R/R_q = 100$.

intermediate i_x. This reflects the fact that there coexists the stationary trajectory and the running trajectory, and these two trajectories, which have quite different average velocities, are probabilistically realized, leading to the large fluctuation of the current. For larger i_x the fluctuation decreases, since the stationary fixed point disappears. Reflecting the difference of the critical current i_{c2}, the region where the current fluctuation enhances is different for $A > 0$ and $A < 0$ cases, and that leads to quite different current fluctuation as we can see in Fig. 3.11.

Nonreciprocal Bloch oscillation for case (II)

First, we will discuss the effect of nonreciprocity in Bloch oscillation in Josephson junction. For the energy dispersion (3.15), denoting the left and right Brillouin zone boundary $\tilde{q}_{L,R}$, the conditions for the Bloch oscillation for $\tilde{i}_x > 0$ and $\tilde{i}_x < 0$ cases can be written as,

$$\tilde{i}_x \geq \frac{\partial\tilde{\epsilon}(\tilde{q}_R)}{\partial\tilde{q}} =: \tilde{i}^R_{c,bl}, \quad \tilde{i}_x \leq \frac{\partial\tilde{\epsilon}(\tilde{q}_L)}{\partial\tilde{q}} =: -\tilde{i}^L_{c,bl}, \tag{3.19}$$

respectively. The periods of the Bloch oscillation for $\tilde{i}_x > 0$ and $\tilde{i}_x < 0$ cases are,

$$\tilde{\tau}_R = \int_{\tilde{q}_L}^{\tilde{q}_R} \frac{d\tilde{q}}{\tilde{i}_x - \frac{\partial\tilde{\epsilon}}{\partial\tilde{q}}}, \quad \tilde{\tau}_L = \int_{\tilde{q}_R}^{\tilde{q}_L} \frac{d\tilde{q}}{\tilde{i}_x - \frac{\partial\tilde{\epsilon}}{\partial\tilde{q}}}. \tag{3.20}$$

The voltage drop can be calculated by Eq. (3.14) as [108]

$$V_{L,R} = \frac{e}{C}\left\langle \frac{\partial\tilde{\epsilon}}{\partial\tilde{q}} \right\rangle = \frac{e}{C}\left(\tilde{i}_x - \frac{2}{\tilde{\tau}_{L,R}}\right). \tag{3.21}$$

We show the voltage drop calculated by Eq. (3.21) in Figs. 3.12A and B. As we can see, since the critical currents where the Bloch oscillation sets in are different for $\tilde{i}_x > 0$ and $\tilde{i}_x < 0$, i.e., $\tilde{i}^R_{c,bl} \neq \tilde{i}^L_{c,bl}$, $I_x - V$ curve exhibits nonreciprocity.

Nonreciprocal Zener tunneling for case (II)

Next, we discuss the nonreciprocity in Zener tunneling rate. The general expression of the Zener tunneling rate was derived in Ref. [110], where the argument is only for the quadratic charging energy. Generalizing their argument to include the asymmetry of the charging energy, we obtain[4]

$$P_\pm = \exp\left[-\left(\frac{\pi E_J}{2E_Q}\right)^2 \frac{R}{R_q}\frac{1}{|V_{C,\pm}||v_\pm|}\right], \quad \left(R_q = \frac{e^2}{2\pi\hbar}\right) \tag{3.22}$$

where we neglected the effect of the fluctuation of the charge. Here

$$V_{C,\pm} = \frac{d}{d\tilde{q}}(E'_{\rm ch}(\tilde{q}) - E'_{\rm ch}(\tilde{q} \mp 2))\Big|_{\tilde{q}=\tilde{q}_R/\tilde{q}_L},$$

and, as we can easily see, $|V_{C,+}| = |V_{C,-}|$. $v_\pm$ is the velocity of the charge at $\tilde{q}_{R,L}$ given by the solution of Eq. (3.14), i.e.,

$$v_\pm = \tilde{i}_x - \frac{\partial\tilde{\epsilon}}{\partial\tilde{q}}\Big|_{\tilde{q}=\tilde{q}_R/\tilde{q}_L} = \tilde{i}_x \mp \tilde{i}^{R/L}_{c,bl}, \tag{3.23}$$

where $\tilde{i}^{R/L}_{c,bl}$ are defined in Eq. (3.19). As we noted $\tilde{i}^R_{c,bl} \neq \tilde{i}^L_{c,bl}$, so $|v_+(\tilde{i}_x)| \neq |v_-(-\tilde{i}_x)|$ and $P_+ \neq P_-$. The Landau-Zener tunneling probability $P_\pm$ obtained from Eq. (3.22) is shown in Fig. 3.12D. We can see the threshold behavior coming from the dissipation [120].

Here we note the importance of the effect of dissipation in obtaining the nonreciprocal Zener tunneling rate. In the present semiclassical approximation, there occurs no quantum tunneling when the classical solution does not reach the band crossing point due to the dissipation. Then the asymmetric threshold current is the origin of the nonreciprocal tunneling rate, and hence the dissipation is required for the nonreciprocity. On the other hand, it was shown in Ref. [80] that the nonreciprocal Landau-Zener tunneling occurs if we have nonzero shift vector even without the dissipation. Here, as we discussed in

[4]For the derivation, see Appendix B.2.

section 3.3, we are considering the system where $\mathcal{P}'$ and $\mathcal{T}'$ is broken by the asymmetry of the dispersion relation, but the system still has $\mathcal{P}'\mathcal{T}'$ symmetry. Then, from the general transformation rule [82], the shift vector is identically zero. Furthermore, we can show that, in the absence of the shift vector, there is no nonreciprocity in the LZ rate even in the presence of the asymmetry in the band energy. To show this, we observe that, in the absence of shift vector, the amplitude for the tunneling process during one cycle of Bloch oscillation under the electric field $E = -E_x < 0$ is given as [80],

$$a_+^{(-E_x)} = ie^{i\arg A_{+-}(-\pi)} \int_{-\pi}^{\pi} dk_1 |A_{+-}|(k_1) e^{-i\int_{-\pi}^{k_1} dk_2 \frac{\Delta(k_2)}{-eE_x}}, \tag{3.24}$$

where $A_{+-} = \langle u_+|\partial_k|u_-\rangle$, $|u_\pm\rangle$ is the wavefunction for upper/lower band, and $\Delta(k)$ is the k dependent difference of the upper band energy and the lower band energy. Although the standard estimation utilizes the integration path in the complex k plane, here we only consider the integration path on the real k line. From Cauchy's theorem, this does not spoil any generality of our result. Then, the expression for the reverse process with the electric field $E = E_x > 0$ is given as,

$$a_+^{(E_x)} = ie^{i\arg A_{+-}(\pi)} \int_{\pi}^{-\pi} dk_1 |A_{+-}|(k_1) e^{-i\int_{\pi}^{k_1} dk_2 \frac{\Delta(k_2)}{eE_x}},$$

By taking the complex conjugate of Eq. (3.24), we can show that $\left(a_+^{(-E_x)}\right)^* = e^{i\chi} a_+^{(E_x)}$, where

$$\chi = -\arg A_{+-}(-\pi) - \arg A_{+-}(\pi) - \int_{-\pi}^{\pi} dk_2 \frac{\Delta(k_2)}{eE_x}.$$

Therefore, we conclude that $\left|a_+^{(-E_x)}\right| = \left|a_+^{(E_x)}\right|$ in the absence of shift vector, even if the system breaks $\mathcal{P}$ symmetry. The situation is different if we include the dissipation to the system, as we can see from Eq. (3.22). Since the semiclassical dynamics of Q reflects the asymmetry of the dispersion through the dissipative term, the nonreciprocal LZ effect is realized.

3.5 Discussion

Nonlinear capacitance

Here, we estimate the nonlinear capacitance α [99–103] using the scaling form derived by the Thomas-Fermi approximation [102, 103]:

$$\begin{aligned} \alpha &\propto \left[\frac{(4\pi)^2}{\epsilon_{F,2}} \left(S\lambda_2\lambda_2^{-2}e^{-2}\right)^{-2} - \frac{(4\pi)^2}{\epsilon_{F,1}} \left(S\lambda_1\lambda_1^{-2}e^{-2}\right)^{-2}\right] \frac{1}{e^3}, \\ &\propto \left[\frac{1}{n_2} - \frac{1}{n_1}\right] \frac{4\pi}{eS^2} \end{aligned} \tag{3.25}$$

where S is the area of the cross section of the Josephson Junction, $\lambda_{1/2}$, $\epsilon_{F,1/2}$ and $n_{1/2}$ are the Thomas-Fermi screening lengths, the Fermi energy and the carrier density of the bulk superconductors, and we replaced $d/d\epsilon$ with $1/\epsilon_F$ (ϵ_F is the Fermi energy) for the order estimation. Now, the linear capacitance in the Thomas-Fermi approximation can be written as

$$C = \frac{\epsilon_r}{4\pi} \frac{S}{a + \lambda_1 + \lambda_2}, \tag{3.26}$$

where ϵ_r and a are the relative dielectric constant and the thickness of the thin film, respectively.

First we consider the case (I), where the dynamics is governed by Eqs. (3.10) and (3.11). Then, in the dimensionless unit, we get

$$\begin{aligned} A &= \alpha C^{3/2} \sqrt{E_J} \\ &\propto \left[\frac{\epsilon_r}{n_2 S(a + \lambda_1 + \lambda_2)} - \frac{\epsilon_r}{n_1 S(a + \lambda_1 + \lambda_2)} \right] \sqrt{\frac{E_J}{2E_Q}} \end{aligned} \tag{3.27}$$

Now, we set the typical values $n_{1,2} \sim 10^{22}\,\mathrm{cm}^{-3}$, $\epsilon_r \sim 10$, $S \sim 0.1\,\mu\mathrm{m}^2$, $a = 1\,\mathrm{nm}$, $E_Q/E_J \sim 10^{-1}$ and assume $a \gg \lambda_{1,2}$. Then, $A \sim 10^{-5}$.

If we consider the case (II), where the dynamics is governed by Eqs. (3.14) and (3.15), in dimensionless unit,

$$\tilde{A} = \alpha C e \sim \left[\frac{\epsilon_r}{n_2 S(a + \lambda_1 + \lambda_2)} - \frac{\epsilon_r}{n_1 S(a + \lambda_1 + \lambda_2)} \right]. \tag{3.28}$$

Since $E_J \propto S$ and $E_Q \propto 1/S$, $E_J/E_Q \ll 1$ is satisfied for the system with small S. Therefore, we assume small Josephson junction and set $S = 0.01\mu\mathrm{m}^2$, $n_{1,2} \sim 10^{22}\,\mathrm{cm}^{-3}$, $\epsilon_r \sim 10$, $a = 1\,\mathrm{nm}$ and assume $a \gg \lambda_{1,2}$. Then, $\tilde{A} \sim 10^{-4}$.

Experimental measurement

From the above estimate, $A \sim 10^{-5}$ for case (I) and $\tilde{A} \sim 10^{-4}$ for case (II), so the asymmetry is relatively small in the experimental settings, but it is possible to measure the 2ω response $V_{2\omega}$ to the AC driving current $I_x(t) = I_a \cos \omega t$ with small ω with a high precision. Assuming ω is small compared to the characteristic frequency of the dynamics, we can calculate the 2ω component of the response voltage by the adiabatic approximation:

$$\begin{aligned} V_{2\omega} &= \frac{\omega}{2\pi} \int_0^{2\pi/\omega} dt \cos(2\omega t) V(I_a \cos \omega t) \\ &= \frac{1}{4\pi} \int_0^{2\pi} d\tau \cos\tau \left[V\left(I_a \cos\frac{\tau}{2}\right) + V\left(-I_a \cos\frac{\tau}{2}\right) \right]. \end{aligned} \tag{3.29}$$

Now, we estimate $V_{2\omega}$ for three cases: (A): case (I) with $T = 0$, (B): case (I) with $T > 0$ and (C): case (II). As we discussed, the asymmetry of V is pronounced near the various critical value of i_x or $\tilde{i}_x$, so, to obtain large $V_{2\omega}$ we set the amplitude of the external voltage I_a near these critical currents, i.e., (A) I_c, (B) $i_{c2}I_c$ and (C) $\tilde{i}_{c,bl}^{L/R} e/(RC)$.

For the case (A), i.e., case (I) with $T = 0$, if we set $I_0 > I_C$, the above measurement of 2ω component reflects the difference of i_{c1}^R and i_{c1}^L. We set the critical current density $I_c/S = 100\,\mathrm{A/cm^2}$ and the resistance times area $RS = 10^{-5}\,\Omega\,\mathrm{cm^2}$, and the capacitance $C/S \sim 10^{-5}\,\mathrm{F/cm^2}$, where we used Eq. (3.26) with $a = 1\,\mathrm{nm}$, $S = 0.1\,\mu\mathrm{m^2}$ and $\epsilon_r = 10$. Then we get $r^{-1} \sim 0.1$, and for $A \sim 10^{-5}$, $A' = 0.5A$, the numerical calculation yields $V_{2\omega} \sim 0.00001 RI_c \sim 10\,\mathrm{nV}$.

Next, we consider the case (B), i.e., case (I) with $T > 0$. We use the same parameters as the case (A) and set $T = 50\,\mathrm{K}$. Then, the numerical calculation yields $V_{2\omega} \sim 0.00001 RI_c \sim 10\,\mathrm{nV}$.

For the case (C), i.e., case (II), for $\tilde{A} = 10^{-4}$ and $\tilde{A}' = 0.5\tilde{A}$, the numerical calculation yields $V_{2\omega} \sim 0.0001 e/C \sim 10\,\mathrm{nV}$, where we used the parameters $C/S \sim 10^{-5}\,\mathrm{F/cm^2}$ and $S = 0.01\mu\mathrm{m^2}$.

In summary, $V_{2\omega}$ is about $10\,\mathrm{nV}$ for the usual Josephson junction systems, and it can be measured by the current experimental technology. As concrete superconducting materials, it is better to use different superconductors with the different carrier density in the normal state, so that the nonlinear capacitance becomes large.

Conclusion

We have shown that, in inversion asymmetric Josephson junctions, the nonreciprocal $I_x - V$ curve is realized if we include the asymmetry of the charging energy both for the system with (I) $E_J/E_Q \gg 1$ and (II) $E_J/E_Q \ll 1$. In case (I), the nonreciprocity is realized when the shunt resistance is large so that the dynamics of the Josephson phase is underdamped. When the thermal fluctuation is small, the nonreciprocity is enhanced near the critical current of the hysterisis. When the thermal fluctuation is not negligible, we expect the large nonreciprocity near the critical current of the dynamical transition where the minimum of the distribution function changes from the static configuration to the running configuration. In case (II), the nonreciprocal Bloch oscillation leads to nonreciprocal $I - V$ curve, and also the Zener tunneling exhibits nonreciprocity. In both cases, the nonreciprocity induced by the nonlinear capacitance can be detected by 2ω component measurement of the voltage drop $V_{2\omega}$ induced by the external AC current $I_x(t) = I_a \cos\omega t$, in the current experimental technology.

Chapter 4

Summary and perspectives

In chapter 2, we discussed the quantum dynamics of the vortices in the superconductors in the presence of dissipation. We showed that the dilute bosons in the presence of strong dissipation does not exhibit superfluidity even at zero temperature, based on the physical argument, the numerical quantum Monte Carlo calculation, and the perturbative field theoretical calculation.

Theoretically, the effect of the dissipation caused by the normal core on the motion of the vortex has been known for a long time [54]. However, the discussion has been mainly at the classical level, and its effect at the quantum regime near zero temperature remained unclear. To clarify it, we constructed the model describing the dynamics of the vortices in the presence of low energy excitation at the normal core. Although the effect of dissipation on the single particle problems is well-known [36, 52, 121], the effect of dissipation in the many body problems have not been discussed in detail. We quantitatively showed that the dissipation suppresses the genuine many-body effect, i.e., superfluidity.

As we discussed, our theory describes the physics of the low temperature metallic phase of two dimensional superconductors, i.e., "failed superconductor". Not only that, our model gives the concrete prediction that the failed superconductor should be present for the moderately clean regime and absent for the superclean regime. This prediction can be verified experimentally by measuring the relaxation time of the sample through the residual resistivity at the normal state. Therefore, we believe that our model plays an important role in understanding the generic failed superconductor phase in highly crystalline superconductors.

As a future work, it will be interesting to discuss the effect of dissipation on the many-body fermionic systems or phonon systems. For fermionic systems, the effect of low energy degrees of freedom is well explored in the field theoretical model [122, 123], but the fermionic dissipative model in the first quantized formulation seems to be less explored. For phonon systems, depending on the density of states at low energy, the combination of the phonon degrees of freedom and the dissipative low energy degrees of freedom may lead to the novel phase of matter if both degrees of freedom are relevant in the sense of renormalization group. Also, since our model is relevant to the failed superconductors where the control parameter is the magnetic field, for other experiments where the control parameter is the dirtiness of the sample or the gate voltage [11], our model does not apply. Whether or not our theory give insights into these situations is

unclear, and clarifying whether or not the vortices play important role in those situations is an important future work.

In chapter 3, we discussed the nonreciprocity of Josephson junctions where the inversion symmetry is broken by the asymmetric charging energy. In the case of large junctions where the capacitance is large, the dynamics of the junction is described by the phase degree of freedom, while for small junctions the charge degree of freedom is a good quantum number.

In the former case, we showed that the nonreciprocity is realized when the shunt resistance is large so that the dynamics of the Josephson phase is underdamped, while for the system with small shunt resistance the nonreciprocity is not observed. When the thermal fluctuation can be neglected, $I - V$ curve shows hysteresis behavior, and the nonreciprocity is enhanced near the critical current of the hysteresis. In the presence of thermal fluctuation, the hysteresis disappears, and the voltage drop is appreciable above some critical current. This can be understood as a consequence of the dynamic transition, where the minimum of the large deviation function switches from the static configuration to the running configuration. We showed that the nonreciprocity is large near the critical current of this transition.

In the latter case, the dynamics of the charge degree of freedom is described by the Bloch oscillation phenomenon, where the charge accumulated on the junction periodically exhibits tunneling because of the Josephson coupling. The period of the Bloch oscillation is different for the positive external current and the negative external current, and that leads to the nonreciprocity in $I - V$ curve. Also, the rate of Zener tunneling shows nonreciprocity. Although we can show that nonzero Berry connection is necessary for the nonreciprocal Zener tunneling in the absence of dissipation [80], the Josephson junction is inherently dissipative because of the shunt resistance, so that nonreciprocal Zener tunneling is realized in Josephson junctions with asymmetric charging energy even without the Berry connection.

The natural question to ask is the role of the superconductivity in the nonreciprocal response. Even without the superconductivity, the asymmetric charging energy already breaks the inversion symmetry, so we expect the nonreciprocal response. In this case, $I - V$ curve is determined by the dynamics of the charge degree of freedom, and we need to investigate the nonreciprocity of the single electron tunneling and the Coulomb blockade phenomenon [124].

In this thesis, we discussed the dynamics of the two systems related to superconductivity where the dissipation plays an important role. Since the dissipation leads to the nonlocal action in imaginary time, it leads to the phenomenon qualitatively different from the clean systems where the action is local in time. Understanding the effect of dissipation on many-body systems is demanded because of the experimental progress in cold atom systems, where the many body phenomena like the antiferromagnetism [125] is observed. The solid state systems are much more dirty compared to the cold atom systems and we do observe robust thermodynamic phase even in the presence of the environment in solids, but the number of particles in cold atom systems is extremely small compared to the solid state systems, so the thermodynamic phase is expected to be less robust against the environmental effect for cold atom systems. Therefore, it will be important to understand the effect of environment on cold atom systems and see whether or not the

interesting thermodynamic phase survives even in the presence of dissipation.

Appendix A

Appendix to chapter 2

A.1 Microscopic derivation of Green function in Keldysh formalism

Here, we will discuss the microscopic derivation of Green function in the Keldysh formulation. The action of the system is as follows:

$$S = \int_C dt \Big[\sum_{\boldsymbol{k}} \bar{\psi}_{\boldsymbol{k}} (i\partial_t - \xi_{\boldsymbol{k}}) \psi_{\boldsymbol{k}} - \frac{g}{2} \sum_i \rho_i^2 \\ - \sum_i \rho_i \sum_\alpha (V_\alpha a_{i\alpha} + V_\alpha^* \bar{a}_{i\alpha}) + \sum_{i,\alpha} \bar{a}_{i\alpha} (i\partial_t - \epsilon_\alpha) a_{i\alpha} \Big],$$

where C is the Keldysh contour and $\rho_i = \bar{\psi}_i \psi_i$. Introducing $\psi^{cl,q} = (\psi^+ \pm \psi^-)/\sqrt{2}$, $a^{cl,q} = (a^+ \pm a^-)/\sqrt{2}$, $\rho^{cl,q} = (\rho^+ \pm \rho^-)/\sqrt{2}$, $\Psi = (\psi^{cl}, \psi^q)^T$, $A = (a^{cl}, a^q)^T$ and $P = (\rho^{cl}, \rho^q)$, it can be transformed into,

$$S = \sum_{\boldsymbol{k}} \int_{-\infty}^{\infty} dt \Psi_{\boldsymbol{k}}^\dagger \mathfrak{g}_{\boldsymbol{k}}^{-1} \Psi_{\boldsymbol{k}} - \frac{g}{2} \sum_i \int_{-\infty}^{\infty} dt P_i^T \sigma_x P_i \\ - \int_{-\infty}^{\infty} dt \sum_{i,\alpha} [V_\alpha P_i \sigma_x A_{i\alpha} + V_\alpha^* P_i \sigma_x A_{i\alpha}^\dagger] + \sum_{i,\alpha} \int_{-\infty}^{\infty} dt A_{i\alpha}^\dagger \mathfrak{D}_\alpha^{-1} A_{i\alpha},$$

where

$$\mathfrak{g}_{\boldsymbol{k}}^{-1} = \begin{pmatrix} 0 & i\partial_t - \xi_{\boldsymbol{k}} - i0 \\ i\partial_t - \xi_{\boldsymbol{k}} + i0 & 2i0 \coth(\beta \xi_{\boldsymbol{k}}/2) \end{pmatrix}, \quad \mathfrak{D}_\alpha^{-1} = \begin{pmatrix} 0 & i\partial_t - \epsilon_\alpha - i0 \\ i\partial_t - \epsilon_\alpha + i0 & 2i0 \coth(\beta \epsilon_\alpha/2) \end{pmatrix}.$$

Then, integrating over $A, A^\dagger$, we obtain

$$S = \sum_{\boldsymbol{k}} \int_{-\infty}^{\infty} dt \Psi_{\boldsymbol{k}}^\dagger \mathfrak{g}_{\boldsymbol{k}}^{-1} \Psi_{\boldsymbol{k}} - \frac{g}{2} \sum_i \int_{-\infty}^{\infty} dt P_i^T \sigma_x P_i - \sum_i \int_{-\infty}^{\infty} dt P_i^T \left(\sum_\alpha |V_\alpha|^2 \sigma_x \mathfrak{D}_\alpha \sigma_x \right) P_i. \tag{A.1}$$

Here,

$$\sum_\alpha |V_\alpha|^2 \sigma_x \mathfrak{D}_\alpha(\omega)\sigma_x = \begin{pmatrix} 0 & \sum_\alpha \frac{|V_\alpha|^2}{\omega-\epsilon_\alpha-i0} \\ \sum_\alpha \frac{|V_\alpha|^2}{\omega-\epsilon_\alpha+i0} & -2i\pi\coth(\beta\omega/2)\sum_\alpha |V_\alpha|^2\delta(\omega-\epsilon_\alpha) \end{pmatrix}$$
$$=: \frac{1}{2}\begin{pmatrix} 0 & \mathrm{Re}\Sigma(\omega)+i\mathrm{Im}\Sigma(\omega) \\ \mathrm{Re}\Sigma(\omega)-i\mathrm{Im}\Sigma(\omega) & -2i\coth(\beta\omega/2)\mathrm{Im}\Sigma(\omega) \end{pmatrix},$$

and

$$P = \frac{1}{\sqrt{2}}\begin{pmatrix} \bar\psi^{cl}\psi^{cl}+\bar\psi^q\psi^q & \bar\psi^q\psi^{cl}+\bar\psi^{cl}\psi^q \end{pmatrix}^T,$$

We note that $\mathrm{Re}\Sigma(0) < 0$, so $\mathrm{Re}\Sigma(\omega)$ represents the effective attractive interaction. Here we just concentrate on the effect of $\mathrm{Im}\Sigma(\omega) = A(\omega)$ which describes the dissipation. Here we consider the decomposition $\psi^{cl} = \sqrt{\rho_0} + \phi^{cl}$, $\psi^q = \phi^q$ and expand up to second order terms in ϕ. Then,

$$\bar\psi^{cl}\bar\psi^q\psi^{cl}\psi^{cl} + \bar\psi^{cl}\bar\psi^q\psi^q\psi^q + h.c. = \rho_0\bar\phi^{cl}\bar\phi^q + 2\rho_0\bar\phi^q\phi^{cl} + \rho_0\phi^{cl}\phi^q + 2\rho_0\bar\phi^{cl}\phi^q + \mathcal{O}(\phi^3),$$

and

$$\sqrt{2}P^T = \rho_0\begin{pmatrix} 1 & 0 \end{pmatrix} + \sqrt{\rho_0}\begin{pmatrix} \phi^{cl}+\bar\phi^{cl} & \phi^q+\bar\phi^q \end{pmatrix} + \begin{pmatrix} \bar\phi^{cl}\phi^{cl}+\bar\phi^q\phi^q & \bar\phi^q\phi^{cl}+\bar\phi^{cl}\phi^q \end{pmatrix}.$$

Then,

$$2P^T\sigma_x P = \begin{pmatrix} \bar\phi^{cl} & \phi^{cl} & \bar\phi^q & \phi^q \end{pmatrix}\begin{pmatrix} 0 & 0 & 2\rho_0 & \rho_0 \\ 0 & 0 & \rho_0 & 2\rho_0 \\ 2\rho_0 & \rho_0 & 0 & 0 \\ \rho_0 & 2\rho_0 & 0 & 0 \end{pmatrix}\begin{pmatrix} \phi^{cl} \\ \bar\phi^{cl} \\ \phi^q \\ \bar\phi^q \end{pmatrix}$$

and

$$2P_{-\omega}^T\begin{pmatrix} 0 & iA(\omega) \\ -iA(\omega) & -2iA(\omega)\coth(\beta\omega/2) \end{pmatrix}P_\omega$$
$$= i\rho_0 A(\omega)\begin{pmatrix} \bar\phi_\omega^{cl} & \phi_{-\omega}^{cl} & \bar\phi_\omega^q & \phi_{-\omega}^q \end{pmatrix}\begin{pmatrix} 0 & 0 & 1 & 1 \\ 0 & 0 & 1 & 1 \\ -1 & -1 & -2\coth(\beta\omega/2) & -2\coth(\beta\omega/2) \\ -1 & -1 & -2\coth(\beta\omega/2) & -2\coth(\beta\omega/2) \end{pmatrix}\begin{pmatrix} \phi_\omega^{cl} \\ \bar\phi_{-\omega}^{cl} \\ \phi_\omega^q \\ \bar\phi_{-\omega}^q \end{pmatrix}.$$

In total, Eq. (A.1) can be rewritten as,

$$S = \frac{1}{2}\sum_{\boldsymbol{k},\omega}\varphi_{\boldsymbol{k},\omega}^\dagger\begin{pmatrix} 0 & \omega\sigma_z - \hat H_{\boldsymbol{k}} - i\hat a(\omega) \\ \omega\sigma_z - \hat H_{\boldsymbol{k}} + i\hat a(\omega) & 2i\coth(\beta\omega/2)\hat a(\omega) \end{pmatrix}\varphi_{\boldsymbol{k},\omega},$$

where

$$\varphi_{\boldsymbol{k},\omega}^T = \begin{pmatrix} \phi_{\boldsymbol{k},\omega}^{cl} & \bar\phi_{-\boldsymbol{k},-\omega}^{cl} & \phi_{\boldsymbol{k},\omega}^q & \bar\phi_{-\boldsymbol{k},-\omega}^q \end{pmatrix}$$

and, assuming $\mu = \rho_0 g$,

$$\hat{H}_{\boldsymbol{k}} = \begin{pmatrix} \epsilon_{\boldsymbol{k}} + g\rho_0 & g\rho_0 \\ g\rho_0 & \epsilon_{\boldsymbol{k}} + g\rho_0 \end{pmatrix}, \quad \hat{a}(\omega) = \rho_0 A(\omega) \begin{pmatrix} 1 & 1 \\ 1 & 1 \end{pmatrix}.$$

Therefore, the Green functions for the Bogoliubov quasiparticle are

$$G^{A/R} = \frac{1}{\omega^2 - \omega_{\boldsymbol{k}}^2 \mp 2i\rho_0 A \epsilon_{\boldsymbol{k}}} \begin{pmatrix} \omega + \epsilon_{\boldsymbol{k}} + g\rho_0 \pm i\rho_0 A & -g\rho_0 \mp i\rho_0 A \\ -g\rho_0 \mp i\rho_0 A & -\omega + \epsilon_{\boldsymbol{k}} + g\rho_0 \pm i\rho_0 A \end{pmatrix},$$

and

$$\begin{aligned} G^K &= \coth(\beta\omega/2)[G^R - G^A] \\ &= \frac{-2i\coth(\beta\omega/2)\rho_0 A}{\omega^4 - (2\epsilon_{\boldsymbol{k}}^2 + 4g\rho_0\epsilon_{\boldsymbol{k}})\omega^2 + \epsilon_{\boldsymbol{k}}^4 + 4g\rho_0\epsilon_{\boldsymbol{k}}^3 + 4\rho_0^2\epsilon_{\boldsymbol{k}}^2(g^2 + A^2)} \begin{pmatrix} (\omega + \epsilon_{\boldsymbol{k}})^2 & -(\omega^2 - \epsilon_{\boldsymbol{k}}^2) \\ -(\omega^2 - \epsilon_{\boldsymbol{k}}^2) & (\omega - \epsilon_{\boldsymbol{k}})^2 \end{pmatrix}. \end{aligned}$$

Appendix B

Appendix to chapter 3

B.1 Projection operator analysis

In this section, we will discuss γ^{-1} expansion of the Fokker-Planck equation, following van Kampen's [126] procedure for the elimination of fast variables. Those who are only interested in the final results can skip the detailed derivation and directly go to Eqs. (B.24) and (B.25).

Here we consider the following Langevin equation:

$$\begin{cases} \dot{x} = \partial_p G(p) \\ \dot{p} = -\partial_x V(x) - m\gamma\dot{x} + \xi(t), \end{cases} \tag{B.1}$$

where $\langle \xi(t)\xi(t') \rangle = 2m\gamma k_B T \delta(t-t')$. Instead of the variables φ and Q, we used the notation similar to the Browinan particle. We can easily transform Eq. (B.1) into Eq. (3.9) in the main text by the substitution $m\gamma \to R^{-1}$, $x \to \hbar\varphi/(2e)$, $p \to Q$, $G \to E_{\rm ch}$ and

$$V \to -\frac{\hbar I_x}{2e}\varphi - \frac{I_c \hbar}{2e}\cos\varphi. \tag{B.2}$$

Physically, $G(p)$ and $V(x)$ represent the kinetic energy and the potential energy, respectively. If we set $G(p) = p^2/(2m)$, we get the usual Langevin equation for the Brownian particle. Here we consider the more general $G(p)$ including the odd powers of p, which corresponds to the odd power of Q of the charging energy $E_{\rm ch}$ in the main text. Using the Chapman-Kolmogorov expansion [127], this Langevin equation can be transformed to the following Fokker-Planck equation for the probability distribution $\rho(x,p,t)$.

$$\begin{aligned} \partial_t \rho &= [-(\partial_p G)\partial_x + \partial_x V \partial_p]\rho + m\gamma\partial_p((\partial_p G)\rho + \beta^{-1}\partial_p \rho) \\ \Leftrightarrow \partial_t \rho &= L_1 \rho + \frac{1}{\epsilon} L_0 \rho \quad (\epsilon = 1/\gamma), \end{aligned} \tag{B.3}$$

where

$$L_0 = m\partial_p((\partial_p G) + \beta^{-1}\partial_p), \quad L_1 = -(\partial_p G)\partial_x + \partial_x V \partial_p.$$

Here we note the following property of the operator L_0:

$$\begin{aligned} L_0^T = m(-(\partial_p G) + \beta^{-1}\partial_p)\partial_p &= m(-(\partial_p G) + \beta^{-1}\partial_p)\partial_p(e^{\beta G}e^{-\beta G}) \\ &= e^{\beta G} m\partial_p((\partial_p G) + \beta^{-1}\partial_p)e^{-\beta G} \\ &= e^{\beta G} L_0 e^{-\beta G}. \end{aligned}$$

This property can be used to define the following inner product:

$$(\phi, \psi) = \int dxdp\, e^{\beta G}\phi\psi, \tag{B.4}$$

where the following convenient relation holds:

$$\begin{aligned} (\phi, L_0\psi) &= \int dxdp\, e^{\beta G}\phi L_0\psi \\ &= \int dxdp\, \psi L_0^T(e^{\beta G}\phi) \\ &= \int dxdp\, e^{\beta G}\psi L_0\phi = (\psi, L_0\phi), \end{aligned}$$

which means that L_0 is symmetric operator for the inner product defined in Eq. (B.4).

Now we define the projection operator $\mathcal{P}$ which satisfies,

$$\mathcal{P}L_0 = 0.$$

$\mathcal{P}$ can be constructed from the full set of left null vector $\{\tilde{\alpha}_r\}_r$ of L_0, $\tilde{\alpha}_r L_0 = 0$, as

$$\mathcal{P}_{q,q'} = \sum_r \alpha_r(q)\tilde{\alpha}_r(q'), \quad \alpha_r(q) = e^{-\beta G}\tilde{\alpha}_r(q),$$

where $q = (x, p)$ and we used the inner product (B.4) to define the right vector $\alpha_r(q)$ from the left vector $\tilde{\alpha}_r(q)$. This $\mathcal{P}$ has a nice property that

$$L_0\mathcal{P} = 0,$$

since

$$L_0\alpha_r = L_0(e^{-\beta G}\tilde{\alpha}_r) = e^{-\beta G}L_0^T\tilde{\alpha}_r = 0.$$

We further define the projection operator $\mathcal{Q} = 1 - \mathcal{P}$. Then, from Eq. (B.3),

$$\begin{aligned} \partial_t\mathcal{P}\rho &= \mathcal{P}L_1\mathcal{P}\rho + \mathcal{P}L_1\mathcal{Q}\rho, \\ \partial_t\mathcal{Q}\rho &= \frac{1}{\epsilon}\mathcal{Q}L_0\mathcal{Q}\rho + \mathcal{Q}L_1\mathcal{P}\rho + \mathcal{Q}L_1\mathcal{Q}\rho. \end{aligned}$$

We rewrite the above equation as

$$\begin{aligned} \partial_t v &= Av + Bw, \\ \partial_t w &= \frac{1}{\epsilon}Fw + Cv + Dw, \end{aligned}$$

where

$$A = \mathcal{P}L_1\mathcal{P}, \quad B = \mathcal{P}L_1\mathcal{Q}, \quad C = \mathcal{Q}L_1\mathcal{P}, \quad D = \mathcal{Q}L_1\mathcal{Q},$$
$$F = \mathcal{Q}L_0\mathcal{Q}, \quad \mathcal{P}\rho = v, \quad \mathcal{Q}\rho = w.$$

Then, the reduced equation for v is,

$$\partial_t v = [A - \epsilon BF^{-1}C + \epsilon^2(BF^{-1}DF^{-1}C - BF^{-2}CA)]v + \mathcal{O}(\epsilon^3)v, \tag{B.5}$$

and the third order term is

$$\epsilon^3[-BF^{-1}DF^{-1}DF^{-1}C + BF^{-2}CBF^{-1}C + BF^{-2}DF^{-1}CA + BF^{-1}DF^{-2}CA - BF^{-3}CA^2]v. \tag{B.6}$$

Now we apply the above scheme to our present model. We will show that $\mathcal{O}(\epsilon^2)$ term vanishes, and calculate $\mathcal{O}(\epsilon)$ term and $\mathcal{O}(\epsilon^3)$ term.

First, we construct the left null vector of L_0:

$$L_0^T\tilde{\alpha} = m(-(\partial_p G) + \beta^{-1}\partial_p)\partial_p\tilde{\alpha} = 0.$$

We set $\partial_p\tilde{\alpha} = \psi$ and $\psi = e^{\beta G}\bar{\psi}$. Then, $\partial_p\bar{\psi} = 0$, so $\psi = e^{\beta G}c(x)$. Therefore $\partial_p\tilde{\alpha} = c(x)e^{\beta G}$, so $\phi = c(x)\int^p dp e^{\beta G} + d(x)$ we impose the condition that the left vector ϕ is normalizable, i.e., $\int dpdx e^{-\beta G}\phi^2 < \infty$. Then $c(x) = 0$. Therefore, we obtain $\tilde{\alpha}_r = \phi_r(x)$, where $\phi_r(x)$ are the complete basis in x space. Now we can construct the projection operator as

$$\mathcal{P}_{q,q'} = e^{-\beta G(p)}\sum_r \phi_r(x)\phi_r(x') = e^{-\beta G(p)}\delta(x - x').$$

Then, $v = \mathcal{P}\rho = e^{-\beta G}\tilde{\rho}, \quad \tilde{\rho}(x,t) = \int dp\, \rho(x,p,t)$, and

$$\begin{aligned} Av = \mathcal{P}(-\partial_p G\partial_x + \partial_x V\partial_p)e^{-\beta G}\tilde{\rho} &= \mathcal{P}(-\partial_p G e^{-\beta G}\partial_x\tilde{\rho} + \tilde{\rho}\partial_x V(\partial_p e^{-\beta G})) \\ &= e^{-\beta G}\int dp(-\partial_p G e^{-\beta G}\partial_x\tilde{\rho} + \tilde{\rho}\partial_x V(\partial_p e^{-\beta G})) \\ &= 0, \end{aligned}$$

and

$$Cv = \mathcal{Q}(-\partial_p G\partial_x + \partial_x V\partial_p)e^{-\beta G}\tilde{\rho} = \partial_p e^{-\beta G}(\beta^{-1}\partial_x\tilde{\rho} + \tilde{\rho}\partial_x V).$$

Now we solve $Cv = Fw$ where $\mathcal{Q}w = w$ to obtain $w = F^{-1}Cv$. To do that, we first calculate Fw:

$$Fw = L_0 w = m\partial_p((\partial_p G) + \beta^{-1}\partial_p)w = \partial_p e^{-\beta G}(\beta^{-1}\partial_x\tilde{\rho} + \tilde{\rho}\partial_x V).$$

We integrate over p for both sides:

$$m((\partial_p G) + \beta^{-1}\partial_p)w = e^{-\beta G}(\beta^{-1}\partial_x\tilde{\rho} + \tilde{\rho}\partial_x V) + c(x). \tag{B.7}$$

We set $w = e^{-\beta G}\bar{w}$. Then, Eq. (B.7) can be rewritten as,

$$\partial_p \bar{w} = \frac{\beta}{m}((\beta^{-1}\partial_x\tilde{\rho} + \tilde{\rho}\partial_x V) + e^{\beta G}c(x)). \tag{B.8}$$

we integrate both sides of Eq. (B.8) over p to obtain

$$w = e^{-\beta G}\frac{\beta}{m}[p(\beta^{-1}\partial_x\tilde{\rho} + \tilde{\rho}\partial_x V) + e^{-\beta G}\int^p dp' e^{\beta G(p')}c(x)] + e^{-\beta G}d(x).$$

From the normalizability condition, $c = 0$, and from the condition $Qw = w$, we obtain

$$w = e^{-\beta G}\frac{1}{m}(p - \langle p\rangle)(\partial_x\tilde{\rho} + \beta\tilde{\rho}\partial_x V),$$

where the averaging is with respect to the weight $e^{-\beta G(p)}$:

$$\langle f(p)\rangle = \frac{\int dp' e^{-\beta G(p')}f(p')}{\int dp' e^{-\beta G(p')}}.$$

From now on, we choose the origin in p space so that $\langle p\rangle = 0$. Then, since $w = F^{-1}Cv$,

$$\begin{aligned} BF^{-1}Cv = Bw &= \mathcal{P}(-\partial_p G\partial_x + \partial_x V\partial_p)e^{-\beta G}\frac{p}{m}(\partial_x\tilde{\rho} + \beta\tilde{\rho}\partial_x V) \\ &= e^{-\beta G}\left[\int dp(-\partial_p G)e^{-\beta G}\frac{p}{m}\right]\partial_x(\partial_x\tilde{\rho} + \beta\tilde{\rho}\partial_x V) \\ &= -e^{-\beta G}\frac{1}{\beta m}\partial_x(\partial_x\tilde{\rho} + \beta\tilde{\rho}\partial_x V). \end{aligned} \tag{B.9}$$

This is the term at order $\mathcal{O}(\gamma^{-1})$.

We next consider the second order terms. Noting $Av = 0$, among the two terms shown in Eq. (B.5), we need to consider

$$\begin{aligned} BF^{-1}DF^{-1}Cv &= BF^{-1}\mathcal{Q}(-\partial_p G\partial_x + \partial_x V\partial_p)e^{-\beta G}\frac{p}{m}(\partial_x\tilde{\rho} + \beta\tilde{\rho}\partial_x V) \\ &= BF^{-1}[(-\partial_p G\partial_x + \partial_x V\partial_p)e^{-\beta G}\frac{p}{m} + e^{-\beta G}\frac{1}{m\beta}\partial_x]D_x\tilde{\rho} \end{aligned}$$

where $D_x = \partial_x + \beta(\partial_x V)$. We need to solve following the equation for w:

$$\begin{aligned} &Fw = DF^{-1}Cv \\ \Leftrightarrow &m\partial_p((\partial_p G) + \beta^{-1}\partial_p)w = m^{-1}[\beta^{-1}(\partial_p p e^{-\beta G})\partial_x D_x\tilde{\rho} + \partial_x V(\partial_p e^{-\beta G}p)D_x\tilde{\rho})]. \end{aligned} \tag{B.10}$$

We integrate over p on both sides of Eq. (B.10) and set $w = e^{-\beta G}\bar{w}$:

$$m\beta^{-1}\partial_p\bar{w} = m^{-1}p[\beta^{-1}\partial_x D_x\tilde{\rho} + \partial_x V D_x\tilde{\rho})] + e^{\beta G}c(x). \tag{B.11}$$

We further integrate over p in Eq. (B.11) to obtain,

$$\begin{aligned} &m\beta^{-1}\bar{w} = \frac{p^2}{2m}[\beta^{-1}\partial_x D_x\tilde{\rho} + \partial_x V D_x\tilde{\rho})] + \int^p dp' e^{\beta G(p')}c(x) + d(x) \\ \Leftrightarrow &w = \frac{\beta}{m}e^{-\beta G}\frac{p^2}{2m}[\beta^{-1}\partial_x D_x\tilde{\rho} + \partial_x V D_x\tilde{\rho})] + e^{-\beta G}\frac{\beta}{m}\int^p dp' e^{\beta G(p')}c(x) + e^{-\beta G}\frac{\beta}{m}d(x). \end{aligned}$$

From the normalizability, $c = 0$, and from the condition $Qw = w$, we obtain

$$w = F^{-1}DF^{-1}Cv = e^{-\beta G}\frac{p^2 - \langle p^2\rangle}{2m^2}D_x^2\tilde{\rho}.$$

Then,

$$BF^{-1}DF^{-1}Cv = -e^{-\beta G}\int dp'\beta^{-1}e^{-\beta G(p')}\frac{p'}{m^2}\partial_x D_x^2\tilde{\rho} = 0.$$

Therefore, the terms at order $\mathcal{O}(\gamma^{-2})$ vanishes.

Now we move on to the third order terms. Among the five terms in Eq. (B.6), we need to consider following two terms:

$$\epsilon^3[-BF^{-1}DF^{-1}DF^{-1}C + BF^{-2}CBF^{-1}C]v. \tag{B.12}$$

First, we consider the first term in Eq. (B.12):

$$\begin{aligned}
BF^{-1}D(F^{-1}DF^{-1}Cv) &= BF^{-1}De^{-\beta G}\frac{p^2 - \langle p^2\rangle}{2m^2}D_x^2\tilde{\rho} \\
&= BF^{-1}\mathcal{Q}(-\partial_p G\partial_x + \partial_x V\partial_p)e^{-\beta G}\frac{p^2 - \langle p^2\rangle}{2m^2}D_x^2\tilde{\rho} \\
&= BF^{-1}[(-\partial_p G\partial_x + \partial_x V\partial_p)e^{-\beta G}\frac{p^2 - \langle p^2\rangle}{2m^2}D_x^2\tilde{\rho} \\
&\quad - e^{-\beta G}\int dp'(-\partial_p G(p'))e^{-\beta G(p')}\frac{p'^2 - \langle p^2\rangle}{2m^2}\partial_x D_x^2\tilde{\rho}] \\
&= BF^{-1}(-\partial_p G\partial_x D_x^2\tilde{\rho} + \partial_x V D_x^2\tilde{\rho}\partial_p)e^{-\beta G}\frac{p^2 - \langle p^2\rangle}{2m^2}.
\end{aligned} \tag{B.13}$$

To calculate $F^{-1}DF^{-1}DF^{-1}Cv$, we need to solve $Fw = DF^{-1}DF^{-1}Cv$ for w:

$$\begin{aligned}
&Fw = DF^{-1}DF^{-1}Cv \\
\Leftrightarrow &m\partial_p((\partial_p G) + \beta^{-1}\partial_p)w = (-\partial_p G\partial_x D_x^2\tilde{\rho} + \partial_x V D_x^2\tilde{\rho}\partial_p)e^{-\beta G}\frac{p^2 - \langle p^2\rangle}{2m^2}.
\end{aligned} \tag{B.14}$$

Now we integrate both sides of Eq. (B.14) over p:

$$\begin{aligned}
&m((\partial_p G) + \beta^{-1}\partial_p)w \\
=&\beta^{-1}\left[e^{-\beta G}\frac{p^2 - \langle p^2\rangle}{2m^2} - \int^p dp' e^{-\beta G(p')}\frac{p'}{m^2}\right]\partial_x D_x^2\tilde{\rho} + (\partial_x V D_x^2\tilde{\rho})e^{-\beta G}\frac{p^2 - \langle p^2\rangle}{2m^2} + c(x).
\end{aligned} \tag{B.15}$$

We introduce $w = e^{-\beta G}\bar{w}$. Then, Eq. (B.15) can be rewritten as,

$$m\beta^{-1}\partial_p\bar{w} = \beta^{-1}[\frac{p^2 - \langle p^2\rangle}{2m^2}D_x^3\tilde{\rho} - \partial_x D_x^2\tilde{\rho}e^{\beta G}\int^p dp' e^{-\beta G(p')}\frac{p'}{m^2}] + e^{\beta G}c(x). \tag{B.16}$$

We integrate both sides of Eq. (B.16) over p:

$$m\beta^{-1}w = \beta^{-1}e^{-\beta G}\left[\frac{p^3/3 - \langle p^2\rangle p}{2m^2}D_x^3\tilde{\rho} - \partial_x D_x^2\tilde{\rho}\int^p dp'' e^{\beta G(p'')}\int^{p''} dp' e^{-\beta G(p')}\frac{p'}{m^2}\right] + e^{-\beta G}\int^p dp' e^{\beta G(p')}c(x) + e^{-\beta G}d(x).$$

From the normalizability, $c = 0$, and from $Qw = w$,

$$w = e^{-\beta G}\left[\frac{p^3 - \langle p^3\rangle - 3\langle p^2\rangle p}{6m^3}D_x^3\tilde{\rho} - (g(p) - \langle g(p)\rangle)\partial_x D_x^2\tilde{\rho}\right],$$
$$\left(g(p) = \int^p dp'' e^{\beta G(p'')}\int^{p''} dp' e^{-\beta G(p')}\frac{p'}{m^3}\right).$$

Now we apply B to w:

$$\begin{aligned} Bw =& BF^{-1}DF^{-1}DF^{-1}Cv \\ =& \mathcal{P}(-\partial_p G\partial_x + \partial_x V\partial_p)e^{-\beta G}[\frac{p^3 - \langle p^3\rangle - 3\langle p^2\rangle p}{6m^3}D_x^3\tilde{\rho} - (g(p) - \langle g(p)\rangle)\partial_x D_x^2\tilde{\rho}] \\ =& -\beta^{-1}e^{-\beta G}\int dp e^{-\beta G}[\frac{p^2 - \langle p^2\rangle}{2m^3}\partial_x D_x^3\tilde{\rho} - g'(p)\partial_x^2 D_x^2\tilde{\rho}] \\ =& \beta^{-1}\partial_x^2 D_x^2\tilde{\rho}e^{-\beta G}\langle g'(p)\rangle, \end{aligned} \tag{B.17}$$

here,

$$g'(p) = e^{\beta G(p)}\int^p dp' e^{-\beta G(p')}\frac{p'}{m^3}.$$

Now, we calculate the second term in Eq. (B.12):

$$BF^{-2}C(BF^{-1}Cv) = -BF^{-2}\frac{1}{\beta m}D_x\partial_p e^{-\beta G}\partial_x D_x\tilde{\rho}.$$

To calculate $F^{-1}CBF^{-1}Cv$, we need to solve $Fw = CBF^{-1}Cv$ for w:

$$\begin{aligned} & Fw = CBF^{-1}Cv \\ \Leftrightarrow & m\partial_p((\partial_p G) + \beta^{-1}\partial_p)w = \frac{-1}{\beta m}\partial_p e^{-\beta G}D_x\partial_x D_x\tilde{\rho}. \end{aligned} \tag{B.18}$$

Integrating both sides of Eq. (B.18) with respect to p,

$$((\partial_p G) + \beta^{-1}\partial_p)w = \frac{-1}{\beta m^2}e^{-\beta G}D_x\partial_x D_x\tilde{\rho} + c(x). \tag{B.19}$$

Introducing $w = e^{-\beta G}\bar{w}$, Eq. (B.19) can be rewritten as,

$$\partial_p\bar{w} = \frac{-1}{m^2}D_x\partial_x D_x\tilde{\rho} + e^{\beta G}c(x), \tag{B.20}$$

and integrating both sides of Eq. (B.20) over p,

$$\bar{w} = \frac{-p}{m^2} D_x \partial_x D_x \tilde{\rho} + \int^p dp' e^{\beta G(p')} c(x) + d(x),$$

then, from the normalizability and $Qw = w$,

$$w = F^{-1} C B F^{-1} C v = \frac{-p}{m^2} e^{-\beta G} D_x \partial_x D_x \tilde{\rho},$$

To calculate $F^{-1}F^{-1}CBF^{-1}Cv$ we further solve the equation $Fw = F^{-1}CBF^{-1}Cv$ for w:

$$\begin{aligned} &Fw = F^{-1} C B F^{-1} C v \\ \Leftrightarrow &m\partial_p((\partial_p G) + \beta^{-1}\partial_p) w = \frac{-p}{m^2} e^{-\beta G} D_x \partial_x D_x \tilde{\rho}. \end{aligned} \tag{B.21}$$

Integrating both sides of Eq. (B.21) over p,

$$\begin{aligned} &m((\partial_p G) + \beta^{-1}\partial_p) w = \int^p dp' \frac{-p'}{m^2} e^{-\beta G(p')} D_x \partial_x D_x \tilde{\rho} + c(x) \\ \Leftrightarrow &m\beta^{-1}\partial_p \bar{w} = e^{\beta G} \int^p dp' \frac{-p'}{m^2} e^{-\beta G(p')} D_x \partial_x D_x \tilde{\rho} + e^{\beta G} c(x) \\ \therefore &m\beta^{-1}\bar{w} = \int^p dp'' e^{\beta G(p'')} \int^{p''} dp' \frac{-p'}{m^2} e^{-\beta G(p')} D_x \partial_x D_x \tilde{\rho} + \int^p dp' e^{\beta G(p')} c(x) + d(x) \\ \therefore &w = -\beta e^{-\beta G} (g(p) - \langle g(p) \rangle) D_x \partial_x D_x \tilde{\rho}, \end{aligned}$$

where we used the normalizability and the condition $Qw = w$ in the last line. Now we apply B to w:

$$\begin{aligned} Bw =& BF^{-2} C B F^{-1} C v \\ =& \mathcal{P}(-\partial_p G \partial_x + \partial_x V \partial_p)(-\beta) e^{-\beta G} (g(p) - \langle g(p) \rangle) D_x \partial_x D_x \tilde{\rho} \\ =& \beta^{-1} e^{-\beta G} \langle g'(p) \rangle \partial_x (D_x \partial_x D_x \tilde{\rho}) \end{aligned} \tag{B.22}$$

Therefore, combining Eqs. (B.17) and (B.22), at order $\mathcal{O}(\gamma^{-3})$,

$$\beta^{-1}\gamma^{-3} e^{-\beta G} \langle g'(p) \rangle \partial_x [D_x \partial_x - \partial_x D_x] D_x \tilde{\rho} \tag{B.23}$$

Combining Eqs. (B.9) and (B.23), in total,

$$\partial_t \tilde{\rho} = \partial_x \left(\frac{1}{m\gamma\beta} - \frac{\langle g'(p) \rangle}{\beta\gamma^3} [\partial_x D_x - D_x \partial_x] \right) (D_x \tilde{\rho}), \tag{B.24}$$

where we again note that,

$$\tilde{\rho}(x,t) = \int dp \rho(x,p,t), \quad D_x = \partial_x + \beta(\partial_x V), \quad \langle g'(p) \rangle = \frac{\int_{-\infty}^{\infty} dp \int_{-\infty}^{p} dp' e^{-\beta G(p')} \frac{p'}{m^3}}{\int_{-\infty}^{\infty} dp e^{-\beta G(p')}}. \tag{B.25}$$

This equation is invariant under the inversion $x \to -x$, so up to order $\mathcal{O}(\gamma^{-3})$, the system does not exhibit nonreciprocity.

For example, if we take the usual kinetic energy $G(p) = p^2/(2m)$, then,

$$\langle g'(p) \rangle = -\frac{1}{m^2\beta}. \tag{B.26}$$

Therefore, Eq. (B.24) becomes

$$\partial_t \tilde{\rho} = \frac{1}{m\beta\gamma}\partial_x \left(1 + \frac{1}{m\gamma^2}\partial_x^2 V(x)\right)(D_x\tilde{\rho}). \tag{B.27}$$

This expression reproduces the γ^{-1} expansion up to third order terms [126]. Also, up to order $\mathcal{O}(\gamma^{-1})$, this equation is known as the Smoluchowski equation.

We can also take the limit $\beta \to \infty$ in Eq. (B.24) to discuss the fluctuationless case. In this limit, denoting $m^2\beta\langle g'(p)\rangle \to_{\beta\to\infty} -\mathfrak{g}$, from Eq. (B.24),

$$\partial_t \tilde{\rho} = \frac{1}{m\gamma}\partial_x \left(1 + \frac{\mathfrak{g}}{m\gamma^2}\partial_x^2 V\right)(\partial_x V\tilde{\rho}). \tag{B.28}$$

Not surprisingly, the equation becomes first order differential equation in x, since there is no fluctuation which leads to the higher order derivatives in x. Eq. (B.28) is the deterministic Liouville equation equivalent to the following deterministic equation:

$$\dot{x} = -\frac{\partial_x V}{m\gamma} - \frac{\mathfrak{g}}{m^2\gamma^3}(\partial_x^2 V)(\partial_x V). \tag{B.29}$$

Comparing to Eq. (B.1), we note that, up to $\mathcal{O}(\gamma^{-1})$, Eq. (B.29) is equivalent to Eq. (B.1) at $T = 0$ and without the inertia term. Therefore, the overdamped approximation where we drop the inertia term is the first order term of γ^{-1} expansion. Furthermore, we can see that Eq. (B.29) is invariant under $x \to -x$, so again the system do not exhibits the nonreciprocity in this fluctuationless case.

B.2 Derivation of Zener tunneling rate

For convenience, we restate the setting of the Josephson junction. We consider the situation where the two superconductors are connected by the Josephson coupling and shunted by the ohmic resistor. Then, denoting the voltage drop across the circuit as V and the total current as I_x, we obtain

$$V = \frac{\partial E_C}{\partial Q} = \frac{d\phi}{dt} = RI_3, \quad I_x = I_1 + I_2 + I_3 = \frac{dQ}{dt} + E_J \sin\phi + \frac{V}{R}, \tag{B.30}$$

where E_C is the charging energy of the capacitor, and the circuit is as is shown below.

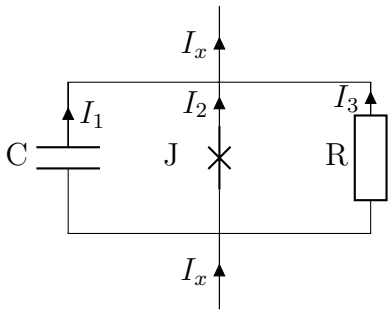

Then, the equations describing this circuit is,

$$\frac{d\phi}{dt} = V = \frac{\partial E_C}{\partial Q}, \quad \frac{dQ}{dt} = I_x - E_J \sin\phi - \frac{1}{R}\frac{\partial E_C}{\partial Q},$$

so if we drive the circuit by the current I_x, the phase slip $d\phi/dt$ leads to the voltage drop V.

Now, the second equation of (B.30) can be transformed to

$$R\,(I_1 + I_2) + V = RI_x (=: V_x). \tag{B.31}$$

This equation can be regarded as the balance of voltage drop of the following circuit:

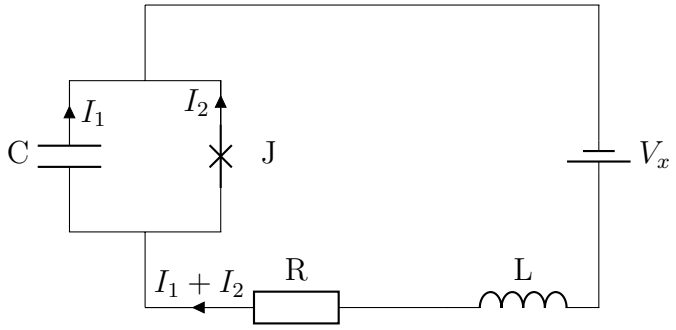

$I_1 + I_2$ is now the current flowing through the whole circuit, and V is the voltage drop across the Josephson junction. Here we introduced the inductor L, which provides the high frequency cutoff of the Ohmic conductance. In this setting, we set the external voltage V_x and measures the voltage drop V.

Now we write the Lagrangian of the above system. To do that, we need the following degrees of freedom: $\{\phi, Q; q, p; X_k, P_k\}$. Among them, Q, ϕ represents the degrees of freedom of Josephson junction; q, p represents the normal current $I_1 + I_2$, i.e., $\dot{q} = I_1 + I_2$ and p is conjugate to q; X_k, P_k is the degrees of freedom of heat bath, and couples to q. The coupling of q to ϕ is represented as $\Delta L = \dot{q}\phi/(2e)$, or equivalently $\Delta L = -\dot{\phi}q/(2e)$, which only differs from the former by the total time derivative. For the former case, $\phi/(2e)$ is treated as the vector potential for q, p, while for the latter case, $-q/(2e)$ is treated as the vector potential for ϕ, Q. Here we consider the first case. Then, the total Lagrangian is,

$$L = Q\dot{\phi} + \frac{L\dot{q}^2}{2} - \left(E_c(Q) - E_J \cos\phi + \sum_k \left[\frac{M_k \dot{X}_k^2}{2} + \frac{M_k \omega_k^2}{2} \left(X_k + \lambda_k \frac{q}{M_k \omega_k^2} \right)^2 \right] \right) + \frac{\dot{q}\phi}{2e}. \tag{B.32}$$

Then, the equation of motion is,

$$\dot{Q} = -E_J \sin\phi + \frac{\dot{q}}{2e}, \quad 0 = \dot{\phi} - \frac{\partial E_C}{\partial Q}, \tag{B.33}$$
$$L\ddot{q} + \frac{\dot{\phi}}{2e} = -\sum_k \lambda_k \left(X_k + \lambda_k \frac{q}{M_k \omega_k^2} \right).$$

After integrating out X_k and P_k, we get

$$\ddot{q} + \frac{\dot{\phi}}{2eL} = -\frac{R}{L}\dot{q}$$
$$\therefore v = e^{-Rt/L}\left(v(0) + \frac{1}{2eL}\int_0^t dt' e^{Rt'/L}\dot{\phi}(t') \right), \quad (v = \dot{q}).$$

Now we assume the modulation of $\dot{\phi}$ is slow compared to the time scale L/R. Then,

$$v = \dot{q} \cong \frac{\dot{\phi}}{2eR}$$

Then, from (B.33),

$$\dot{Q} = -E_J \sin\phi + \frac{\dot{\phi}}{(2e)^2 R}, \quad \dot{\phi} = \frac{\partial E_C}{\partial Q},$$

which is the desired equation for the circuit dynamics. Therefore, we use the Lagrangian (B.32) in the following.

Here, we use the real-time formalism to calculate the density matrix. The expression is given as,

$$\rho(t, \phi_{+f}, \phi_{-f})$$
$$= \int dq_f dq_i \int Dq_+ Dq_- \tilde{\rho}(t, \phi_{+f}, \phi_{-f}; \{q_+(\tau), q_-(\tau)\}) \exp\left(iS[\{q_+(\tau), q_-(\tau)\}] \right),$$

where S is the Caldeira-Leggett action [36]

$$S[q_+, q_-]$$
$$= \int_0^t d\tau V_x q_q(\tau) + \int_0^t d\tau \int_0^t ds \left[-q_q(\tau) Z_s(\tau - s) q_{cl}(s) + \frac{i}{2} q_q(\tau) G_q(\tau - s) q_q(s) \right], \tag{B.34}$$

$$Z_s(t) = \int Z_s(\omega) e^{-i\omega t} \frac{d\omega}{2\pi}, \quad G_q(t) = \int \omega \coth\left(\frac{\omega}{2T} \right) \mathrm{Re}[Z_s(\omega)] e^{-i\omega t} \frac{d\omega}{2\pi},$$

and

$$V_x(t) = \int_0^t Z_s(t - s) I_x(s) ds.$$

And we defined $q_{cl} = (q_+ + q_-)/2$, $q_q = q_+ - q_-$. The initial conditions are $q_{cl}(0) = q_q(t) = 0$, $q_{cl}(t) = q_f$, $q_q(0) = q_i$ Here, $\tilde{\rho}(t, \phi_{+f}, \phi_{2f}; \{q_+(\tau), q_-(\tau)\})$ is obtained by solving the dynamics of ϕ in the presence of $q(t)$:

$$\tilde{\rho}(t, \phi_{+f}, \phi_{-f}; \{q_+(\tau), q_-(\tau)\}) = \int \rho(0, Q_+, Q_-)\psi_{Q_+q_+}(t, \phi_+)\psi^*_{Q_-q_-}(t, \phi_-)dQ_+dQ_-,$$

where the wave function ψ_{Qq} obeys the following equation:

$$i\frac{d}{dt}\psi_{Qq}(t, \phi) = \left[E_C\left(-i2e\frac{\partial}{\partial\phi}\right) - E_J\cos\phi - \frac{\dot{q}(t)\phi}{2e}\right]\psi_{Qq}(t, \phi), \quad \psi_{Qq}(0) = \frac{e^{i\frac{Q\phi}{2e}}}{\sqrt{2\pi}}$$

We set $\psi = e^{i(q(t)-q(0))\phi/(2e)}\tilde{\psi}$. Then,

$$i\frac{d}{dt}\tilde{\psi}_{Qq}(t, \phi) = \left[E_C\left(-i2e\frac{\partial}{\partial\phi} + q(t) - q(0)\right) - E_J\cos\phi\right]\tilde{\psi}_{Qq}(t, \phi), \quad \tilde{\psi}_{Qq}(0) = \frac{e^{i\frac{Q\phi}{2e}}}{\sqrt{2\pi}}.$$

Because of the periodicity of ϕ, in an analogous manner to the Bloch function, the solution can be written as,

$$\tilde{\psi}_{Qq}(t) = e^{iQ\phi/(2e)}\sum_n c_n(t)\frac{e^{-in\phi}}{\sqrt{2\pi}}.$$

Then c_n is the solution of the following equation:

$$i\frac{dc_n}{dt} = E_C\left(Q + q(t) - q(0) - 2en\right)c_n - \frac{E_J}{2}(c_{n+1} + c_{n-1}). \tag{B.35}$$

Now,

$$\begin{aligned}\tilde{\rho}(t, \phi_{+f}, \phi_{-f}; \{q_+(\tau), q_-(\tau)\}) &= \int \rho(0, Q_+, Q_-)\sum_{n,m} c_n[q_+]c^*_m[q_-] \\ &\quad \times e^{i[Q_+ + q_+(t) - q_+(0) - 2en]\phi_+/(2e)}e^{-i[Q_- + q_-(t) - q_-(0) - 2em]\phi_-/(2e)}dQ_+dQ_- \\ &= \int \rho(0, Q_+, Q_-)\sum_{n,m} c_n[q_+]c^*_m[q_-] \\ &\quad \times e^{i[Q_+ + q_f - q_i/2 - 2en]\phi_+/(2e)}e^{-i[Q_- + q_f + q_i/2 - 2em]\phi_-/(2e)}dQ_+dQ_-\end{aligned}$$

Here, we introduce

$$\begin{aligned}\tilde{q}_+(\tau) &= q_+(\tau) + Q_+ - q_+(0) = q_+(\tau) + Q_+ - q_i/2 =: q_+(\tau) + q_{s+}, \\ \tilde{q}_-(\tau) &= q_-(\tau) + Q_- - q_-(0) = q_-(\tau) + Q_- + q_i/2 =: q_-(\tau) + q_{s-}\end{aligned}$$

Then,

$$\begin{aligned}\tilde{q}_+(t) &= q_+(t) + Q_+ - q_i/2 = q_f + Q_+ - q_i/2 =: q_{+0}, \quad \tilde{q}_+(0) = Q_+ \\ \tilde{q}_-(t) &= q_-(t) + Q_- + q_i/2 = q_f + Q_- + q_i/2 =: q_{-0}, \quad \tilde{q}_-(0) = Q_-.\end{aligned}$$

Now we relabel $\tilde{q}$ as q. Then,

$$\tilde{\rho}(t,\phi_{+f},\phi_{-f};\{q_+(\tau),q_-(\tau)\}) = \int \rho(0,Q_+,Q_-)\sum_{n,m} c_n[q_+]c_m^*[q_-] \times e^{i[q_{+0}-2en]\phi_+/(2e)}e^{-i[q_{-0}-2em]\phi_-/(2e)}dQ_+dQ_-,$$

and

$$\begin{aligned}&\rho(t,\phi_{+f},\phi_{-f})\\ &=\int dq_{+0}dq_{-0}\int_{Q_+}^{q_{+0}}Dq_+\int_{Q_-}^{q_{-0}}Dq_-\\ &\qquad\times\tilde{\rho}(t,\phi_{+f},\phi_{-f};\{q_+(\tau),q_-(\tau)\})\exp\left(iS[\{q_+(\tau)-q_{s+},q_-(\tau)-q_{s-}\}]\right)\\ &=\sum_{n,m}\int\frac{dq_{+0}dq_{-0}}{2\pi}\rho_{nm}(t,q_{+0},q_{-0})e^{i[q_{+0}-2en]\phi_+/(2e)}e^{-i[q_{-0}-2em]\phi_-/(2e)},\end{aligned}$$

where

$$\rho_{nm}(t,q_{+0},q_{-0}) = \int J_q^{nm}(t,q_{+0},q_{-0},Q_+,Q_-)\rho(0,Q_+,Q_-)dQ_+dQ_-,$$

and

$$\begin{aligned}&J_q^{nm}(t,q_{+0},q_{-0},Q_+,Q_-)\\ &=\int_{Q_+}^{q_{+0}}Dq_+\int_{Q_-}^{q_{-0}}Dq_-c_n[q_+(\tau)]c_m^*[q_-(\tau)]\exp\left(iS[\{q_+(\tau)-q_{s+},q_-(\tau)-q_{s-}\}]\right).\end{aligned}$$

For later use, we solve Eq. (B.35) for $c_0(0)=1$, $c_1(0)=0$. Because of the shift of q mentioned above, (B.35) is now written as

$$i\frac{dc_n}{dt} = E_C\left(q(t)-2en\right)c_n - \frac{E_J}{2}(c_{n+1}+c_{n-1}). \tag{B.36}$$

We introduce

$$c_0(t) = \exp\left(-i\int_0^t E_C(q(\tau))d\tau\right)u_0(t),\quad c_1(t) = \exp\left(-i\int_0^t E_C(q(\tau)-2e)d\tau\right)u_1(t).$$

Then, assuming only c_1 and c_0 is nonzero, Eq. (B.36) becomes

$$\begin{aligned}\frac{du_0}{dt} &= \frac{iE_J}{2}\exp\left(i\int_0^t[E_C(q(\tau))-E_C(q(\tau)-2e)]d\tau\right)u_1,\\ \frac{du_1}{dt} &= \frac{iE_J}{2}\exp\left(-i\int_0^t[E_C(q(\tau))-E_C(q(\tau)-2e)]d\tau\right)u_0.\end{aligned}$$

integrating these equations over 0 to t and using $u_0(0)=1$ and $u_1(0)=0$,

$$\begin{aligned}u_0(t) &= 1+\frac{iE_J}{2}\int_0^t d\tau'\exp\left(i\int_0^{\tau'}[E_C(q(\tau))-E_C(q(\tau)-2e)]d\tau\right)u_1(\tau'),\\ u_1(t) &= \frac{iE_J}{2}\int_0^t d\tau'\exp\left(-i\int_0^{\tau'}[E_C(q(\tau))-E_C(q(\tau)-2e)]d\tau\right)u_0(\tau').\end{aligned}$$

Then,

$$
\begin{aligned}
u_0(t) &= 1 - \frac{E_J^2}{4}\int_0^t d\tau' \exp\left(i\int_0^{\tau'}[E_C(q(\tau)) - E_C(q(\tau)-2e)]d\tau\right) \\
&\quad\times \int_0^{\tau'} d\tau'' \exp\left(-i\int_0^{\tau''}[E_C(q(\tilde{\tau})) - E_C(q(\tilde{\tau})-2e)]d\tilde{\tau}\right) u_0(\tau'') \\
&= 1 - \frac{E_J^2}{4}\int_0^t d\tau' \int_0^{\tau'} d\tau'' \exp\left(i\int_{\tau''}^{\tau'}[E_C(q(\tau)) - E_C(q(\tau)-2e)]d\tau\right) u_0(\tau'') \\
&= 1 - \frac{E_J^2}{4}\int_0^t d\tau' \int_0^{\tau'} d\tau'' \exp\left(i\int_{\tau''}^{\tau'}[E_C(q(\tau)) - E_C(q(\tau)-2e)]d\tau\right) + \mathcal{O}(E_J^4) \\
&= \exp\left[-\frac{E_J^2}{4}\int_0^t d\tau' \int_0^{\tau'} d\tau'' \exp\left(i\int_{\tau''}^{\tau'}[E_C(q(\tau)) - E_C(q(\tau)-2e)]d\tau\right)\right] + \mathcal{O}(E_J^4)
\end{aligned}
$$

Here, Zener tunneling rate is given as,

$$
\Gamma_\uparrow = \frac{I_x}{2e} w(2e/I_x) = \frac{I_x}{2e}\int \rho_{00}(2e/I_x; q_D, q_D) dq_D,
$$

i.e., we consider the case where $q_{+0} = q_{-0} = q_D$. In that case, since the Caldeira-Leggett action (B.34) is invariant under the shift of the classical component $q_{cl} \to q_{cl} + q_D$, the following relation holds:

$$
S[\{q_+(\tau) - q_{s+}, q_-(\tau) - q_{s-}\}] = S[\{q_+(\tau), q_-(\tau)\}].
$$

Then,

$$
\begin{aligned}
w(t) &= \int dq_D dQ_+ dQ_- \rho(0, Q_+, Q_-) \int_{Q_+}^{q_D} Dq_+ \int_{Q_-}^{q_D} Dq_- c_0[q_+(\tau)] c_0^*[q_-(\tau)] \\
&\qquad\times \exp\left(iS[\{q_+(\tau), q_-(\tau)\}]\right) \\
&= \int dq_D dQ_+ dQ_- \rho(0, Q_+, Q_-) \int_{Q_+}^{q_D} Dq_+ \int_{Q_-}^{q_D} Dq_- u_0[q_+(\tau)] u_0^*[q_-(\tau)] \\
&\qquad\times \exp\left(iS[\{q_+(\tau), q_-(\tau)\}] - i\int_0^t [E_C(q_+(\tau)) - E_C(q_-(\tau))]d\tau\right). \qquad \text{(B.37)}
\end{aligned}
$$

Now we note that the action in the exponent in Eq. (B.37) is for the dissipative system with the energy potential $E_C(q)$ in the Keldysh formalism. Then, the natural way to interpret Eq. (B.37) is that it is the expectation value of the quantity $u_0[q_+(\tau)]u_0^*[q_-(\tau)]$.

Now,

$$\begin{aligned}
&u_0[q_+(\tau)]u_0^*[q_-(\tau)] \\
&= \exp\left\{-\frac{E_J^2}{4}\int_0^t d\tau' \int_0^{\tau'} d\tau'' \left[\exp\left(i\int_{\tau''}^{\tau'} [E_C(q_+(\tau)) - E_C(q_+(\tau) - 2e)]d\tau\right)\right.\right. \\
&\qquad \left.\left. + \exp\left(-i\int_{\tau''}^{\tau'} [E_C(q_-(\tau)) - E_C(q_-(\tau) - 2e)]d\tau\right)\right]\right\} \\
&=: e^{-f}.
\end{aligned}$$

Now, we approximate the above expression only by considering the zeroth order terms in q_q. Then,

$$\langle f\rangle \cong \frac{E_J^2}{2}\int_0^t d\tau' \int_0^{\tau'} d\tau'' \mathrm{Re}\exp\left(i\int_{\tau''}^{\tau'} [E_C(\langle q_{cl}(\tau)\rangle) - E_C(\langle q_{cl}(\tau)\rangle - 2e)]d\tau\right)$$

Here we note that the expression $E_C(\langle q_{cl}(\tau)\rangle) - E_C(\langle q_{cl}(\tau)\rangle - 2e) =: \Delta(\langle q_{cl}(\tau)\rangle)$ is the energy difference between the band in the first Brillouin zone and the one shifted by $2e$. This term becomes zero when the two bands touch. Also, the integrand is symmetric with respect to the change $\tau' \leftrightarrow \tau''$. Then,

$$\langle f\rangle \cong \frac{E_J^2}{4}\mathrm{Re}\int_0^t d\tau' \int_0^t d\tau'' \exp\left(i\left[\int_0^{\tau'} \Delta(\langle q_{cl}(\tau)\rangle)d\tau - \int_0^{\tau''} \Delta(\langle q_{cl}(\tau)\rangle)d\tau\right]\right)$$

Now we approximate this integral by the method of steepest descent. The saddle point is the time $t = t_0$ where the two band crosses. Then,

$$\langle f\rangle \cong \frac{E_J^2}{4}\frac{2\pi}{\langle q'_{cl}(t_0)\rangle \Delta'(\langle q_{cl}(t_0)\rangle)} = \frac{E_J^2\pi}{2\Delta'(\langle q_{cl}(t_0)\rangle)}\frac{1}{\langle q'_{cl}(t_0)\rangle} =: \frac{I_Z}{\langle q'_{cl}(t_0)\rangle}$$

Then, the expression of the Zener tunneling probability is,

$$P = \exp\left[-\frac{I_Z}{\langle q'_{cl}(t_0)\rangle}\right].$$

In the presence of the antisymmetry of the dispersion, $\langle q'_{cl}(t_0)\rangle$ is different for the right-moving case and the left-moving case. In the limit of $1/R_s \to 0$, $\langle q'_{cl}(t_0)\rangle = I_x$ for both left and right-moving case, and we obtain the symmetric Zener tunneling probability.

Bibliography

[1]P. W. Anderson, *Basic notions of condensed matter physics* (CRC Press, 2018).

[2]M. Tinkham, *Introduction to Superconductivity* (Courier Corporation, Jan. 2004).

[3]M. P. A. Fisher and D. H. Lee, "Correspondence between two-dimensional bosons and a bulk superconductor in a magnetic field", Physical Review B **39**, 2756–2759 (1989).

[4]D.-H. Lee and M. P. A. Fisher, "Anyon superconductivity and the fractional quantum hall effect", Physical Review Letters **63**, 903–906 (1989).

[5]M. P. A. Fisher, "Quantum phase transitions in disordered two-dimensional superconductors", Physical Review Letters **65**, 923–926 (1990).

[6]M. P. A. Fisher, G. Grinstein, and S. M. Girvin, "Presence of quantum diffusion in two dimensions: universal resistance at the superconductor-insulator transition", Physical Review Letters **64**, 587–590 (1990).

[7]S. M. Girvin, M. Wallin, M.-C. Cha, M. P. A. Fisher, and A. P. Young, "Universal Conductivity at the Superconductor-Insulator Transition in Two-Dimensions", Progress of Theoretical Physics Supplement **107**, 135–144 (1992).

[8]D. B. Haviland, Y. Liu, and A. M. Goldman, "Onset of superconductivity in the two-dimensional limit", Physical Review Letters **62**, 2180–2183 (1989).

[9]Y. Saito, T. Nojima, and Y. Iwasa, "Quantum phase transitions in highly crystalline two-dimensional superconductors", Nature Communications **9**, 778 (2018).

[10]Y. Saito, T. Nojima, and Y. Iwasa, "Highly crystalline 2d superconductors", Nature Reviews Materials **2**, 1–18 (2016).

[11]A. Kapitulnik, S. A. Kivelson, and B. Spivak, "Colloquium: Anomalous metals: Failed superconductors", Reviews of Modern Physics **91**, 011002 (2019).

[12]R. Wakatsuki, Y. Saito, S. Hoshino, Y. M. Itahashi, T. Ideue, M. Ezawa, Y. Iwasa, and N. Nagaosa, "Nonreciprocal charge transport in noncentrosymmetric superconductors", Science Advances **3**, e1602390 (2017).

[13]S. Hoshino, R. Wakatsuki, K. Hamamoto, and N. Nagaosa, "Nonreciprocal charge transport in two-dimensional noncentrosymmetric superconductors", Physical Review B **98**, arXiv: 1805.05735, 054510 (2018).

[14]K. Hamamoto, T. Park, H. Ishizuka, and N. Nagaosa, "Scaling theory of a quantum ratchet", Physical Review B **99**, 064307 (2019).

[15]S. Chakravarty, G.-L. Ingold, S. Kivelson, and A. Luther, "Onset of Global Phase Coherence in Josephson-Junction Arrays: A Dissipative Phase Transition", Physical Review Letters **56**, 2303–2306 (1986).

[16]S. Chakravarty, G.-L. Ingold, S. Kivelson, and G. Zimanyi, "Quantum statistical mechanics of an array of resistively shunted Josephson junctions", Physical Review B **37**, 3283–3294 (1988).

[17]C. Caroli, P. G. De Gennes, and J. Matricon, "Bound Fermion states on a vortex line in a type II superconductor", Physics Letters **9**, 307–309 (1964).

[18]M. Stone, "Spectral flow, Magnus force, and mutual friction via the geometric optics limit of Andreev reflection", Physical Review B **54**, 13222–13229 (1996).

[19]N. B. Kopnin and M. M. Salomaa, "Mutual friction in superfluid ^{3}He : Effects of bound states in the vortex core", Physical Review B **44**, 9667–9677 (1991).

[20]N. B. Kopnin, *Theory of nonequilibrium superconductivity*, International series of monographs on physics 110 (Oxford Univ. Press, Oxford, 2009).

[21]Y. Saito, Y. Nakamura, M. S. Bahramy, Y. Kohama, J. Ye, Y. Kasahara, Y. Nakagawa, M. Onga, M. Tokunaga, T. Nojima, et al., "Superconductivity protected by spin–valley locking in ion-gated mos 2", Nature Physics **12**, 144–149 (2016).

[22]M. Greiter, F. Wilczek, and E. Witten, "Hydrodynamic Relations in Superconductivity", Modern Physics Letters **B3**, 903 (1989).

[23]D. Son and M. Wingate, "General coordinate invariance and conformal invariance in nonrelativistic physics: Unitary Fermi gas", Annals of Physics **321**, 197–224 (2006).

[24]I. J. R. Aitchison, P. Ao, D. J. Thouless, and X.-M. Zhu, "Effective Lagrangians for BCS superconductors at $T = 0$", Physical Review B **51**, 6531–6535 (1995).

[25]I. J. R. Aitchison, G. Metikas, and D. J. Lee, "Finite-temperature time-dependent effective theory for the Goldstone field in a BCS-type superfluid", Physical Review B **62**, 6638–6648 (2000).

[26]M. E. Fisher, M. N. Barber, and D. Jasnow, "Helicity modulus, superfluidity, and scaling in isotropic systems", Physical Review A **8**, 1111–1124 (1973).

[27]S. Sachdev, "Quantum Impurity in a Nearly Critical Two-Dimensional Antiferromagnet", Science **286**, 2479–2482 (1999).

[28]V. N. Popov, *Functional integrals and collective excitations*, Cambridge monographs on mathematical physics (Cambridge Univ. Press, Cambridge, 1987).

[29]A. A. Abrikosov, L. P. Gorkov, and I. E. Dzyaloshinski, *Methods of quantum field theory in statistical physics* (Courier Corporation, 2012).

[30]H. T. C. Stoof, D. B. M. Dickerscheid, and K. Gubbels, *Ultracold quantum fields* (Springer, Berlin, 2009).

[31]M. Imada, A. Fujimori, and Y. Tokura, "Metal-insulator transitions", Reviews of Modern Physics **70**, 1039–1263 (1998).

[32]M. P. A. Fisher, P. B. Weichman, G. Grinstein, and D. S. Fisher, "Boson localization and the superfluid-insulator transition", Physical Review B **40**, 546–570 (1989).

[33]K. Huang and H.-F. Meng, "Hard-sphere Bose gas in random external potentials", Physical Review Letters **69**, 644–647 (1992).

[34]A. V. Lopatin and V. M. Vinokur, "Thermodynamics of the Superfluid Dilute Bose Gas with Disorder", Physical Review Letters **88**, 235503 (2002).

[35]M. V. Feigelman, V. B. Geshkenbein, L. B. Ioffe, and A. I. Larkin, "Two-dimensional Bose liquid with strong gauge-field interaction", Physical Review B **48**, 16641–16661 (1993).

[36]A. Caldeira and A. Leggett, "Path integral approach to quantum Brownian motion", Physica A: Statistical Mechanics and its Applications **121**, 587–616 (1983).

[37]R. P. Feynman, "The λ-Transition in Liquid Helium", Physical Review **90**, 1116–1117 (1953).

[38]R. P. Feynman, "Atomic Theory of the λ Transition in Helium", Physical Review **91**, 1291–1301 (1953).

[39]E. L. Pollock and D. M. Ceperley, "Path-integral computation of superfluid densities", Physical Review B **36**, 8343–8352 (1987).

[40]D. M. Ceperley, "Path integrals in the theory of condensed helium", Reviews of Modern Physics **67**, 279–355 (1995).

[41]P. Nozieres, *Theory Of Quantum Liquids* (CRC Press, Mar. 2018).

[42]P. W. Anderson, "Coherent Excited States in the Theory of Superconductivity: Gauge Invariance and the Meissner Effect", Physical Review **110**, 827–835 (1958).

[43]D. J. Scalapino, S. R. White, and S. Zhang, "Insulator, metal, or superconductor: The criteria", Physical Review B **47**, 7995–8007 (1993).

[44]A. J. Leggett, "Bose-Einstein condensation in the alkali gases: Some fundamental concepts", Reviews of Modern Physics **73**, 307–356 (2001).

[45]D. Dalidovich and P. Phillips, "Fluctuation Conductivity in Insulator-Superconductor Transitions with Dissipation", Physical Review Letters **84**, 737–740 (2000).

[46]L. Zhu, Y. Chen, and C. M. Varma, "Local quantum criticality in the two-dimensional dissipative quantum XY model", Physical Review B **91**, 205129 (2015).

[47]L. Zhu, C. Hou, and C. M. Varma, "Quantum criticality in the two-dimensional dissipative quantum XY model", Physical Review B **94**, 235156 (2016).

[48]C. Hou and C. M. Varma, "Phase diagram and correlation functions of the two-dimensional dissipative quantum XY model", Physical Review B **94**, 201101 (2016).

[49]M. P. A. Fisher and G. Grinstein, "Quantum Critical Phenomena in Charged Superconductors", Physical Review Letters **60**, 208–211 (1988).

[50]S. Sachdev, *Quantum Phase Transitions* (Cambridge University Press, Cambridge, Apr. 2011).

[51]Z. Cai, U. Schollwöck, and L. Pollet, "Identifying a Bath-Induced Bose Liquid in Interacting Spin-Boson Models", Physical Review Letters **113**, 260403 (2014).

[52]A. O. Caldeira and A. J. Leggett, "Quantum tunnelling in a dissipative system", Annals of Physics **149**, 374–456 (1983).

[53]N. Nagaosa, *Quantum Field Theory in Condensed Matter Physics*, Theoretical and Mathematical Physics (Springer-Verlag, Berlin Heidelberg, 1999).

[54]J. Bardeen and M. J. Stephen, "Theory of the Motion of Vortices in Superconductors", Physical Review **140**, A1197–A1207 (1965).

[55]O. S. Duarte and A. O. Caldeira, "Effective Coupling between Two Brownian Particles", Physical Review Letters **97**, 250601 (2006).

[56]A. Kamenev, *Field theory of non-equilibrium systems* (Cambridge University Press, 2011).

[57]S. M. Apenko, "Critical temperature of the superfluid transition in Bose liquids", Physical Review B **60**, 3052–3055 (1999).

[58]U. Weiss, *Quantum Dissipative Systems*, 4th (WORLD SCIENTIFIC, 2012).

[59]R. P. Feynman, "Slow Electrons in a Polar Crystal", Physical Review **97**, 660–665 (1955).

[60]D. C. Khandekar, K. V. Bhagwat, and S. V. Lawande, "Polaron effective mass", Physical Review B **37**, 3085–3088 (1988).

[61]M. Boninsegni, N. Prokof'ev, and B. Svistunov, "Worm Algorithm for Continuous-Space Path Integral Monte Carlo Simulations", Physical Review Letters **96**, 070601 (2006).

[62]M. Boninsegni, N. V. Prokof'ev, and B. V. Svistunov, "Worm algorithm and diagrammatic Monte Carlo: A new approach to continuous-space path integral Monte Carlo simulations", Physical Review E **74**, 036701 (2006).

[63]F. Mezzacapo and M. Boninsegni, "Superfluidity and Quantum Melting of p-H_2 Clusters", Physical Review Letters **97**, 045301 (2006).

[64]F. Mezzacapo and M. Boninsegni, "Structure, superfluidity, and quantum melting of hydrogen clusters", Physical Review A **75**, 033201 (2007).

[65]R. A. Aziz, V. P. S. Nain, J. S. Carley, W. L. Taylor, and G. T. McConville, "An accurate intermolecular potential for helium", The Journal of Chemical Physics **70**, 4330–4342 (1979).

[66]V. Ambegaokar and M. Troyer, "Estimating errors reliably in Monte Carlo simulations of the Ehrenfest model", American Journal of Physics **78**, 150–157 (2010).

[67]S. A. Chin, "Symplectic integrators from composite operator factorizations", Physics Letters A **226**, 344–348 (1997).

[68]P. Werner, M. Troyer, and S. Sachdev, "Quantum Spin Chains with Site Dissipation", Journal of the Physical Society of Japan **74**, 67–70 (2005).

[69]P. Werner, K. Völker, M. Troyer, and S. Chakravarty, "Phase Diagram and Critical Exponents of a Dissipative Ising Spin Chain in a Transverse Magnetic Field", Physical Review Letters **94**, 047201 (2005).

[70]A. Griffin, *Excitations in a Bose-condensed liquid* (Cambridge University Press, Cambridge, 1993).

[71]J. Keeling, "Superfluid Density of an Open Dissipative Condensate", Physical Review Letters **107**, 080402 (2011).

[72]B. D. Josephson, "Relation between the superfluid density and order parameter for superfluid He near Tc", Physics Letters **21**, 608–609 (1966).

[73]C. A. Müller, "Josephson relation for disordered superfluids", Physical Review A **91**, 023602 (2015).

[74]M. Stone, "Magnus force on skyrmions in ferromagnets and quantum Hall systems", Physical Review B **53**, 16573–16578 (1996).

[75]L. L. Foldy, "Charged Boson Gas", Physical Review **124**, 649–651 (1961).

[76]S. R. Hore and N. E. Frankel, "Dielectric response of the charged Bose gas in the random-phase approximation", Physical Review B **12**, 2619–2628 (1975).

[77]J. C. Lee, "Dielectric approach to a dense charged boson gas at $T = 0$", Physical Review B **12**, 2644–2655 (1975).

[78]P. Ao and D. J. Thouless, "Berry's phase and the Magnus force for a vortex line in a superconductor", Physical Review Letters **70**, 2158–2161 (1993).

[79]Y. Tokura and N. Nagaosa, "Nonreciprocal responses from non-centrosymmetric quantum materials", Nature Communications **9**, 1–14 (2018).

[80]S. Kitamura, N. Nagaosa, and T. Morimoto, "Nonreciprocal landau–zener tunneling", Communications Physics **3**, 1–8 (2020).

[81]M. V. Berry, "Quantal phase factors accompanying adiabatic changes", Proceedings of the Royal Society **A392**, 45–57 (1984).

[82]T. Morimoto and N. Nagaosa, "Topological nature of nonlinear optical effects in solids", Science Advances **2**, e1501524 (2016).

[83]D. Jalas, A. Petrov, M. Eich, W. Freude, S. Fan, Z. Yu, R. Baets, M. Popović, A. Melloni, J. D. Joannopoulos, M. Vanwolleghem, C. R. Doerr, and H. Renner, "What is — and what is not — an optical isolator", Nature Photonics **7**, 579–582 (2013).

[84]F. Fratini, E. Mascarenhas, L. Safari, J.-P. Poizat, D. Valente, A. Auffèves, D. Gerace, and M. F. Santos, "Fabry-Perot Interferometer with Quantum Mirrors: Nonlinear Light Transport and Rectification", Physical Review Letters **113**, 243601 (2014).

[85]A. Rosario Hamann, C. Müller, M. Jerger, M. Zanner, J. Combes, M. Pletyukhov, M. Weides, T. M. Stace, and A. Fedorov, "Nonreciprocity Realized with Quantum Nonlinearity", Physical Review Letters **121**, 123601 (2018).

[86]M. Nakamura, S. Horiuchi, F. Kagawa, N. Ogawa, T. Kurumaji, Y. Tokura, and M. Kawasaki, "Shift current photovoltaic effect in a ferroelectric charge-transfer complex", Nature Communications **8**, 1–6 (2017).

[87]Z. Sun, Y. Yi, T. Song, G. Clark, B. Huang, Y. Shan, S. Wu, D. Huang, C. Gao, Z. Chen, et al., "Giant nonreciprocal second-harmonic generation from antiferromagnetic bilayer cri 3", Nature **572**, 497–501 (2019).

[88]O. E. Alon, V. Averbukh, and N. Moiseyev, "Selection rules for the high harmonic generation spectra", Physical Review Letters **80**, 3743–3746 (1998).

[89]D. E. Parker, T. Morimoto, J. Orenstein, and J. E. Moore, "Diagrammatic approach to nonlinear optical response with application to Weyl semimetals", Physical Review B **99**, 045121 (2019).

[90]T. Ideue, K. Hamamoto, S. Koshikawa, M. Ezawa, S. Shimizu, Y. Kaneko, Y. Tokura, N. Nagaosa, and Y. Iwasa, "Bulk rectification effect in a polar semiconductor", Nature Physics **13**, 578–583 (2017).

[91]G. Carapella and G. Costabile, "Ratchet Effect: Demonstration of a Relativistic Fluxon Diode", Physical Review Letters **87**, 077002 (2001).

[92]J. B. Majer, J. Peguiron, M. Grifoni, M. Tusveld, and J. E. Mooij, "Quantum Ratchet Effect for Vortices", Physical Review Letters **90**, 056802 (2003).

[93]F. Raissi and J. E. Nordman, "Josephson fluxonic diode", Applied Physics Letters **65**, 1838–1840 (1994).

[94]P. Recher, Y. V. Nazarov, and L. P. Kouwenhoven, "Josephson light-emitting diode", Physical Review Letters **104**, 156802 (2010).

[95]F. Hassler, Y. V. Nazarov, and L. P. Kouwenhoven, "Quantum manipulation in a josephson light-emitting diode", Nanotechnology **21**, 274004 (2010).

[96]J. Hu, C. Wu, and X. Dai, "Proposed design of a josephson diode", Physical Review Letters **99**, 067004 (2007).

[97]S. Savel'ev and F. Nori, "Experimentally realizable devices for controlling the motion of magnetic flux quanta in anisotropic superconductors", Nature Materials **1**, 179–184 (2002).

[98]M. J. Martínez-Pérez and F. Giazotto, "Efficient phase-tunable Josephson thermal rectifier", Applied Physics Letters **102**, 182602 (2013).

[99]M. Büttiker, H. Thomas, and A. Prêtre, "Mesoscopic capacitors", Physics Letters A **180**, 364–369 (1993).

[100]M. Buttiker, "Capacitance, admittance, and rectification properties of small conductors", Journal of Physics: Condensed Matter **5**, 9361–9378 (1993).

[101]T. Christen and M. Büttiker, "Low Frequency Admittance of a Quantum Point Contact", Physical Review Letters **77**, 143–146 (1996).

[102]Z.-s. Ma, J. Wang, and H. Guo, "Weakly nonlinear ac response: Theory and application", Physical Review B **59**, 7575–7578 (1999).

[103]B. Wang, X. Zhao, J. Wang, and H. Guo, "Nonlinear quantum capacitance", Applied Physics Letters **74**, 2887–2889 (1999).

[104]P. Hänggi, P. Talkner, and M. Borkovec, "Reaction-rate theory: fifty years after Kramers", Reviews of Modern Physics **62**, 251–341 (1990).

[105]S. H. Strogatz, *Nonlinear Dynamics and Chaos : With Applications to Physics, Biology, Chemistry, and Engineering* (CRC Press, May 2018).

[106]Y. M. Ivanchenko and L. A. Zil'berman, "The Josephson Effect in Small Tunnel Contacts", Soviet Physics JETP **28**, 1272 (1969).

[107]V. Ambegaokar and B. I. Halperin, "Voltage Due to Thermal Noise in the dc Josephson Effect", Physical Review Letters **22**, 1364–1366 (1969).

[108]K. K. Likharev and A. B. Zorin, "Theory of the Bloch-wave oscillations in small Josephson junctions", Journal of Low Temperature Physics **59**, 347–382 (1985).

[109]G. Schön and A. D. Zaikin, "Quantum coherent effects, phase transitions, and the dissipative dynamics of ultra small tunnel junctions", Physics Reports **198**, 237–412 (1990).

[110]A. D. Zaikin and D. S. Golubev, "Effect of environment on interband tunneling in ultrasmall Josephson junctions", Physics Letters A **164**, 337–344 (1992).

[111]L. S. Kuzmin, Y. A. Pashkin, D. S. Golubev, and A. D. Zaikin, "Charge transport and Zener tunneling in small Josephson junctions with dissipation", Physical Review B **54**, 10074–10080 (1996).

[112]J. Guckenheimer and P. J. Holmes, *Nonlinear Oscillations, Dynamical Systems, and Bifurcations of Vector Fields*, Applied Mathematical Sciences (Springer-Verlag, New York, 1983).

[113]J. L. García-Palacios and F. J. Lázaro, "Langevin-dynamics study of the dynamical properties of small magnetic particles", Physical Review B **58**, 14937–14958 (1998).

[114]H. Risken and T. Frank, *The Fokker-Planck Equation: Methods of Solution and Applications*, 2nd ed., Springer Series in Synergetics (Springer-Verlag, Berlin Heidelberg, 1996).

[115]P. Hänggi and F. Marchesoni, "Artificial Brownian motors: Controlling transport on the nanoscale", Reviews of Modern Physics **81**, 387–442 (2009).

[116]L. P. Fischer, P. Pietzonka, and U. Seifert, "Large deviation function for a driven underdamped particle in a periodic potential", Physical Review E **97**, 022143 (2018).

[117]A. C. Barato and U. Seifert, "Thermodynamic Uncertainty Relation for Biomolecular Processes", Physical Review Letters **114**, 158101 (2015).

[118]P. Pietzonka, A. C. Barato, and U. Seifert, "Universal bounds on current fluctuations", Physical Review E **93**, 052145 (2016).

[119]H.-M. Chun, L. P. Fischer, and U. Seifert, "Effect of a magnetic field on the thermodynamic uncertainty relation", Physical Review E **99**, 042128 (2019).

[120]D. S. Golubev and A. D. Zaikin, "Effect of external circuit on the charge dynamics of ultrasmall Josephson junctions", Physics Letters A **148**, 479–484 (1990).

[121]A. Schmid, "Diffusion and Localization in a Dissipative Quantum System", Physical Review Letters **51**, 1506–1509 (1983).

[122]J. A. Hertz, "Quantum critical phenomena", Physical Review B **14**, 1165–1184 (1976).

[123]A. J. Millis, "Effect of a nonzero temperature on quantum critical points in itinerant fermion systems", Physical Review B **48**, 7183–7196 (1993).

[124]D. Averin and K. Likharev, "Coulomb blockade of single-electron tunneling, and coherent oscillations in small tunnel junctions", Journal of Low Temperature Physics **62**, 345–373 (1986).

[125]A. Mazurenko, C. S. Chiu, G. Ji, M. F. Parsons, M. Kanász-Nagy, R. Schmidt, F. Grusdt, E. Demler, D. Greif, and M. Greiner, "A cold-atom fermi–hubbard antiferromagnet", Nature **545**, 462–466 (2017).

[126]N. Van Kampen, "Elimination of fast variables", Physics Reports **124**, 69–160 (1985).

[127]A. Altland and B. D. Simons, *Condensed Matter Field Theory*, 2nd ed. (Cambridge University Press, Cambridge, 2010).